Early cretaceous topographic evolution associated with the collapse of the Mongol-Okhotsk orogen in Western Transbaikalia: an integrated analysis

Anastasia V Arzhannikova, Elena I Demonterova, Alexander V Sizov, Marc Jolivet, Ekaterina A Mikheeva, Alexei V Ivanov, Sergey G Arzhannikov, Valentin B Khubanov

Early Cretaceous topographic evolution associated with the collapse of the Mongol-Okhotsk orogen in Western Transbaikalia: an integrated analysis

Anastasia V. Arzhannikova[a,*], Elena I. Demonterova[a], Alexander V. Sizov [a,b], Marc Jolivet[c], Ekaterina A. Mikheeva[a], Alexei V. Ivanov[a], Sergey G. Arzhannikov[a], Valentin B. Khubanov[d]

a Institute of the Earth's Crust, Russian Academy of Sciences, Siberian Branch, Irkutsk, Russia

b Geological Institute, Russian Academy of Sciences, Moscow, Russia

c Laboratoire Géosciences Rennes, CNRS-UMR6118, Université de Rennes, Rennes, France

d Geological Institute, Russian Academy of Sciences, Siberian Branch, Ulan-Ude, Russia

*Corresponding author: Arzhannikova Anastasia, arzhan@crust.irk.ru

Abstract

The Early Cretaceous topographic evolution of Transbaikalia was largely governed by the tectonic evolution of the Mongol-Okhotsk orogenic belt. The collapse of the Mongol-Okhotsk orogen triggered the formation of metamorphic core complexes and associated extensional basins, widespread throughout Transbaikalia, North Mongolia, and North China. Numerous lithofacies and biostratigraphic studies have been carried out from the sedimentary deposits of the Transbaikalia basins. However, the absence of absolute ages for the sedimentary series, as well as sediment source-to-sink analysis do not allow to accurately characterize the regional topographic evolution. We focused our study on the Gusinoozersk Basin of Western Transbaikalia, where extensive sedimentary sections of Lower Cretaceous deposits have been preserved. We provide new U/Pb (LA-ICP-MS) data on detrital zircons from sedimentary series and $^{40}Ar/^{39}Ar$ data on intruding rocks. We review the paleontological data to clarify the age of the paleogeographic events associated with the collapse of the Mongol-Okhotsk orogen, as well as to correct the age of faunal complexes in Western Transbaikalia. Our geochronological results show that the formation of the Cretaceous basins of Transbaikalia began around ~~130~~136 – ~~136~~ 130 Ma, accompanying the main episode of extension associated with the exhumation of the metamorphic core complexes. The lowest coarse-clastic formation characterizes the rapid subsidence and the predominance of

proximal sediment sources. Distal provinces also made a contribution to sedimentation indicating the rise of a positive topography characterizing the exhumation of the metamorphic core complexes. Overlying fine-grained formations indicate a significant smoothing of the topography, suggesting that from middle Aptian, Western Transbaikalia developed in a relatively calm tectonic regime. We also show that the basins of Transbaikalia were formed both in conjunction with the exhumation of metamorphic cores complexes and reactivated structural sutures. Revised data on dinosaur fauna and palynology, together with the dating of host deposits, provide insights on the Early Cretaceous paleoenvironmental evolution.

Keywords: U–Pb detrital zircons dating; sediment source-to-sink analysis; topographic evolution; Western Transbaikalia.

1. Introduction

The Mesozoic topographic and environmental evolution of Transbaikalia was largely driven by the tectonic evolution of the Mongol-Okhotsk orogenic belt (see fig. 1A for location). The belt was formed as a result of the closure of the Mongol-Okhotsk Ocean which extended between the Siberian and Mongolian-North China continents from the Late Paleozoic to the Mesozoic (Zonenshain et al., 1990; Sengör and Natal'in, 1996; Yin and Nie, 1996; Zorin, 1999). Most geodynamic models indicate a scissor-like closure of the ocean from West to East from the Permian to the Middle Jurassic (Zonenshain et al. 1990; Nie et al., 1990; Nie, 1991; Yin and Nie, 1993; 1996; Zorin et al., 1998; Davis et al., 1998; Gordienko, Kuzmin, 1999; Zorin, 1999; Darby et al., 2001; Parfenov et al., 2003; Donskaya et al., 2013; Demonterova et al., 2017; Sorokin et al., 2020; Wang et al., 2022 and others). Recent detrital zircon U-Pb data from marine and continental deposits along the Mongol-Okhotsk suture showed that the last stage of the oceanic closure was segmental. Some terranes in the central part of the ocean accreted to the Siberian continent 5–10 Ma later than in the western and eastern parts (Guo et al., 2017; Arzhannikova et al., 2022).

Although this geodynamic event has been widely studied, the topographic evolution of the Mongol-Okhotsk belt is still poorly understood. Widespread magmatism and thrusting related to subduction and collision suggested that the Mongol–Okhotsk belt formed as a plateau-like uplift (Zorin, 1999). Paleomagnetic data obtained from the Mesozoic deposits of Southeastern Siberia and Northern Mongolia indicate left-lateral strike-slip motion along the Mongol-Okhotsk suture zone during and after the collision, caused by the clockwise rotation of the Siberian continent (Parfenov et al., 2001; Metelkin et al., 2004, 2010). Yang et al. (2015) proposed that this major left-lateral strike-slip motion triggered the gravitational collapse of the thickened upper crust, leading to the development of rift basins. Detrital zircon dating and sedimentology study in the Tugnui Basin, one of the oldest Mesozoic basins of Transbaikalia (see fig. 1B for location), revealed rapid geodynamic changes from ~~the Mongol–Okhotsk~~ collision to widespread rifting at about 168 Ma (Arzhannikova et al., 2020). The paleogeographic reconstruction showed that the region was subjected to several stages of compression and extension associated with an oblique collision that took place at different times in the Middle and Upper Jurassic in different regions of Transbaikalia (Yang et al., 2016; Arzhannikova et al., 2020; 2022). The main stage of collapse of the Mongol-Okhotsk orogen is associated with the exhumation of metamorphic core complexes and the formation of rift basins, widely distributed over Transbaikalia, North Mongolia (Fig. 1B), and within the North China Craton. This widespread, highly distributed extension phase occurred between 138 Ma and 110 Ma, with a peak at 130–125 Ma (Zheng et al., 1991; Sklyarov et al., 1997; Zorin et al., 1997; Zorin, 1999; Donskaya et al., 2008; Daoudene et al., 2013, 2017; Wang et al., 2011, 2012; Ivanov et al., 2015; Zhang et al., 2019). Numerous paleontological, paleobotanical, lithofacies and biostratigraphic studies have been carried out from the sedimentary deposits of the Transbaikalia rift basins (e.g. Martinson, 1961; Kolesnikov, 1961; 1964; Otchirov, 1964; Serdobolskaya and Kozubova, 1976; Skoblo et al., 2001; Jolivet et al., 2017; Arzhannikova et al., 2018). However, the absence of absolute ages for the sedimentary series ~~does~~ did not allow to accurately characterize the regional topographic and environmental evolution.

The Cretaceous basins of Transbaikalia are nonetheless key objects to study the destruction of the Mongol-Okhotsk orogen and the corresponding paleoenvironmental evolution. These basins represent a unique record of the Cretaceous fauna, flora, climate and topography of this huge region. One of the key depressions, where extensive sedimentary sections of Cretaceous deposits have been preserved, is the Gusinoozersk Basin of Western Transbaikalia (see fig. 1B for location). Sediments of this depression are well characterized by fossil fauna. Bonebeds containing the remains of dinosaurs and other vertebrates were found in the sediments of the basal Murtoi Formation. Based on the correlation of vertebrate faunas, ~~an assumption was made about~~ the age of the sediments was estimated ranging from Late Baremian to Middle Aptian (Dmitriev, 1960; Nessov and Starkov, 1992; Averianov et al, 2003), thus from ~127 to 120 Ma (here and further the stratigraphic age is established according to www.stratigraphy.org assessed on 30th May 2022). However, later studies of the fauna suggested that deposits in the Gusinoozersk Basin could begin to accumulate earlier, starting from the Late Berriasian – Valanginian (Skoblo et al., 2001) (~140 Ma) or Late Valanginian – Barremian (Averianov et al., 2022) (~133–125 Ma). Constraining the time span in the geological record of well-preserved sediments is key to determine the paleoenvironment of the region, as well as the age and correlation of non-marine vertebrates of the Early Cretaceous in Transbaikalia, Mongolia, and China.

The objective of this study was to bracket the age of the sedimentary series of the Gusinoozersk Basin based on U/Pb (LA-ICP-MS) dating of detrital zircons and $^{40}Ar/^{39}Ar$ dating of an intruding dike. Carrying out absolute dating made it possible to clarify the age of the paleogeographic events associated with the collapse of the Mongol-Okhotsk orogen, as well as to correct the age of faunal complexes in Western Transbaikalia. This last point represents a leap forwards to biostratigraphic correlations in various regions of Central Asia.

A recent revision of the dinosaur fauna (Averianov et al., 2022) has made it possible to take a fresh look at the faunal list of the complex of fossil vertebrates in the Gusinoozersk Basin.

This~~, which~~, together with new data on age and paleogeography in this study, provides a more complete picture of the Early Cretaceous paleoenvironments of Western Transbaikalia.

2. Geological setting

The Gusinoozersk Basin is a Cretaceous NE-SW oriented depression bounded to the NW and SE by the Khambin and Monostoy ridges, respectively (Fig. 2). The Gusinoozersk Basin was first described as a typical graben (Luchitsky, 1975). According to Leonov (1983), two synsedimentary tectonic structures, the Khambin and Monostoy faults, were involved in the formation of the basin, and the onset of sedimentation was associated with the activation of the Khambin Fault (see fig. 2 for location). Later, Bulnaev (2006) established this depression as monoclinal, formed due to unilateral synsedimentary subsidence along the Monostoy Fault, which runs along the eastern flank of the basin (see fig. 2 for location). Indeed, the thickness of sediments in the depression is not constant, increasing from the western edge to the East. This indicates that the role of the Monostoy Fault in the development of the basin was predominant (Bulnaev, 2006). Below we present a description of the igneous complexes within the Khambin and Monostoy ridges, as potential sediment sources, as well as a description of the sedimentary deposits of the Gusinoozersk Basin.

2.1. Igneous complexes of the Khambin and Monostoy ridges

The Khambin Ridge, framing the Gusinoozersk Basin ~~from~~ to the west, is composed of two igneous complexes. The “Ichetui” bimodal volcanics are identified in the southern part of the ridge (see fig. 2). They are also distributed within several grabens of Western Transbaikalia and composed of trachybasalts, trachyandesites, trachydacites and trachyrhyodacites. The “Ichetui” volcanic rocks have been dated by different geochronological methods from ~~145~~ 168 to ~~168~~ 145 Ma in different places of Western Transbaikalia (Gordienko et al., 1997; Ivanov et al., 1995; Vorontsov et al., 1999; Andryushchenko et al., 2010; Arzhannikova et al., 2018). Specifically, for the Khambin Ridge, two dates were obtained with ages of ~~156~~ 159 and ~~159~~ 156 Ma

(Andryushchenko et al., 2010). The northern part of the Khambin Ridge is characterized by the Sogotinsk igneous complex (see fig. 2). Three phases of intrusion are distinguished within the complex: monzonites and quartz monzonites; syenites, quartz syenites and granosyenites; and moderately alkaline granites and leucogranites. Geochronological dating of the Sogotinsk complex by the K-Ar method provided an age range of ~~220~~271 – ~~271~~ 220 Ma for the granitoids, while the Rb-Sr method gave an age range of ~~267~~287 – ~~287~~ 267 Ma (Platov et al., 2013).

The Monostoy Ridge is mainly composed of Paleozoic meta-sedimentary series, locally intruded by the Triassic granitoids of the Malo-Kunaley complex and some Early Jurassic bimodal association (Fig. 2). The Malo-Kunaley complex is represented by peralkaline granites, granosyenites and alkaline syenites. A Late Triassic age of 2~~1~~20 – 2120~~0~~ Ma was determined for the Malo-Kunaley granites ~~by~~ from whole rock Rb-Sr and zircon U-Pb ~~methods~~analysis~~, including for the area within the northeastern part of the Monostoy Ridge~~ (Yarmolyuk et al., 2000; Litvinovsky et al., 2001; Reichow et al., 2010). The Early Jurassic bimodal association is widespread in Western Transbaikalia. Within the Monostoy Ridge it is composed of a thick (over 2000 m) bimodal volcanic sequence (trachybasalts, trachyandesite-basalts, alkaline trachydacites) with an age, determined by whole rock Rb-Sr ~~method~~analysis, of ~194 Ma (Yarmolyuk et al., 2000).

2.2. Sedimentary deposits of the Gusinoozersk Basin

The age of the sedimentary deposits is debated. The main studies were carried out in the 1950-1960s. Various complexes of freshwater mollusks characteristic of the Middle, Upper Jurassic - Lower Cretaceous were found in different parts of the sedimentary section of the basin (e.g. Martinson, 1955). According to Otchirov (1964), sedimentation began in the Gusinoozersk Basin from the Early Jurassic and continued up to the upper Lower Cretaceous. Kolesnikov (1961; 1964), based on lithological, paleontological and geological data, attributed the entire section of the Mesozoic continental deposits to the Middle Jurassic - Lower Cretaceous. Based on geological mapping, Komarov (1962) divided the stratigraphic section, from base to top, into the Sanga,

Selenga, Bain-Zurkhen and Kholboldzhin Fms. All formations were described as conformable and span from the Upper Jurassic to the Lower Cretaceous (Fig. 3).

Subsequently, a rich collection of fossil mollusks, ostracods and plants, as well as fragmentary remains of bones and teeth of dinosaurs was collected (Scoblo, 1967). This new collection, as well as geological drilling data for coal exploration, raised disagreements on the Mesozoic stratigraphy of the Gusinoozersk Basin, leading to different interpretations of the complex geological structures of this region. The scheme proposed by Scoblo (1967) differs significantly from those of Martinson (1961), Kolesnikov (1961; 1964) or Otchirov (1964). In particular, it suggests a complete absence of Middle and Upper Jurassic sediments in the Gusinoozersk Basin. Later, numerous fossil findings made it possible to expand the lists of ancient fauna and flora and significantly correct the stratigraphy and distribution of fossil organisms (Scoblo et al., 2001). In our work, we adhere to the stratigraphic scheme published in (Scoblo et al., 2001), which is best characterized by fossil fauna. The Gusinoozersk series are subdivided into four formations (bottom-up) (Fig. 3):

1. The Murtoi Fm. (K_1mr) (analogous to the lower sub-formation of the Sanga Fm. according to Komarov (1962), (Fig. 3)), is 300-450 m thick and occurs along the western side of the Gusinoozersk Basin, at the foot of the Khambin Ridge. The Murtoi Fm. rests on the underlying Middle and Upper Jurassic volcanic rocks through an erosional unconformity. It is composed of interbedded conglomerates, gravelstones, sandstones and silicic volcanic rocks. Up section, the conglomerates become finer, and the number and thickness of the sandstone interlayers increase. The sorting and rounding of pebbles increase up section, which is interpreted as a decrease in fluvial-environment deposits and a correlative increase in lacustrine deposits (Skoblo et al., 2001). In the Mogoito locality (see fig. 2) the Murtoi Fm. contains various fossil bivalves, gastropods, scattered fragmental remains of vertebrates such as palaeonisciform, acipenceriform and teleostean actinopterygians, macrobaenid turtles, lizards, various ornithischian and saurischian dinosaurs, pterosaurs, birds, and eutherian mammals (Skoblo et al., 2001; Averianov and

Skutschas, 2001; 2009; Averianov et al, 2003; Skutschas, 2008). New data on fauna and palynology from the Mogoito locality make it possible to estimate the age of the formation as Late Valanginian – Barremian (~133–125 Ma), although some of the data are quite contradictory and require further clarification (Averianov et al., 2022).

2. The Ubukun Fm. (K_1 ub) (analogous to the upper sub-formation of the Sanga Fm. according to Komarov (1962), (Fig. 3)) is 300-450 m thick and characterized by deep-lake sediment facies. Mudstones are widespread in the lower part of the formation, interbedded with siltstones and fine-grained sandstones higher-up in the section. Sandstones with small coal lenses dominate t~~T~~he upper part of the section ~~is dominated by sandstones with small coal lenses~~. The fossil fauna (mostly ostracods) is exclusively limnophilic, characteristic of a lake at least 50 m deep (Skoblo et al., 2001). Sandy facies with coal lenses in the upper part of the formation indicate shallowing of the lake and development of swamps. The biostratigraphic age of the Ubukun Fm. is determined as Hauterivian (132.6–129.4 Ma) (Skoblo et al., 2001).

3. The Selenga Fm. (K_1sl) forms the lower part of the coal-bearing strata of the Gusinoozersk series, and shows the greatest regional distribution. It is characterized by transgression-regression cycles and divided into two sub-formations. The Lower Selenga sub-formation (K_1 sl_1) corresponds to the Selenga Fm., and the Upper Selenga sub-formation (K_1 sl_2) corresponds to the Bain-Zurkhen Fm. according to Komarov (1962), (Fig. 3)). The Lower Selenga Sfm., with a total thickness of up to 600 m is represented by interbedded gravelstones, sandstones, siltstones, mudstones, and coal. The grain size is decreasing up section. The sub-formation is characterized by three ostracod horizons. The Upper Selenga Sfm., up to 500 m thick, lacks gravelstones and is dominated by finer-grained sediments. The number and thickness of coal seams in the Upper Selenga Sfm. is greater than in the Lower Selenga Sfm. Different parts of the section display carbonaceous sandy shale layers (“paper” oil shale) with fish, pelecypod and ostracod horizons. The sub-formation is also characterized by various bivalves and gastropods. The

biostratigraphic age of the entire Selenga Fm. is determined as Hauterivian-Barremian (~130 Ma) (Skoblo et al., 2001).

4. The Kholboldzhin Fm. (K_1 hl) forms the upper part of the Mesozoic deposits in the Gusinoozersk Basin (Fig. 3). It has a thickness of up to 1200 m and conformably overlies the Selenga Fm. The deposits are represented by polymictic arkose sandstones, siltstones and coal. The coal occurrence in this formation is the highest in the Gusinoozersk Basin, displaying more than 16 coal seams with a thickness of 2-4 to 53 m. The deposits contain ostracods and small bivalves. The biostratigraphic age of the Kholboldzhin Fm. is determined as Barremian-Aptian (~129.4–113 Ma) (Skoblo et al., 2001).

The Monostoy foothill series form a separate stratigraphic unit along the foot of the Monostoy Ridge and is represented by colluvions, conglomerates, breccias, gravelstones with sandstone interbeds. Drilling data show that sediments of this series are laterally correlated to fine-grained sediments in the basin, starting from the Lower Selenga Sfm. (Bulnaev, 2006; Skoblo et al., 2001) (Fig.3). This indicates that, starting from the time of the accumulation of the Lower Selenga Sfm., the Monostoy Fault played the main role in the subsidence of the basin.

The correlation of sections in several areas of the Gusinoozersk Basin is based on the complexes of fauna (especially ostracods and mollusks) and takes into account all the geological and structural data. Though numerous intra-formation erosion surfaces are exposed, the overall stratigraphy seems conformable, without major erosion lags. Biostratigraphically, this is confirmed by the succession of faunal complexes and the stability of the plant association throughout the Lower Cretaceous. The composition of the flora from individual formations and sub-formations indicates that they evolved under similar paleoenvironmental conditions (Skoblo, 1967; Skoblo et al., 2001). At the same time, the variations in sediment facies assemblages and depositional environments indicate different dynamics of basin subsidence.

The discussion above clearly shows that the age and stratigraphy of the deposits of the Gusinoozersk Basin have been debated for many decades. So far, no geochronological data have

been published on the Late Mesozoic sedimentary deposits of the basin, nor data on the evolution of sediment sources. Such data are nonetheless necessary to fully constrain the onset of formation of the Cretaceous basins in Transbaikalia and assess the morphostructural and paleoenvironmental evolution associated with the collapse of the Mongol-Okhotsk orogen.

3. Detrital zircon U-Pb (LA-ICP-MS) and igneous rocks $^{40}Ar/^{39}Ar$ dating

3.1. Sampling sites

In this study, we selected samples from three key formations of the Gusinoozersk Basin and performed U–Pb (LA-ICP-MS) analysis of detrital zircons to clarify the depositional age and determine the evolution of the source-to-sink pattern. The samples were taken from the basal Murtoi Fm., the Lower Selenga Sfm. and the Kholboldzhin Fm, covering the entire section of the Cretaceous deposits (Figs. 2, 3).

The Murtoi Fm. was sampled from an outcrop located near the Murtoi Valley (N51°09.745′; E106°13.630′) (Fig. 4, sample Gus-17-1, see Fig. 2 for location). The deposits are poorly sorted conglomerates composed of largely self-supported, moderately to well-rounded pebbles and cobbles up to 20 cm in size with a limited sandy matrix. Pebbles and cobbles consist mainly of intermediate and felsic volcanic rocks with mafic inclusions. The deposits are interpreted as proluvial-alluvial facies from braided rivers. Sample Gus-17-1, collected for U-Pb (LA-ICP-MS) detrital zircon dating was taken from the sandy matrix (Fig. 4C).

Within the studied outcrop, the conglomerates are intruded by the Murtoi dike belonging to the Khurai-Baiba dike complex (Komarov, 1962) (Fig. 4A, B). The apparent width of the dike is 9 m. The dike has a lamprophyric composition with inclusions of granitoid xenoliths (Khubanov et al., 2017). There are at least three magmatic intrusion phases, similar in composition but different in degree of crystallization (Andryushchenko et al., 2010). The dike was previously dated by Rb-Sr and K-Ar methods, which yielded ages of 117 ± 6 Ma and 122 Ma (without stated uncertainty), respectively (Litvinovsky et al., 1989). To clarify the age of the intrusion within the

studied outcrop and to establish the upper limit of the age of the sampled sedimentary unit, a sample Mur-17-1 was taken from the dike for $^{40}Ar/^{39}Ar$ analysis.

The Lower Selenga Sfm. is represented by a 90-meter thick section in the undercut of a road, NW of the basin (N51°16.491′; E106°22.275′) (Fig. 5A, see position of sample Gus-14-6 on fig. 2 for location) (Jolivet et al., 2017). The deposits are tilted westward. The lower (eastern) part of the section is represented by medium- and fine-grained light grey sandstones alternating with siltstones and rare thin coal interlayers. In the upper part of the section, the coal layers become thicker (up to 1 m) and are interbedded with siltstones and fine-grained sandstones. According to Martinson (1961) and Jolivet et al. (2017) such deposits characterize a subsiding, wet, densely-vegetated alluvial plain environment. The change from coarse-grained to fine-grained deposits with an increase in the proportion of coals indicates a retrogradation trend and a transition to a lacustrine depositional environment. The fine-grained deposits and the occurrence of coal interlayers suggest a low-relief topography in the area of the basin and a relatively low input of clastic sediments. A sample for U-Pb (LA-ICP-MS) dating of detrital zircons (Gus-14-6) was collected from a medium-grained sandstone at 61 m from the base of the logged section (Fig. 5A).

The Kholboldzhin Fm. is represented by a 70-meter thick section within the Gusinoozersk coal deposit on the eastern shore of Lake Gusinoe (N51°09.284′; E106°25.795′) (see position of sample Gus-14-1 on fig. 2 for location) (Jolivet et al., 2017). The section displays interbedded grey siltstones with plant remains, rare interlayers of fine- to medium-grained sandstone, and coal seams up to 3 m thick (Fig. 5B, C). This facies assemblage is interpreted as lacustrine to marsh depositional environments. The upper ~20 m of the section are represented mainly by fine- to medium-grained sandstones with a calcareous and clay cement, interpreted as meandering river facies (Jolivet et al., 2017). A sample for detrital zircon dating (Gus-14-1) was collected from one of the fine-to-medium-grained sandstone interbeds in the lower part of the section (23 m from bottom) (Fig. 5B).

3.2. Analytical methods and results

Sample preparation for detrital zircons analysis was carried out at the Centre for Geodynamics and Geochronology of the Institute of the Earth's Crust SB RAS. U-Pb (LA-ICP-MS) analysis was made at the Analytical center of mineralogical, geochemical and isotope studies at the Geological Institute, SB RAS. The sample preparation and analytical procedures are the same as described in Arzhannikova et al. (2020). The isotopic ratios measurement technique is described in detail in Khubanov et al. (2016) and Buyantuev et al. (2017). For this study, more than 100 zircon grains were selected from each sample, with no differentiation of size (the size of the analyzed grains varied from 60 μm to 180 μm) or morphology. U-Pb analysis was performed using an ICP-MS Element XR (ThermoFisher Scientific) coupled to an UP-213 laser (New Wave). Zircons 91500 (1065 Ma) (Wiedenbeck et al., 1995), Plešovice (337 Ma) (Slama et al., 2008), and GJ-1 (608.5 Ma) (Jackson et al., 2004) were used as external standards. The relative errors in the measurement for isotope ratios in the reference standards varied within ranges of 1%–2.3% for $^{208}Pb/^{232}Th$, 2.1%–2.6% for $^{207}Pb/^{206}Pb$, 1.1%–2.6% for $^{206}Pb/^{238}U$ and 2%–2.5% for $^{207}Pb/^{235}U$. Analytical results were processed using the GLITTER (Griffin et al., 2008) software. Only data with a concordance >90% were taken into account in the interpretation. The abundance histograms and probability density curves for each sample were plotted for $^{206}Pb/^{238}U$ ages with 2σ analytical uncertainty using the Dezirteer software (Powerman et al., 2021). Most U-Pb ages cluster below 400 Ma with few outliers showing older ages (Supplementary Data, Tables S1-S3). Therefore, we used only grains younger than 400 Ma to plot the diagrams (Fig. 6).

$^{40}Ar/^{39}Ar$ dating was carried out at the Centre for Geodynamics and Geochronology of the Institute of the Earth's Crust SB RAS using an ARGUS VI mass spectrometer coupled to a double-vacuum resistance oven. The age was calculated relative to the BERN4M standard with an age of 18.885 ± 0.097 Ma, which makes it possible to directly compare the $^{40}Ar/^{39}Ar$ and U-Pb ages (Ivanov et al., 2017).

Ninety-one concordant U-Pb zircon ages were obtained from the basal Murtoi Fm. (sample Gus-17-1). They are statistically distributed into the following populations: 150-165, 170-

185, 215-245, 250-270 and 280–300 Ma. The youngest zircon has an age of 136.1 ± 43.9 Ma (Fig. 6A; Supplementary Data, Tables S1). In the Lower Selenga Sfm. (sample Gus-14-6), 76 concordant U-Pb zircon ages were obtained. The main age population ranges 175–210 Ma, and is complemented by a minor group with ages of 225–245 Ma and few, scattered older ages. The youngest zircon present in the sample has an age of 1165.9 ± 21.7 Ma (Fig. 6B; Supplementary Data, Tables S2). In the Kholboldzhin Fm. (sample Gus-14-1), 103 concordant U-Pb zircon ages were obtained. Zircon ages are distributed into one major population at 160–230 Ma with a main peak at 191 Ma. A few older outliers are also present as in the Lower Selenga sample. The youngest zircon in the sample is 159.860 ± 21.75 Ma (Fig. 6C; Supplementary Data, Tables S3).

The $^{40}Ar/^{39}Ar$ plateau age of lamprophyre sample Mur-17-1 lamprophyres collected from the Murtoi dike is 130.0 ± 10.7 Ma (Fig. 7A). The same plateau steps form an inverse isochron with age of 130.2 ± 1.4 Ma and initial $^{40}Ar/^{36}Ar$=285 ± 63. Because the initial argon isotope composition is equal to the atmospheric value (~300), the calculation of the plateau age, which assumes the atmospheric initial value, is justified. Further, we use the plateau age because it has lower analytical uncertainty.

4. Discussion

4.1. Age and evolution of provenance of the Gusinoozersk Basin deposits

In sample Gus-17-1 from the Murtoi Fm. the age population of 150–160 165 Ma forms a significant age peak (see Fig. 6A). This age range corresponds to that of the “Ichetui” bimodal volcanics identified in the southern part of the Khambin Ridge (see Fig. 2). The main age population of 215–270 Ma corresponds in age to the Sogotinsk igneous complex identified in the ~~southern~~ northern part of the Khambin Ridge (see Fig. 2). The small age population of 280–300 Ma zircons in this sample can ~~also~~ be attributed to the Angara-Vitim batholith~~Sogotinsk complex~~. Finally, tracing the provenance of the 170–185 Ma zircons is a challenge. Almost no igneous rocks of this age have been found in Western Transbaikalia or Northern Mongolia. The only dating

of syenites in this range (178 ± 3 Ma) is situated in the Burgutuy massif of the Buteel metamorphic core complex (Mazukabzov et al., 2006) (see Fig. 1B for location).

In sample Gus-14-6 from the Lower Selenga Sfm., most zircons ages range 175–210 Ma (see fig. 6B), which can be attributed to the syenites of the Burgutuy massif, as well as to the Early Jurassic bimodal association, identified within the Monostoy Ridge. A small population with an age of 225–245 Ma matches the age of the Sogotinsk igneous complex.

In sample Gus-14-1 from the Kholboldzin Fm., almost all zircons ages are 160–230 Ma, with the maximum number occurring between 160 and 200 Ma (see ~~fig~~Fig. 6C), as in the Selenga Sfm~~. sample~~.

As ~~can be seen from~~evidenced by the histogram of the age distribution of detrital zircons from the Murtoi Fm. (Fig. 6A), the contribution of proximal sources located in the Khambin Ridge in the total amount of zircons is major. The mostly coarse-grained deposits suggest that most of the clastic material was transported by braided rivers draining the Khambin Rigde. The minor zircon population of 170–185 Ma indicates a small contribution to the sedimentation from more distant provinces located to the south in the area of the Burgutuy massif of the Buteel metamorphic core complex (see fig. 1B for location). In the overlying Selenga and Kholboldzhin Fms., zircons brought from the Khambin Ridge are practically absent, except for a small population with an age of 225–245 Ma. The main source of sediments in these formations appears to be the Monostoy Ridge and the Buteel metamorphic core complex. Syn-tectonic biotite $^{40}Ar/^{39}Ar$ age and U-Pb age of metamorphic zircon from the footwall of the Buteel metamorphic core complex indicate that its exhumation occurred between 138 Ma and 122 Ma (Mazukabzov et al., 2011), possibly exposing the 178 ± 3 Ma Burgutuy massif to erosion and providing a new sediment source for the Gusinoozersk Basin. A fine-grained lithology of the Selenga and Kholboldzhin Fms. sediments reflects a smoothing of the topography in the region, suggesting a low-intensity tectonic regime. The slow subsidence of the basin during the accumulation of the Selenga and Kholboldzhin Fms. was largely compensated by sedimentation mainly occurring in lacustrine-swamp depositional

environments with an occasional supply of coarser alluvial material associated with erosion of the sides of the basin. All formations contain a few zircons with ages of ~~290~~280 ~~–~~330 Ma that match the age of the Angara-Vitim batholith (Litvinovsky et al., 2011) located to the north of the Gusinoozersk Basin. Judging by the significant occurrence of Late Carboniferous–Early Permian detrital U–Pb zircon ages in the Lower–Middle Jurassic deposits of the Verkhoyansk margin and the Irkutsk Basin (see fig. 1B for location), the Angara–Vitim batholith region represented an uplifted area up to the beginning of the Middle Jurassic (Prokopiev et al., 2008; Demonterova et al. , 2017; Mikheeva, 2017). Until that time, the rivers draining the southern part~~region~~ of the Angara-Vitim batholith transported the clastic material southward to the Mongol-Okhotsk continental margin. The closure of the Mongol-Okhotsk Ocean in the region of Western Transbaikalia at the Early and Middle Jurassic boundary led to a reorganization of the drainage network and a change in the direction of transport of sedimentary material to the north (Arzhannikova et al., 2020). The occurrence of zircon ages corresponding to sources both north and south of Western Transbaikalia in one sample indicates recycling of sediments from previous deposits (Yang et al., 2013), as it has been observed for the Middle Jurassic deposits of the neighboring Tugnui Basin (Arzhannikova et al., 2020) (see fig. 1B for location). The pre-existing cover sequence at the Mongol-Okhotsk continental margin, containing zircons derived from the Angara-Vitim batholith, was probably still largely preserved by the Early Cretaceous and participated to the clastic material source. Although the contribution of recycled zircons to the deposits of the Gusinoozersk Basin is not significant: in the Murtoi Fm., zircons with the age of the Angara-Vitim batholith do not exceed 7%, and only single grains of this age are found in the overlying formations.

Single zircon grains with ages ranging from 330 to 400 Ma are found in samples from the Lower Selenga Sfm. and Kholboldzhin Fm. There are no zircon~~s~~s of this age in the sample from the Murtoi Fm. In the adjacent areas, volcanic rocks with such ages are not known (Wang et al., 2022); therefore, the question of the provenance of these zircons remains open.

The youngest generations of zircons in the samples were found in the Murtoi Fm. and Lower Selenga Sfm. These are composed of a very few single grains with ages ranging from ~116 to 145 Ma (Fig. 6 A, B). These ages correspond to the ages of single paleovolcanoes of trachybasaltic and trachyandesite composition in the Khambin Ridge (~~124~~127–~~127~~–124 Ma) (Andryushchenko et al., 2010), large volcanoes of alkaline rhyolites (~140 Ma), including those within the Monostoy Ridge (Yarmolyuk et al., 2000), as well as two stages of magmatic activity that occurred in Western Transbaikalia at ~~135~~143–~~143~~–135 Ma and ~~111~~131–~~131~~–111 Ma (Vorontsov et al., 2016). In their study, Vorontsov et al. (2016) pointed out that after 135 Ma, the emitted volume of volcanic rocks sharply decreased and their composition changed from bimodal associations to basaltoid ones. The predominance of mafic rocks among the Early Cretaceous volcanics (up to 90%) (Donskaya et al., 2013; Sheldrick et al., 2020) possibly explains the small amount of zircons of this age in the samples.

Thus, our geochronological studies made it possible to clarify the onset time of the formation of the Gusinoozersk Basin. While it was previously considered as Middle Jurassic to Early Cretaceous (Komarov, 1962; Martinson, 1961; Kolesnikov, 1964; Otchirov, 1964; Skoblo et al., 2001 and others), our detrital zircon U-Pb age data from the basal Murtoi Fm. indicate that the basin began to subside not earlier than ~136 million years ago (according to the age of the youngest zircon in the sample). However, this age of ~136 Ma relies on a single grain and is therefore statistically very weak. A more representative number of young zircons (3 grains) have an age of 150–153 Ma (Supplementary Data, Tables S1). However, the age of ~136 Ma is in better agreement with the biostratigraphic data. Based on freshwater mollusks, Kolesnikov (1980) estimated the age of the Murtoi Fm as Berriasian – Valanginian (~145–132.9 Ma). Based on the age of the ostracods, Scoblo et al. (2001) dated the Murtoi Fm. as Berriasian–Hauterivian (~145–129.4 Ma). The spore-pollen assemblages associated with the overlying Selenga and Kholboldzhin Fms. are characterized by Late Jurassic species, while the flora macro-remains in the same deposits are Early Cretaceous (see for example the Old Zagustay samples in Jolivet et

al., 2017). Jolivet et al. (2017) also reported the occurrence of few Cretaceous spores and pollens from the Selenga SFfm., finally suggesting that the Selenga, Bainzorkhen and Kholboldshin Fms beare of late Late Jurassic – Early Cretaceous age. Averianov et al. (2022) identified spore-pollen spectra from the Murtoi Fm., which correspond to those that were widespread across Siberia in the Lower Cretaceous. For some species (*Foraminisporis asymmetricus* and *Rouuseisporites reticulatus*), the lower stratigraphic limit corresponds to the middle of the lower Valanginian (Averianov et al., 2022), which is in good agreement with the lower age limit of the formation at ~136 Ma obtained in our work from the dating of the youngest zircon. This result suggests that the Jurassic spore-pollen spectra found in the Selenga and Kholboldzhin Fms. (Jolivet et al., 2017) were indeed recycled from the Jurassic sediments widespread in the region in the Lower Cretaceous. This would explain the discrepancy between those Jurassic spore-pollen spectra and the Lower Cretaceous age of the flora macro-remains found in the same formations. Indeed, while spores and pollens are small and resistant enough to be recycled from older sediment deposits (Stanley, 1966), macro-remains, and especially soft parts such as leafs are impossible to recycled. Since the $^{40}Ar/^{39}Ar$ dating of the Khurai-Baiba dike complex, intruding the deposits of the Murtoi Fm., showed an upper age limit of 130.0 ± 10.7 Ma for the basal formation, we suggest that the formation of the Gusinoozersk Basin started at 130136–136–130 Ma. These data are consistent with the biostratigraphic age of the Murtoi Fm.; However, our new geochronological data narrows the age interval for the beginning of sedimentation in the Gusinoozersk Basin.

4.2. Taphonomy of the Mogoito locality series and paleoenvironmental application

Based on the fossils found at the Mogoito locality, we can model the paleoenvironment at the time of the onset of sedimentation in the Gusinoozersk Basin during deposition of the Murtoi Fm. It yielded the largest number of vertebrate remains from the Gusinoozersk Basin. The Mogoito locality consists of a series of natural outcrops in shallow ravines and scours on the western bank of Lake Gusinoe exposing sediments from the Murtoi Fm. The locality represents an important source of information about the Early Cretaceous vertebrate fauna of Central Asia. The lower

alluvial-proluvial part of the Murtoi section in Mogoito locality is made of large and medium pebble conglomerates of varying rounding, gravelstone and sandstone containing rare fragmentary dinosaur fossils and remains of petrified wood. The upper alluvial part of the section is composed of alluvial cross-bedded fine-to-coarse grain sandstone alternating with a thinner layer of shale and siltstone with remains of bivalve mollusks and vertebrates. The remains of fossil bones are randomly scattered in the sediments. There are no articulated skeletal elements here, and most of the bones are highly fragmented. Some bones were carried by water currents and rounded.

~~The main part~~A major amount of ~~the~~ fossils belongs to the sauropods *Tengrisaurus starkovi* (Averianov and Skutschas, 2017; Averianov et al., 2021) belonging to the titanosaurs group. Remains of another sauropod (Sauropoda indet.) are also present but yet under study (Averianov et al., 2022). Three theropod groups have been identified from the Mogoito locality based on the isolated bones and teeth: Ornithomimosauria, Therizinosauroidea, and Dromaeosauridae (Averianov et al., 2003; Averianov and Skutschas, 2009; Averianov et al., 2022). All available remains previously identified as Ornithopoda indet. as well as a *Psittacosaurus* sp. (Averianov and Skutschas, 2009) from Mogoito locality can be attributed to a representative of the basal ornithischian clade Jeholosauridae indet. (Averianov et al., 2022). Remains of other diapsid reptiles such as lizards, pterosaurs, turtles *Kirgizemys dmitrievi* and choristoderes *Khurendukhosaurus* sp. (Skutschas and Vitenko, 2017) are also found. The fossil crocodyliforms, another reptile group found in more southern Late Mesozoic vertebrate faunas in Mongolia, have not been recorded so far from there. This is most likely due to the cool climate, which is not suitable for crocodyliforms. ~~Although~~ although it is impossible to exclude the possibility that they simply did not get into the paleontological record. Fish remains *Stichopterus* sp., Paleonisciformes indet., cf. *Irenichthys* sp. (Averianov and Skutschas, 2009) are found in alluvial deposits. The discovery of the eutherian mammal *Murtoilestes abramovi* (Averianov and Skutschas, 2001) in one of the Mogoito gullies is noteworthy.

The Mogoito locality is largely similar to the Khuren Dukh locality of Mongolia, sharing the macrobaenid turtle *Kirgizemys* and the long-necked choristodere *Khurendukhosaurus* (Averianov and Skutschas, 2000). However, abundant remains of *Psittacosaurus* at the Khuren Dukh locality (Kalandadze and Kurzanov, 1974) are not known in the Mogoito locality. Apparently, this indicates an older age of the sediments in Mogoito, because when present, *Psittacosaurus* is the most abundant dinosaur taxon in an assemblage (Averianov et al., 2022).

~~We cannot use d~~Dinosaurs cannot be used as good indicators of climate because some of them thrived and even bred in the cool temperate climate above the Arctic Circle, such as in Kakanaut locality (Chukotka, Russia). A CLAMP analysis of the Maastrichtian Kakanaut coastal paleoflora, using the Physg3brcAZ and the WorldClim2 calibration data sets, yielded a mean annual temperature of ~12 °C, the warmest month having a mean temperature of ~21 °C, and the coldest month a mean temperature of ~5 °C (Zolina et al., 2020). However, the absence of crocodyliforms and the presence of turtles and choristoderes in the Mogoito locality suggest a temperate climate, with an annual mean temperature well above freezing level but below 14°C (Markwick, 1998; Mannion et al., 2015; Amiot, 2011). The sedimentation age of the Murtoi Fm. (136–130 Ma, this study) coincides with the global cooling Weissert Event, which took place at ~133 Ma (Cavalheiro et al., 2021) during the earliest Cretaceous (Berriasian to Barremian) and can be characterized as something “in-between” a hothouse and an icehouse (Fig. 8). The average global temperature was about 17◦C (Scotese et al., 2021).

All palynological samples from the Mogoito locality revealed only rare palynomorphs including spores and pollen of terrestrial plants and freshwater microphytoplankton. The low counts in palynomorphs could be probably attributed to a taphonomic bias related to the coarse-grained character of the deposits less favorable to the accumulation of light-weighted organic material. Terrestrial palynomorphs are represented by spores of cyatheaceous/dipteridaceous, osmundaceous and schizaeaceous ferns, liverworts and lycopods, ginkgoalean pollen grains and saccate pollen of conifers. Stratigraphically important taxa include *Cicatricosisporites* sp.,

Foraminisporis asymmetricus and *Rouseisporites reticulatus*, which were widespread across Siberia in the Lower Cretaceous (Averianov et al., 2022).

Taking into account the data on ostracods and malacofauna, it can be assumed that in the Murtoi time there were no large deep lakes in the Gusinoozersk Basin. Water bodies rather consisted in a series of small open lakes and oxbow lakes. The climate was cooler than in subsequent ages although absolute temperature ranges are difficult to estimate.

The overlying Ubukun Fm. is represented by lacustrine sediments. All fossil fauna found here is limnophilic. The morphological features of ostracods in the lower part of the formation indicate a depth of the paleolake of 50-100 m. The main representatives of ostracods here are *Mongolianella subexsortis*, *M. rocodi*, *M. substriata*, *Limnocypridea grammi* (Skoblo et al. 2001). In the upper part of the formation, the faunal complex changes. Forms characteristic of small marshy lakes appear. The complex of bivalves given by (Kolesnikov, 1977) contains forms characteristic of the entire Gusinoozersk Series. Vertebrate remains have not been found here, with the exception of one aquatic macrobaenid turtle *Kirgizemys* (similar to those found in the Murtoi Fm.), which, most likely, comes from the Ubukun Fm. (Danilov et al., 2006).

The Selenga and Kholboldzhin Fms. are represented by alluvial and lacustrine-alluvial deposits. The lakes were periodically swamped, and the lacustrine-swampy sediments were later repeatedly eroded by the river. In the Selenga Fm. several marker horizons contain (from bottom to top) *Limnocypridea defense, Darwinula murtoensis, Cypridea selenginensis*, which were living in large open lakes (Skoblo et al., 2001). Marking horizons containing *Cypridea zagustaica* and Ferganoconchidae correspond to the facies of shallow stagnant bodies (Skoblo et al. 2001). According to (Vakhrameev, 1964, 1982), plant remains, such as *Cyparissidium gracile, Pterophyllum sensovianum, Coniopteris (Birisia) onychioides, Sphenopteris (Ruffordia) goeppertii, Onychiopsis elongate, Scleropteris dahurica,* belong to typical Early Cretaceous forms.

A large number of fossil remains of flora and fauna thus make it possible to reconstruct the paleoenvironmental evolution of the basin. The onset of formation of the Gusinoozersk ~~basin~~ Basin

coincided with the global cooling Weissert Event. During that period the temperate climate prevailing in Transbaikalia was favorable to the existence and reproduction of dinosaur, turtles and choristoderes, but not suitable for crocodiles. Following the small-scale open-water lakes and marshes of the Murtoi Fm., deep lakes (or a single, large lake) formed during the deposition time of the Ubukun Fm. This is supported both by the sediment facies and the rich ostracod fauna. Later, in the early Selenga Sub-fm. time, the lakes periodically decreased in size, and in the late Selenga and Kholboldzhin times, there were again a series of small swampy lakes.

4.3. Tectonic evolution of the Gusinoozersk Basin

The vast majority of detrital zircon ages in the sample of the Murtoi Fm. correspond to the age of the volcanic rocks of the Khambin Ridge bordering the basin to the West. There are almost no zircons with ages corresponding to the volcanic rocks of the Monostoy Ridge in the sample. These two results suggest that most of the topographic relief was mainly localized to the West, further suggesting that the subsidence of the Gusinoozersk Basin at the initial stage was mainly controlled by the Khambin Fault. The basin thus initially developed as a west-tilted (actual reference frame) semi-graben (Fig. 9A). By this time, the predominant deposits were proximal deposits from braided rivers draining the Khambin Ridge. In the overlying formations, represented by fine-grained material, there is only minor amount of zircons with ages matching the Khambin volcanic rocks (see Fig. 6B, C). However, these samples contain a zircon age population consistent with the age range of the Early Jurassic bimodal association, identified within the Monostoy Ridge to the East (Yarmolyuk et al., 2000) (see Fig. 2). The absence of "monostoy" zircons in the basal Murtoi Fm. and their presence in the Lower Selenga Sfm. and Kholboldzhin Fm. indicate the formation of a positive relief to the East. This suggests an activation of the Monostoy normal ~~Fault~~ fault later than the accumulation time of the Murtoi Fm. (Fig. 9B). The beginning of the subsidence of the eastern side of the basin was accompanied by simultaneous erosion of the Monostoy Ridge. This is also supported by the deposition of the coarse-grained "Monostoy" facies sediments, starting from the Lower Selenga Sfm. and higher along the section, which facially replaced coal-

bearing deposits (Skoblo et al., 2001) (see fig. 3 and 9B). Since the age of the Lower Selenga Sfm., according to the youngest zircon in the sample, is younger than ~116 Ma, it can be argued that the Monostoy Fault began to control the subsidence of the basin not earlier than this time. As in the case of the Murtoi Fm., the age is estimated from a single grain and should be taken with caution. The next young zircon has an age of ~171 Ma (Supplementary Data, Tables S2), which is obviously older than the age of the underlying Murtoi Fm. The absence of a sufficient amount of young zircons, corresponding to the age of sedimentation of the Selenga Fm., is possibly related to the mafic composition of volcanism characteristic of this time (Vorontsov et al., 2016). Thus, we rely on the only obtained date of ~116 Ma to characterize the age of the Lower Selenga Sfm., but at the same time we assume that the beginning of its deposition may be older, but not older than ~130 Ma. Since the thickness of the sediments in the basin is not constant (there is a trend towards an increase in thickness from the western to the eastern side (Bulnaev, 2006)), the Monostoy Fault most probably played a major role in the second stage of the development of the basin, which started with the beginning of the accumulation of the Selenga Fm. (Fig. 9).

The Khambin and Monostoy faults are trending obliquely to the direction of the Buteel metamorphic core complex, and their activation is not directly related to its tectonic exposure. However, the coincidence in time between the onset of active subsidence in the Gusinoozersk Basin and the exhumation of the Buteel core complex suggest that they interacted structurally during a single process of crustal extension. The Khambin Fault participates to the Dzhida-Vitim structural suture (see fig. 1B for location), which is the boundary between the regions of Late Proterozoic Baikalian and Early Paleozoic Caledonian folding (Luchitsky, 1975). The Mesozoic reactivation of the Dzhida-Vitim structure has been evidenced along its entire length. It controlled the development of the Dzhida-Vitim depression zone, represented by a chain of Mesozoic depressions, which include the Gusinoozersk Basin. Cretaceous reactivation has also been recorded along the Primorsky structural suture in the neighbouring Baikal region (see fig. 1B for location). The apatite fission track data from the Primorsky Ridge and the Olkhon block show

rapid exhumation at ~~120~~140–~~140~~ 120 Ma along the Primorsky suture (Van der Beek et al., 1996; Jolivet et al., 2009). Thus, during the Cretaceous extension, large inherited structures were activated. The basins of Transbaikalia were formed both in conjunction with the exhumation of metamorphic core complexes and mainly located along reactivated structural sutures. While middle to lower crust was exhumed to the surface within the metamorphic core complexes, the probably Cretaceous basins developed along listric faults rooting in the ductile decollement zone at depth (Wernicke, 1981; Donskaya et al., 2008; Mazukabzov et al., 2011).

The basal Murtoi Fm. is composed mainly of poorly sorted conglomerates, which we interpret as representing rapid erosion linked to the active subsidence of the depression at the initial stage and the formation of alluvial fans at the foot of the Khambin Ridge (see fig. 9A). The remote provinces located to the south of the basin also took a small part in the sedimentation during that time – the rivers started transporting clastic material from the Buteel metamorphic core complex. A modern analogue of such rivers could be the Selenga River, whose catchment includes this region. The Selenga River flows to the northeast, passing near the Gusinoozersk Basin through the Monostoy Ridge, and flows into Lake Baikal (see fig. 1B). Among the detrital zircons extracted from modern deposits of the Selenga River Delta (Ivanov et al., 2016), some display U-Pb ages corresponding to the age of syenites of the Burgutuy massif of the Buteel metamorphic core complex. We thus assume that during the accumulation of the Gusinoozersk Basin such a river flowed through the basin towards the Siberian Craton, unloading sediments transported from the southern provinces within the basin. An increase in the contribution of the southern sources up the section indicates either that they have become more eroded or that local sources have decreased.

Fine-grained sediments of the Selenga and Kholboldzhin Fms. (sandstones, siltstones, mudstones with interlayers of coals) indicate that, starting from the middle Aptian (considering that the ~–116 Ma zircon age corresponds to the lower limit of sedimentation), Western Transbaikalia evolved in a relatively calm tectonic regime, characterized by the slow subsidence in the various basins and the continuing denudation of not yet completely eroded ridges. At that

time, the Monostoy Fault still played the main role in the subsidence of the depression. This is confirmed by the deposition of the "Monostoy" conglomerates at the foot of the Monostoy Ridge, laterally replacing the fine-grained sediments of the Selenga and Kholboldzhin fms, and by the occurrence of zircons derived from volcanic rocks located in the Monostoy Ridge. The "Monostoy" facies corresponds to the proximal parts of the alluvial fans deposited by the rivers that were draining the Monostoy Ridge. In the central part of the basin, distal alluvial plain sediment facies accumulated in fluvial and lacustrine-swamp environments (see fig. 9B). The decrease in the subsidence rate of the depression and smoothing of the topography led to the overfilling of the depression with sediments, swamping and peat formation, which gave rise to the formation of coal.

Thus, by the end of the Early Cretaceous, the topography finally flattened out and the Gusinoozersk Basin ceases to be an area of sedimentation. However, it seems that the process of collapse of the Mongol-Okhotsk orogen does not end there, and the extension is shifted closer to the boundary of the Siberian Craton to the area of the Baikal rift system. For example, Van der Beek et al. (1996) and Jolivet et al. (2009) based on apatite fission track data showed the reactivation of the Primorsky and Barguzin faults of the Baikal rift system (see Fig. 1 for location) in the Late Cretaceous and interpreted it as a continuation of postorogenic extension in Transbaikalia.

5. Conclusions

Geochronological dating of sedimentary and igneous rocks of the Gusinoozersk Basin made it possible to clarify the age of paleogeographic events associated with the collapse of the Mongol-Okhotsk orogen in Western Transbaikalia. U/Pb (LA-ICP-MS) dating of detrital zircons from sedimentary deposits and $^{40}Ar/^{39}Ar$ dating of intruding volcanic rocks showed that the formation of the Cretaceous basins of Transbaikalia began around ~~130~~136 ~~–136~~ 130 Ma. It is

related to the main episode of extension associated with the exhumation of metamorphic core complexes.

The lowest coarse-clastic Murtoi Fm. characterizes the rapid subsidence of the basin and the predominance of proximal sediment sources. The provinces located south of the Gusinoozersk Basin also made a contribution to sedimentation indicating the rise of a positive topography associated with the exhumation of the metamorphic core complexes.

From the middle of the Aptian, Western Transbaikalia developed in a relatively calm tectonic regime, as evidenced by fine-grained deposits of the Selenga Sfm. and Kholboldzhin Fm. Within the general pattern of a significant smoothing of the topography, the exposed metamorphic cores complexes continued to be a source of sediments for the basins of Transbaikalia.

The subsidence of the Gusinoozersk Basin was controlled by two side faults: at an early stage, by the Khambin Fault, and at a later stage, by the Monostoy Fault. The Khambin Fault is an inherited Paleozoic structure reactivated during Cretaceous extension. The basins of Transbaikalia were formed both in conjunction with the exhumation of metamorphic cores complexes and reactivated structural sutures.

New data on dinosaur fauna and palynology, together with the dating of host deposits, made it possible to correct the age of faunal assemblages in Western Transbaikalia, which is very important for biostratigraphic correlations in various regions of Central Asia. ~~The currently known data on the palaeoenvironment of the Mogoito locality suggest that the climate was moderately warm but too cold for thermophilic crocodyliforms.~~ The onset of formation of the Gusinoozersk Basin coincided with the global cooling Weissert Event. During that period the temperate climate prevailing in Transbaikalia was favorable to the existence and reproduction of dinosaur, turtles and choristoderes, but not suitable for crocodiles. ~~The time of the onset of sedimentation in the Gusinoozersk Basin probably coincides with the Weissert Event ~133 million years ago marking a profound global cooling that punctuated the Early Cretaceous greenhouse (Cavalheiro et al., 2021; Scotese et al., 2021).~~

Acknowledgments

The study was conducted in the frame of the grant of the Ministry of Science and High Education of the Russian Federation No. 075-15-2022-1100. Detrital zircons were extracted from the bulk sample and prepared for U–Pb analysis at the Centre for Geodynamics and Geochronology of the Institute of the Earth's Crust SB RAS (Irkutsk, Russia). U–Pb isotope analysis of zircons was made at the "Analytical center of mineralogical, geochemical and isotope studies" at the Geological Institute, SB RAS (Ulan-Ude, Russia). After reduction of data in Glitter (Griffin, 2008), all calculations were conducted using Dezirteer program, specially designed for the analysis of U-Pb detrital zircon data (Powerman et al., 2021). The latter can be downloaded for free at http://dezirteer.com/ or used online at https://dezirteer.crust.irk.ru/. We thank three anonymous reviewers for their valuable comments, which greatly improved the original manuscript.

References:

Amiot, R., Wang, X., Zhou, Zh., Wang, X., Buffetaut, E., Lécuyer, C., Ding, Zh., Fluteau, F., Hibino, T., Kusuhashi, N., Mo, J., Suteethorn, V., Wang, Y., Xu, X., Zhang, F., 2011. Oxygen isotopes of East Asian dinosaurs reveal exceptionally cold Early Cretaceous climates. PNAS 108(13), 5179–5183. https://doi.org/10.1073/pnas.1011369108

Andryushchenko, S.V., Vorontsov, A.A., Yarmolyuk, V.V., Sandimirov, I.V., 2010. Evolution of Jurassic-Cretaceous magmatism in the Khambin volcanotectonic complex (Western Transbaikalia). Russ. Geol. Geophys. 51 (7), 734–749. https://doi.org/10.1016/j.rgg.2010.06.002.

Arzhannikova, A.V., Demonterova, E.I., Jolivet, M., Arzhannikov, S.G., Mikheeva, E.A., Ivanov, A.V., Khubanov, V.B., Pavlova, L.A., 2020. Late Mesozoic topographic evolution of

western Transbaikalia: Evidence for rapid geodynamic changes from the Mongol-Okhotsk collision to widespread rifting. Geosci. Front. 11, 1695-1709.

Arzhannikova, A.V., Demonterova, E.I., Jolivet, M., Mikheeva, E.A., Ivanov, A.V., Arzhannikov, S.S., Khubanov, V.B., Kamenetsky, V.S., 2022. Segmental closure of the Mongol-Okhotsk Ocean: insight from detrital geochronology in the East Transbaikalia Basin. Geosci. Front. 13(1), 101254. https://doi.org/10.1016/j.gsf.2021.101254

Arzhannikova, A.V., Frolov, A.O., Arzhannikov, S.G., Demonterova, E.I., Ivanov, A.V., Jolivet, M., Rubtsova, M.N., Dorozhko, A.L., 2018. On correlation between the Jurassic deposits of the Irkutsk basin and Southwestern Transbaikalia from the paleobotanical and geochronological data. Russ. Geol. Geophys. 59 (6), 773–791.

Averianov, A.O., Sizov A.V., Grigoriev D.V., Pestchevitskaya, E.B., Vitenko D.D., Skutschas, P.P., 2022. New data on dinosaurs from the Lower Cretaceous Murtoi Formation of Transbaikalia, Russia. Cretaceous Res. 138, 105287. https://doi.org/10.1016/j.cretres.2022.105287

Averianov, A.O., Sizov, A.V., Skutschas, P.P., 2021. Gondwanan affinities of Tengrisaurus, Early Cretaceous titanosaur from Transbaikalia, Russia (Dinosauria, Sauropoda). Cretaceous Res., 104731.

Averianov, A.O., Skutschas, P.P., 2000. A eutherian mammal from the Early Cretaceous of Russia and biostratigraphy of the Asian Early Cretaceous vertebrate assemblages. Lethaia 33, 330-340.

Averianov, A.O., Skutschas, P.P., 2001. A new genus of eutherian mammal from the Early Cretaceous of Transbaikalia, Russia. Acta Palaeontol. Pol. 46, 431-436.

Averianov, A.O., Skutschas, P.P., 2009. Additions to the Early Cretaceous dinosaur fauna of Transbaikalia, eastern Russia. Proceedings ZIN 313, 363-378.

Averianov, A.O., Skutschas, P.P., 2017. A new lithostrotian titanosaur (Dinosauria, Sauropoda) from the Early Cretaceous of Transbaikalia, Russia. Biol. Commun. 62, 6–18.

Averianov, A.O., Starkov, A. I., Skutschas, P.P., 2003. Dinosaurs from the Early Cretaceous Murtoi Formation in Buryatia, Eastern Russia. J. Vertebr. Paleontol. 23, 586–594.

Bulnaev, K.B., 2006. The formation of "Transbaikal type" depressions. Russ. J. Pac. Geol. 25, 18-30.

Buyantuev, M.D., Khubanov, V.B. and Vrublevskaya, T.T., 2017. U-Pb LA-ICP-MS dating of zircons from subvolcanics of the bimodal dyke series of the Western Transbaikalia: technique, and evidence of the Late Paleozoic extension of the crust. Geodyn. Tectonophys. 8(2), 369-384 (in Russian).

Cavalheiro, L., Wagner, T., Steinig, S., Bottini, C., Dummann, W., Esegbue, O., Gambacorta, G., Giraldo-Gómez, V., Farnsworth, A., Flögel, S., Hofmann, P., Lunt, D.J., Rethemeyer, J., Torricelli, S., Erba, E, 2021. Impact of global cooling on Early Cretaceous high pCO_2 world during the Weissert Event. Nat. Commun. 12, 5411. https://doi.org/10.1038/s41467-021-25706-0

Cramer, B.D., Jarvis, I. 2020. Chapter 11 - Carbon Isotope Stratigraphy. In: Gradstein, F.M., Ogg, J.G., Schmitz, M.D., Ogg, G.M. (Eds.), Geologic Time Scale 2020. Elsevier, pp. 309-343. https://doi.org/10.1016/B978-0-12-824360-2.00011-5.

Danilov, I.G., Averianov, A.O., Skutschas, P.P., Rezvyi, A.S., 2006. *Kirgizemys* (Testudines, 'Macrobaenidae'): New material from the Lower Cretaceous of Buryatia (Russia) and taxonomic revision. Fossil Turtle Research 1, 46–62.

Daoudene, Y., Gapais, D., Cogn_e, J.-P., Ruffet, G., 2017. Late Mesozoic continental extension in northeast Asia – relationship to plate kinematics. BSGF-Earth Sci. B. 188 (1–2), 10.

Daoudene, Y., Ruffet, G., Cocherie, A., Ledru, P., Gapais, D., 2013. Timing of exhumation of the Ereendavaa metamorphic core complex (northeastern Mongolia) – U-Pb and 40Ar/39Ar constraints. J. Asian Earth Sci. 62, 98–116.

Darby, B.J., Davis, G.A., Zheng, Y., 2001. Structural evolution of the southwestern Daqing Shan, Yinshan belt, Inner Mongolia, China. In: Hendrix, M.S., Davis, G.A. (Eds.), Paleozoic and

Mesozoic Tectonic Evolution of Central Asia: from Continental Assembly to Intracontinental Deformation. Mem. Geol. Soc. Am., Boulder, Colorado, p. 194.

Davis, G.A., Wang, C., Zheng, Y.D., Zhang, J.J., Zhang, C.H., Gehrels, G.E., 1998. The enigmatic Yinshan fold-and-thrust belt of northern China: new views on its intraplate contractional styles. Geology 26, 43–46.

Demonterova, E.I., Ivanov, A.V., Mikheeva, E.A., Arzhannikova, A.V., Frolov, A.O., Arzhannikov, S.G., Bryanskiy, N.V., Pavlova, L.A., 2017. Early to Middle Jurassic history of the southern Siberian continent (Transbaikalia) recorded in sediments of the Siberian Craton: Sm-Nd and U-Pb provenance study. BSGF-Earth Sci. B. 188 (1–2), 8.

Dmitriev, G.A., 1960. New finds of dinosaurs in Buryatia. Paleontol. J. 1, 148 (in Russian).

Donskaya, T.V., Gladkochub, D.P., Mazukabzov, A.M., Ivanov, A.V., 2013. Late Paleozoic-Mesozoic subduction-related magmatism at the southern margin of the Siberian continent and the 150 million-year history of the Mongol-Okhotsk Ocean. J. Asian Earth Sci. 62, 79–97.

Donskaya, T.V., Windley, B.F., Mazukabzov, A.M., Kr€oner, A., Sklyarov, E.V., Gladkochub, D.P., Ponomarchuk, V.A., Badarch, G., Reichow, M.K., Hegner, E., 2008. Age and evolution of late Mesozoic metamorphic core complexes in southern Siberia and northern Mongolia. J. Geol. Soc. 165, 405–421.

Gordienko, I.V., Klimuk, V.S., Ivanov, V.G., Posokhov, V.F., 1997. New data on composition and age of bimodal volcanic series of the Tugnui riftogenic depression, Trans-Baikal Region. Dokl. Earth Sci. 353 (2), 273–276.

Gordienko, I.V., Kuz'min, M.I., 1999. Geodynamics and metallogeny of the Mongolo-Transbaikalian region. Russ. Geol. Geophys. 40 (11), 1545–1562 (in Russian).

Griffin, W.L., Powell, W.J., Pearson, N.J., O'Reilly, S.Y., 2008. GLITTER: Data reduction software for laser ablation ICP–MS. In: Sylvester, P.J. (Ed.), Laser Ablation ICPMS in the Earth Sciences. MAC Short-Course series Association, 40, 307-311.

Grossman, E.L., Joachimski, M.M., 2020. Chapter 10 - Oxygen Isotope Stratigraphy. In: Gradstein, F.M., Ogg, J.G., Schmitz, M.D., Ogg, G.M. (Eds.), Geologic Time Scale 2020. Elsevier, pp. 279-307. https://doi.org/10.1016/B978-0-12-824360-2.00010-3.

Guo, Z.H., Yang, Y.T., Zyabrev, S., Hou, Z.H., 2017. Tectonostratigraphic evolution of the Mohe-Upper Amur Basin reflects the final closure of the Mongol-Okhotsk Ocean in the latest Jurassic–earliest Cretaceous. J. Asian Earth Sci. 145 (B), 494–511.

Ivanov, A.V., Demonterova, E.I., Reznitskii, L.Z., Barash, I.G., Arzhannikov, S.G., Arzhannikova, A.V., Hung, C.-H., Chung, S.-L., Iizuka, Y., 2016. Catastrophic outburst and tsunami flooding of Lake Baikal: U-Pb detrital zircon provenance study of the Paleo-Manzurka megaflood sediments. Int. Geol. Rev. 58 (14), 1818-1830. Doi:10.1080/00206814.2015.1064329.

Ivanov, A.V., Meffre, S., Thompson, J., Corfu, F., Kamenetsky, V.S., Kamenetsky, M.B., Demonterova, E.I., 2017. Timing and genesis of the Karoo-Ferrar large igneous province: New high precision U-Pb data for Tasmania confirm short duration of the major magmatic pulse. Chem. Geol. 455, 32-43.

Ivanov, A.V., Demonterova, E.I., He, H.Y., Perepelov, A.B., Travin, A.V., Lebedev, V.A., 2015. Volcanism in the Baikal rift: 40 years of active-versus-passive model discussion. Earth Sci. Rev. 148, 18-43.

Ivanov, V.G., Yarmolyuk, V.V., Smirnov, V.N., 1995. New data on the age of volcanism evidence in West-Zabaikalian Late Mesozoic-Cenozoic volcanic domain. Dokl. Earth Sci. 345 (5), 648–652 (in Russian).

Jackson, S.E., Pearson, N.J., Griffin, W.L., Belousova, E.A., 2004. The application of laser ablation-inductively coupled plasma-mass spectrometry to in situ U-Pb zircon geochronology. Chem. Geol. 211, 47–69.

Jolivet, M., Arzhannikov, S., Chauvet, A., Arzhannikova, A., Vassallo, R., Kulagina, N., Akulova, V., 2013. Accomodating large-scale intracontinental extension and compression in a single

stress-field: A key example from the Baikal Rift System. Gondwana Res. 24(3-4), 918-935. Doi: 10.1016/j.gr.2012.07.017

Jolivet, M., Arzhannikova, A., Frolov, A., Arzhannikov, S., Kulagina, N., Akulova, V., Vassallo, R., 2017. Late Jurassic – Early Cretaceous paleoenvironment evolution of the Transbaikal basins (SE Siberia): implications for the Mongol-Okhotsk orogeny. BSGF-Earth Sci. B. 188(1-2), 9. DOI: 10.1051/bsgf/2017010

——Jolivet, M., De Boisgrollier, T., Petit, C., Fournier, M., Sankov, V.A., Ringenbach, J.-C., Byzov, L., Miroshnichenko, A.I., Kovalenko, S.N. & Anisimova, S.V., 2009. How old is the Baikal Rift Zone? Insight from apatite fission track thermochronology. Tectonics 28, Tc3008.

Kalandadze, N.N., Kurzanov, S.M., 1974. Lower Cretaceous localities of terrestrial vertebrates in Mongolia. In: Kramarenko, N.N. (Ed.), Trudy Sovmestnoi Sovetsko-Mongol'skoi Paleontologicheskoi Ekspeditsii (Proceedings of the Joint Soviet–Mongolian Paleontological Expedition), 1. Nauka, Moscow, pp. 288-295 (in Russian).

Khubanov, V.B., Vrublevskaya, T.T., Tsygankov, A.A., Vladimirov, A.G., Buyantuev, M.D., Sokolova, E.N., Posokhov, V.F., Khromova, E.A., 2017. Melting conditions of granitoid xenoliths in contact with alkaline mafic magma (Gusinoozerskaya dyke, Western Transbaikalia): to the problem of the origin of ultrapotassic acid melts. Geodyn. Tectonophys. 8(2), 347–368. Doi:10.5800/GT-2017-8-2-0245.

Khubanov, V.B., Buyantuev, M.D. and Tsygankov, A.A., 2016. U-Pb dating of zircons from PZ(3)-MZ igneous complexes of Transbaikalia by sector-field mass spectrometry with laser sampling: technique and comparison with SHRIMP. Russ. Geol. Geophys. 57, 1, 190-205.

Kolesnikov, Ch.M., 1961. Stratigraphy of the Mesozoic continental deposits in the Buryat ASSR (Western Zabaikalye). Izv. Akad. Nauk SSSR Ser. Geol. 4, 59-73 (in Russian).

Kolesnikov, Ch.M., 1964. The continental Mesozoic stratigraphy of Zabaikalye. In: Stratigraphy and paleontology of the Mesozoic and Cenozoic deposits in the East Siberia and the Far East. Izd-vo Akademii Nauk SSSR, Moscow-Leningrad, pp. 5-138 (in Russian).

Kolesnikov, Ch.M., 1977. Mesozoic limnic bivalves of USSR. Synopsis of the M.S. thesis, Leningrad, 38 pp. (in Russian).

Kolesnikov, Ch.M., 1980. System, stratigraphic distribution, and zoogeography of the Mesozoic limnic bivalves of the USSR. In: Martinson, G.G. (Ed.), Limnobios of ancient lacustrine basins of Eurasia. Nauka, Leningrad, pp. 9-65 (in Russian).

Komarov, I.V. (ed.), 1962. Geological map of the USSR, scale 1:200,000. West-Zabaikalskaya series, sheet M-48-XI. VSEGEI, Leningrad (in Russian).

Leonov, Yu.G., 1983. Mesozoic tectonics and magmatism of East Asia (Correlation between time of manifestation of tectonic movements and magmatism). Nauka, Moscow, 232 pp. (in Russian).

Litvinovsky B.A., Posokhov V.F., Shadaev M.G., Shalagin V.L., 1989. New data on the age of the Early Cretaceous volcanic rocks of the Western Transbaikalia (Rb–Sr and K–Ar datings). Dokl. Akad. Nauk SSSR 308 (4), 946–949 (in Russian).

Litvinovsky, B.A., Tsygankov, A.A., Jahn, B.M., Katzir, Y., Be'eri-Shlevin, Y., 2011. Origin and evolution of overlapping calc-alkaline and alkaline magmas: The Late Palaeozoic post-collisional igneous province of Transbaikalia (Russia). Lithos 125, 845-874.

Litvinovsky, B.A., Yarmolyuk, V.V., Vorontsov, A.A., Zhuravlev, D.Z., Posokhov, B.F., Sandimirova, G.P., Kuzmin, D.V., 2001. Late Triassic stage of formation of the Mongolian–Transbaikalian alkaline-granitoid province: data of isotope geochemical studies. Russ. Geol. Geophys. 42 (3), 445–455.

Luchitsky I.V., 1975. Mesozoic tectonics of Transbaikalia. Novosibirsk: Nauka, Sib. Dept., 206 pp. (in Russian).

Mannion, P.D., Benson, R.B.J., Carrano, M.T., Tennant, J.P., Judd, J., Butler, R.J., 2015. Climate constrains the evolutionary history and biodiversity of crocodilians. Nat. Commun. 6, 8438. https://doi.org/10.1038/ncomms9438 PMID: 26399170

Markwick, P.J., 1998. Fossil crocodilians as indicators of Late Cretaceous and Cenozoic climates: implications for using palaeontological data in reconstructing palaeoclimate. Palaeogeogr. Palaeoclimatol. Palaeoecol. 137, 205-71.

Martinson, G.G., 1955. About stratigraphy of the Mesozoic continental deposits in Zabaikalye. Dokl. Akad. Nauk SSSR 105 (2), 335-338 (in Russian).

Martinson, G.G., 1961. Mesozoic and Cenozoic mollusks of the continental deposits in the Siberian platform, Zabaikalye and Mongolia. In: Tr. Baikal limnological station, issue 19. Izd-vo Akademii Nauk SSSR, Moscow-Leningrad, 332 pp. (in Russian).

Mazukabzov, A.M., Donskaya, T.V., Gladkochub, D.P., Sklyarov, E.V., Ponomarchuk, V.A. and Salnikova, E.B., 2006. Structure and age of the metamorphic core complex of the Burgutui ridge (southwestern Transbaikal region). Dokl. Earth Sci. 407, 179-183.

Mazukabzov, A.M., Sklyarov, E.V., Donskaya, T.V., Gladkochub, D.P., Fedorovsky, V.S., 2011. Metamorphic core complexes of the Transbaikalia: review. Geodyn. Tectonophys. 2(2), 95-125.

Metelkin, D.V., Vernikovsky, V.A., Kazansky, A.Y., and Wingate, M.T.D., 2010. Late Mesozoic tectonics of Central Asia based on paleomagnetic evidence. Gondwana Research 18, 400-419.

Metelkin, D. V., Gordienko, I. V. and Zhao, X., 2004. Paleomagnetism of Early Cretaceous volcanic rocks from Transbaikalia: argument for Mesozoic strike-slip motions in Central Asian structure. Russ. Geol. Geophys. 45(12), 1349-1363.

Mikheeva, E.A., 2017. Age Limits, Correlation and Source Areas of the Jurassic Sediments in the Irkutsk Basin. Synopsis of the M.S. thesis, IEC SB RAS, Irkutsk, 16 pp. (in Russian).

Nesov, L.A., Starkov, A.I., 1992. Cretaceous vertebrates of Gusinoe Lake depression in Transbaikalia and their contribution into dating and determination of sedimentation conditions. Russ. Geol. Geophys. 6 (378), 10-19 (in Russian).

Nie, S., 1991. Paleoclimatic and paleomagnetic constraints on the Paleozoic Reconstructions of south China, north China and Tarim. Tectonophysics 196, 279–308.

Nie, S., Rowley, D.B., Ziegler, A.M., 1990. Constraints on the location of Asian microcontinents in Paleo-Tethys during late Palaeozoic. In: McKerrow, W.S., Scotese, C.R. (Eds.), Palaeozoic Palaeogeography and Biogeography, vol. 12. Geol. Soc. Mem. Am., pp. 12397–12409.

Otchirov, Ts.O., 1964. Geology of the Gusino-Ivolginsk part of Buryatia. Buryat Publ. House, Ulan-Ude, 155 pp. (in Russian).

Parfenov, L.M., Berzin, N.A., Khanchuk, A.I., Badarch, G., Belichenko, V.G., Bulgatov, A.N., Dril, S.I., Kirillova, G.L., Kuzmin, M.I., Nockleberg, W., Prokopyev, A.V., Timofeev, V.F., Tomurtogoo, O., Yan, X., 2003. A model for the formation of orogenic belts in Central and NE Asia. Russ. J. Pac. Geol. 22 (6), 7–41.

Parfenov, L.M., Popeko, L.I., Tomurtogoo, O., 2001. Problems of tectonics of the Mongol-Okhotsk orogenic belt. Russian Journal of Pacific Geology 16, 797–830.

Platov V.S., Tereshchenkov V.G., Savchenko A.A., Busuek S.M., Anosova G.B., Polyansky S.A., 2013. State geological map of the Russian Federation, scale 1:200,000. Sheet M-48-V. Selenga series. Explanatory note. MF VSEGEI, Moscow.

Powerman, V.I., Buyantuev, M.D., Ivanov, A.V., 2021. A review of detrital zircon data treatment, and launch of a new tool 'Dezirteer' along with the suggested universal workflow. Chem. Geol. 583, 120437 DOI: 10.1016/j.chemgeo.2021.120437

Prokopiev, A.V., Toro, J., Miller, E.L., Gehrels, G.E., 2008. The paleo-Lena River – 200 m.y. of transcontinental zircon transport in Siberia. Geology 36 (9), 699–702.

Qi, X., and Wang, Z. (Eds.), 2008. Geological map of Central Asia and adjacent areas 1:2500000. Geological Publishing House, Beijing.

Reichow, M.K., Litvinovsky, B.A., Parrish, R.R., Saunders, A.D., 2010. Multi-stage emplacement of alkaline and peralkaline syenite-granite suites in the Mongolian-Transbaikalian Belt, Russia: Evidence from U-Pb geochronology and whole rock geochemistry. Chem. Geol. 273(1–2), 120–135. http://dx.doi.org/10.1016/j.chemgeo.2010.02.017

Scotese, C.R., Song, H., Mills, B.J.W., van der Meer, D.G., 2021. Phanerozoic paleotemperatures: The Earth's changing climate during the last 540 million years. Earth-Sci. Rev 215, 103503. https://doi.org/10.1016/j.earscirev.2021.103503.

Sengör, A.M.C., Natal'in, B.A., 1996. Paleotectonics of Asia: fragments of a synthesis. In: Yin, A., Harrison, T.M. (Eds.), The Tectonics of Asia. Cambridge Univ. Press, New York, pp. 486–640.

Serdobolskaya, I.N. and Kozubova, L.A., 1976. On the age of the Ichetui suite in West Transbaikaliya. Russ. Geol. Geophys. 7, 90-93 (in Russian).

Sheldrick, T.C., Barry, T.L., Dash, B. et al., 2020. Simultaneous and extensive removal of the East Asian lithospheric root. Sci Rep 10, 4128. https://doi.org/10.1038/s41598-020-60925-3

Sklyarov, E.V., Mazukabzov, A.M., Mel'nikov, A.I., 1997. Metamorphic Core Complexes of the Cordilleran Type. SPC UIGGM Siberian Branch of the RAS, Novosibirsk, pp. 176 (in Russian).

Skoblo, V.M., 1967. The biostratigraphic scheme of the Lower Cretaceous in the western Zabaikalye. In: The problems of geology of Pribaikalye and Zabaikalye, issue 2(4). Chita (in Russian).

Skoblo, V.M., Lyamina, N.A., Rudnev, A.F., Luzina, I.V., 2001. Continental Upper Mesozoic of Pribaikalia and Transbaikalia (Stratigraphy, Sedimentation Conditions, Correlations). Izd-vo SB RAS, Novosibirsk, pp. 332 (in Russian).

Skutschas, P.P., 2008. A choristoderan reptile from the Lower Cretaceous of Transbaikalia, Russia. Neues Jahrb. fur Geol. Palaontol. - Abh. 247, 63-78.

Skutschas, P.P., Vitenko, D.D., 2017. Early Cretaceous choristoderes (Diapsida, Choristodera) from Siberia, Russia. Cretac. Res. 77, 79-92.

Sláma, J., Košler, J., Condon, D.J., Crowley, J.L., Gerdes, A., Hanchar, J.M., Horstwood, M.S.A., Morris, G.A., Nasdala, L., Norberg, N., Schaltegger, U., Schoene, B., Tubrett, M.N., Whitehouse, M.J., 2008. Plesovice zircon - A new natural reference material for U-Pb and Hf isotopic microanalysis. Chem. Geol. 249, 1–35.

Sorokin, A.A., Zaika, V.A., Kovach, V.P., Kotov, A.B., Xu W.L., Yang, H., 2020. Timing of closure of the eastern Mongol-Okhotsk Ocean: Constraints from U-Pb and Hf isotopic data of detrital zircons from metasediments along the Dzhagdy Transect. GR. 81, 58-78.

Stanley, E.A., 1966. The problem of reworked pollen and spores in marine sediments. Marine Geology, 4(6), 397-408.

Vakhrameev, V.A., 1964. Jurassic and early Cretaceous floras of Eurasia and the paleofloristic provinces of this period. Moscow, 263 pp. (in Russian).

Vakhrameev, V.A., 1982. Division and correlation of continental deposits according to paleobotanical data // Soviet Geology 1, 58-67 (in Russian).

Van der Beek, P., Delvaux, D., Andriessen, P.A.M., and Levi, K.G., 1996. Early Cretaceous denudation related to convergent tectonics in the Baikal Region, SE Siberia // J Geol Soc, London 153, 515-523.

Vorontsov, A.A., Ivanov, V.G., Yarmolyuk, V.V., Kuzmin, M.I., Sandimirova, G.P., Smirnov, V.N., 1999. Late Mesozoic bimodal alkaline volcanic association of Western Transbaikalia and the age of its formation: geological and geochronological (Rb-Sr and K-Ar) data. Dokl. Earth Sci. 369(2), 220-224 (in Russian).

Vorontsov, A.A., Yarmolyuk, V.V., Komaritsyna, T.Yu., 2016. Late Mesozoic-Early Cenozoic rifting magmatism in the Uda sector of Western Transbaikalia. Russ. Geol. Geophys. 57(5), 723-744.

Wang, T., Guo, L., Zheng, Y., Donskaya, T., Gladkochub, D., Zeng, L., Li, J., Wang, Y., Mazukabzov, A., 2012. Timing and processes of late Mesozoic mid-lower-crustal extension in continental NE Asia and implications for the tectonic setting of the destruction of the North China Craton: mainly constrained by zircon U-Pb ages from metamorphic core complexes. Lithos 154, 315–345.

Wang, T., Tong, Y., Xiao, W.J., Guo, L., Windley, B.F., Donskaya, T., Li, S., Narantsetseg, T. and Zhang, J.J., 2022. Rollback, scissor-like closure of the Mongol-Okhotsk Ocean and formation of an orocline: magmatic migration based on a large archive of age data. Natl. Sci. Rev. 9(5), nwab210.

Wang, T., Zheng, Y.D., Zhang, J.J., Zeng, L.S., Donskaya, T.V., Guo, L., Li, J.B., 2011. Pattern and kinematic polarity of late Mesozoic extension in continental NE Asia: perspectives from metamorphic core complexes. Tectonics 30, TC6007. https://doi.org/10.1029/2011TC002896.

Wernicke, B., 1981. Low-angle normal faults in the Basin and Range Province: nappe tectonics in an extending orogen. Nature 291, 645-648

Wiedenbeck, M., Allé, P., Corfu, F., Griffin, W.L., Meier, M., Oberli, F., Van Quadt, A., Roddick, J.C., Spiegel, W., 1995. Three natural zircon standards for U-Th-Pb, Lu-Hf, trace element and REE analyses. Geostandards Newslett. 19, 1–23.

Yang, W., Jolivet, M., Dupont-Nivet, G., Guo, Z., Zhang, Z., Zhang, Z., 2013. Source to sink relations between the Tian Shan and Junggar Basin (northwest China) from Late Palaeozoic to Quaternary: evidence from detrital U-Pb zircon geochronology. Basin Res. 25, 219–240.

Yang, Y.-T., Guo, Z.-X., Song, C.-C., Li, X.-B., and He, S., 2015. A short-lived but significant Mongol–Okhotsk collisional orogeny in latest Jurassic–earliest Cretaceous. Gondwana Research 28(3), 1096-1116.

Yarmolyuk, V.V., Kozlovsky, A.M., Savatenkov, V.M., Kovach, V.P., Kozakov, I.K., Kotov, A.B., Lebedev, V.I. and Eenjin, G., 2016. Composition, Sources, and Geodynamic Nature of Giant Batholiths in Central Asia: Evidence from the Geochemistry and Nd Isotopic Characteristics of Granitoids in the Khangai Zonal Magmatic Area. Petrology 24(5), 433–461.

Yarmolyuk, V.V., Vorontsov, A.A., Ivanov, V.G., Kovalenko, V.I., Baikin, D.N. and Sandimirova, G.P. 2000. Stages of Bimodal and Alkaline Granite Magmatism in the Western Transbaikal Region: Geochronological Data on Rocks from the Tugnui Depression. Dokl. Earth Sci. 373, 811-815.

Yin, A., Nie, S., 1993. An indention model for North and South China collision and the development of the Tan Lu and Honam fault systems, eastern Asia. Tectonics 12, 801–813.

Yin, A., Nie, S., 1996. A Phanerozoic plinspatic reconstruction of China and its neighbouring regions. In: Yin, A., Harrison, T.M. (Eds.), The Tectonic Evolution of Asia. Cambridge University Press, Cambridge, pp. 442–485.

Zhang, K.-J., Yan, L.-L., and Ji, C., 2019. Switch of NE Asia from extension to contraction at the mid-Cretaceous: A tale of the Okhotsk oceanic plateau from initiation by the Perm Anomaly to extrusion in the Mongol–Okhotsk ocean? Earth-Science Reviews 198, 102941.

Zheng, Y., Wang, S., Wang, Y., 1991. An enormous thrust nappe and extensional metamorphic core complex in Sino-Mongolian boundary area. Science in China, ser. B 34, 1145–1152.

Zonenshain, L.P., Kuzmin, M.I., Natapov, L.M., 1990. Geology of the USSR: A Plate tectonic synthesis. American Geophysical Union. Geodyn. 21 https://doi.org/10.1029/GD021.

Zorin, Yu.A., 1999. Geodynamics of the western part of the Mongolia–Okhotsk collisional belt, Trans-Baikal region (Russia) and Mongolia. Tectonophysics 306, 33–56.

Zorin, Yu.A., Belichenko, V.G., Turutanov, E.Kh, Kozhevnikov, V.M., Sklyarov, E.V., Tomurtogoo, O., Khosbayar, P., Arvisbaatar, N., Byambaa, Ch, 1998. Terranes in east Mongolia and central Transbaikalia and evolution of the Okhotsk-Mongolian fold belt. Russ. Geol. Geophys. 39(1), 11–25.

Zorin, Yu.A., Sklyarov, E.V., Mazukabzov, A.M., Belichenko, V.G., 1997. Metamorphic core complexes and Early Cretaceous rifting in the Trans-Baikal region. Russ. Geol. Geophys. 38, 1574–1584.

al., 2020).

Early Cretaceous topographic evolution associated with the collapse of the Mongol-Okhotsk orogen in Western Transbaikalia: an integrated analysis

Anastasia V. Arzhannikova[a,*], Elena I. Demonterova[a], Alexander V. Sizov [a,b], Marc Jolivet[c], Ekaterina A. Mikheeva[a], Alexei V. Ivanov[a], Sergey G. Arzhannikov[a], Valentin B. Khubanov[d]

a Institute of the Earth's Crust, Russian Academy of Sciences, Siberian Branch, Irkutsk, Russia

b Geological Institute, Russian Academy of Sciences, Moscow, Russia

c Laboratoire Géosciences Rennes, CNRS-UMR6118, Université de Rennes, Rennes, France

d Geological Institute, Russian Academy of Sciences, Siberian Branch, Ulan-Ude, Russia

*Corresponding author: Arzhannikova Anastasia, arzhan@crust.irk.ru

Abstract

The Early Cretaceous topographic evolution of Transbaikalia was largely governed by the tectonic evolution of the Mongol-Okhotsk orogen. The collapse of the Mongol-Okhotsk orogen triggered the formation of metamorphic core complexes and associated extensional basins, widespread throughout Transbaikalia, North Mongolia, and North China. Numerous lithofacies and biostratigraphic studies have been carried out from the sedimentary deposits of the Transbaikalia basins. However, the absence of absolute ages for the sedimentary series, as well as sediment source-to-sink analysis do not allow to accurately characterize the regional topographic evolution. We focused our study on the Gusinoozersk Basin of Western Transbaikalia, where extensive sedimentary sections of Lower Cretaceous deposits have been preserved. We provide new U/Pb (LA-ICP-MS) data on detrital zircons from sedimentary series and $^{40}Ar/^{39}Ar$ data on intruding rocks. We review the paleontological data to clarify the age of the paleogeographic events associated with the collapse of the Mongol-Okhotsk orogen, as well as to correct the age of faunal complexes in Western Transbaikalia. Our geochronological results show that the formation of the Cretaceous basins of Transbaikalia began around 136–130 Ma, accompanying the main episode of extension associated with the exhumation of the metamorphic core complexes. The lowest coarse-clastic formation characterizes the rapid subsidence and the predominance of

proximal sediment sources. Distal provinces also made a contribution to sedimentation indicating the rise of a positive topography characterizing the exhumation of the metamorphic core complexes. Overlying fine-grained formations indicate a significant smoothing of the topography, suggesting that from middle Aptian, Western Transbaikalia developed in a relatively calm tectonic regime. We also show that the basins of Transbaikalia were formed both in conjunction with the exhumation of metamorphic cores complexes and reactivated structural sutures. Revised data on dinosaur fauna and palynology, together with the dating of host deposits, provide insights on the Early Cretaceous paleoenvironmental evolution.

Keywords: U–Pb detrital zircons dating; sediment source-to-sink analysis; topographic evolution; Western Transbaikalia.

1. Introduction

The Mesozoic topographic and environmental evolution of Transbaikalia was largely driven by the tectonic evolution of the Mongol-Okhotsk orogenic belt (see fig. 1A for location). The belt was formed as a result of the closure of the Mongol-Okhotsk Ocean which extended between the Siberian and Mongolian-North China continents from the Late Paleozoic to the Mesozoic (Zonenshain et al., 1990; Sengör and Natal'in, 1996; Yin and Nie, 1996; Zorin, 1999). Most geodynamic models indicate a scissor-like closure of the ocean from West to East from the Permian to the Middle Jurassic (Zonenshain et al. 1990; Nie et al., 1990; Nie, 1991; Yin and Nie, 1993; 1996; Zorin et al., 1998; Davis et al., 1998; Gordienko, Kuzmin, 1999; Zorin, 1999; Darby et al., 2001; Parfenov et al., 2003; Donskaya et al., 2013; Demonterova et al., 2017; Sorokin et al., 2020; Wang et al., 2022 and others). Recent detrital zircon U-Pb data from marine and continental deposits along the Mongol-Okhotsk suture showed that the last stage of oceanic closure was segmental. Some terranes in the central part of the ocean accreted to the Siberian continent 5–10 Ma later than in the western and eastern parts (Guo et al., 2017; Arzhannikova et al., 2022).

Although this geodynamic event has been widely studied, the topographic evolution of the Mongol-Okhotsk belt is still poorly understood. Widespread magmatism and thrusting related to subduction and collision suggested that the Mongol–Okhotsk belt formed as a plateau-like uplift (Zorin, 1999). Paleomagnetic data obtained from the Mesozoic deposits of Southeastern Siberia and Northern Mongolia indicate left-lateral strike-slip motion along the Mongol-Okhotsk suture zone during and after the collision, caused by the clockwise rotation of the Siberian continent (Parfenov et al., 2001; Metelkin et al., 2004, 2010). Yang et al. (2015) proposed that this major left-lateral strike-slip motion triggered the gravitational collapse of the thickened upper crust, leading to the development of rift basins. Detrital zircon dating and sedimentology study in the Tugnui Basin, one of the oldest Mesozoic basins of Transbaikalia (see fig. 1B for location), revealed rapid geodynamic changes from collision to widespread rifting at about 168 Ma (Arzhannikova et al., 2020). The paleogeographic reconstruction showed that the region was subjected to several stages of compression and extension associated with an oblique collision that took place at different times in the Middle and Upper Jurassic in different regions of Transbaikalia (Yang et al., 2016; Arzhannikova et al., 2020; 2022). The main stage of collapse of the Mongol-Okhotsk orogen is associated with the exhumation of metamorphic core complexes and the formation of rift basins, widely distributed over Transbaikalia, North Mongolia (Fig. 1B), and within the North China Craton. This widespread, highly distributed extension phase occurred between 138 Ma and 110 Ma, with a peak at 130–125 Ma (Zheng et al., 1991; Sklyarov et al., 1997; Zorin et al., 1997; Zorin, 1999; Donskaya et al., 2008; Daoudene et al., 2013, 2017; Wang et al., 2011, 2012; Ivanov et al., 2015; Zhang et al., 2019). Numerous paleontological, paleobotanical, lithofacies and biostratigraphic studies have been carried out from the sedimentary deposits of the Transbaikalia rift basins (e.g. Martinson, 1961; Kolesnikov, 1961; 1964; Otchirov, 1964; Serdobolskaya and Kozubova, 1976; Skoblo et al., 2001; Jolivet et al., 2017; Arzhannikova et al., 2018). However, the absence of absolute ages for the sedimentary series did not allow to accurately characterize the regional topographic and environmental evolution.

The Cretaceous basins of Transbaikalia are nonetheless key objects to study the destruction of the Mongol-Okhotsk orogen and the corresponding paleoenvironmental evolution. These basins represent a unique record of the Cretaceous fauna, flora, climate and topography of this huge region. One of the key depressions, where extensive sedimentary sections of Cretaceous deposits have been preserved, is the Gusinoozersk Basin of Western Transbaikalia (see fig. 1B for location). Sediments of this depression are well characterized by fossil fauna. Bonebeds containing the remains of dinosaurs and other vertebrates were found in the sediments of the basal Murtoi Formation. Based on the correlation of vertebrate faunas, the age of the sediments was estimated ranging from Late Baremian to Middle Aptian (Dmitriev, 1960; Nessov and Starkov, 1992; Averianov et al, 2003), thus from ~127 to 120 Ma (here and further the stratigraphic age is established according to www.stratigraphy.org assessed on 30th May 2022). However, later studies of the fauna suggested that deposits in the Gusinoozersk Basin could begin to accumulate earlier, starting from the Late Berriasian – Valanginian (Skoblo et al., 2001) (~140 Ma) or Late Valanginian – Barremian (Averianov et al., 2022) (~133–125 Ma). Constraining the time span in the geological record of well-preserved sediments is key to determine the paleoenvironment of the region, as well as the age and correlation of non-marine vertebrates of the Early Cretaceous in Transbaikalia, Mongolia, and China.

The objective of this study was to bracket the age of the sedimentary series of the Gusinoozersk Basin based on U/Pb (LA-ICP-MS) dating of detrital zircons and $^{40}Ar/^{39}Ar$ dating of an intruding dike. Carrying out absolute dating made it possible to clarify the age of the paleogeographic events associated with the collapse of the Mongol-Okhotsk orogen, as well as to correct the age of faunal complexes in Western Transbaikalia. This last point represents a leap forwards to biostratigraphic correlations in various regions of Central Asia.

A recent revision of the dinosaur fauna (Averianov et al., 2022) has made it possible to take a fresh look at the faunal list of the complex of fossil vertebrates in the Gusinoozersk Basin.

This, together with new data on age and paleogeography in this study, provides a more complete picture of the Early Cretaceous paleoenvironments of Western Transbaikalia.

2. Geological setting

The Gusinoozersk Basin is a Cretaceous NE-SW oriented depression bounded to the NW and SE by the Khambin and Monostoy ridges, respectively (Fig. 2). The Gusinoozersk Basin was first described as a typical graben (Luchitsky, 1975). According to Leonov (1983), two synsedimentary tectonic structures, the Khambin and Monostoy faults, were involved in the formation of the basin, and the onset of sedimentation was associated with the activation of the Khambin Fault (see fig. 2 for location). Later, Bulnaev (2006) established this depression as monoclinal, formed due to unilateral synsedimentary subsidence along the Monostoy Fault, which runs along the eastern flank of the basin (see fig. 2 for location). Indeed, the thickness of sediments in the depression is not constant, increasing from the western edge to the East. This indicates that the role of the Monostoy Fault in the development of the basin was predominant (Bulnaev, 2006). Below we present a description of the igneous complexes within the Khambin and Monostoy ridges, as potential sediment sources, as well as a description of the sedimentary deposits of the Gusinoozersk Basin.

2.1. Igneous complexes of the Khambin and Monostoy ridges

The Khambin Ridge, framing the Gusinoozersk Basin to the west, is composed of two igneous complexes. The “Ichetui” bimodal volcanics are identified in the southern part of the ridge (see fig. 2). They are also distributed within several grabens of Western Transbaikalia and composed of trachybasalts, trachyandesites, trachydacites and trachyrhyodacites. The “Ichetui” volcanic rocks have been dated by different geochronological methods from 168 to 145 Ma in different places of Western Transbaikalia (Gordienko et al., 1997; Ivanov et al., 1995; Vorontsov et al., 1999; Andryushchenko et al., 2010; Arzhannikova et al., 2018). Specifically, for the Khambin Ridge, two dates were obtained with ages of ~159 and ~156 Ma (Andryushchenko et al.,

2010). The northern part of the Khambin Ridge is characterized by the Sogotinsk igneous complex (see fig. 2). Three phases of intrusion are distinguished within the complex: monzonites and quartz monzonites; syenites, quartz syenites and granosyenites; and moderately alkaline granites and leucogranites. Geochronological dating of the Sogotinsk complex by the K-Ar method provided an age range of 271–220 Ma for the granitoids, while the Rb-Sr method gave an age range of 287–267 Ma (Platov et al., 2013).

The Monostoy Ridge is mainly composed of Paleozoic meta-sedimentary series, locally intruded by the Triassic granitoids of the Malo-Kunaley complex and some Early Jurassic bimodal association (Fig. 2). The Malo-Kunaley complex is represented by peralkaline granites, granosyenites and alkaline syenites. A Late Triassic age of 220–212 Ma was determined for the Malo-Kunaley granites from whole rock Rb-Sr and zircon U-Pb analysis (Yarmolyuk et al., 2000; Litvinovsky et al., 2001; Reichow et al., 2010). The Early Jurassic bimodal association is widespread in Western Transbaikalia. Within the Monostoy Ridge it is composed of a thick (over 2000 m) bimodal volcanic sequence (trachybasalts, trachyandesite-basalts, alkaline trachydacites) with an age, determined by whole rock Rb-Sr analysis, of ~194 Ma (Yarmolyuk et al., 2000).

2.2. Sedimentary deposits of the Gusinoozersk Basin

The age of the sedimentary deposits is debated. The main studies were carried out in the 1950-1960s. Various complexes of freshwater mollusks characteristic of the Middle, Upper Jurassic - Lower Cretaceous were found in different parts of the sedimentary section of the basin (e.g. Martinson, 1955). According to Otchirov (1964), sedimentation began in the Gusinoozersk Basin from the Early Jurassic and continued up to the upper Lower Cretaceous. Kolesnikov (1961; 1964), based on lithological, paleontological and geological data, attributed the entire section of the Mesozoic continental deposits to the Middle Jurassic - Lower Cretaceous. Based on geological mapping, Komarov (1962) divided the stratigraphic section, from base to top, into the Sanga, Selenga, Bain-Zurkhen and Kholboldzhin Fms. All formations were described as conformable and span from the Upper Jurassic to the Lower Cretaceous (Fig. 3).

Subsequently, a rich collection of fossil mollusks, ostracods and plants, as well as fragmentary remains of bones and teeth of dinosaurs was collected (Scoblo, 1967). This new collection, as well as geological drilling data for coal exploration, raised disagreements on the Mesozoic stratigraphy of the Gusinoozersk Basin, leading to different interpretations of the complex geological structures of this region. The scheme proposed by Scoblo (1967) differs significantly from those of Martinson (1961), Kolesnikov (1961; 1964) or Otchirov (1964). In particular, it suggests a complete absence of Middle and Upper Jurassic sediments in the Gusinoozersk Basin. Later, numerous fossil findings made it possible to expand the lists of ancient fauna and flora and significantly correct the stratigraphy and distribution of fossil organisms (Scoblo et al., 2001). In our work, we adhere to the stratigraphic scheme published in (Scoblo et al., 2001), which is best characterized by fossil fauna. The Gusinoozersk series are subdivided into four formations (bottom-up) (Fig. 3):

1. The Murtoi Fm. (K_1mr) (analogous to the lower sub-formation of the Sanga Fm. according to Komarov (1962), (Fig. 3)), is 300-450 m thick and occurs along the western side of the Gusinoozersk Basin, at the foot of the Khambin Ridge. The Murtoi Fm. rests on the underlying Middle and Upper Jurassic volcanic rocks through an erosional unconformity. It is composed of interbedded conglomerates, gravelstones, sandstones and silicic volcanic rocks. Up section, the conglomerates become finer, and the number and thickness of the sandstone interlayers increase. The sorting and rounding of pebbles increase up section, which is interpreted as a decrease in fluvial-environment deposits and a correlative increase in lacustrine deposits (Skoblo et al., 2001). In the Mogoito locality (see fig. 2) the Murtoi Fm. contains various fossil bivalves, gastropods, scattered fragmental remains of vertebrates such as palaeonisciform, acipenceriform and teleostean actinopterygians, macrobaenid turtles, lizards, various ornithischian and saurischian dinosaurs, pterosaurs, birds, and eutherian mammals (Skoblo et al., 2001; Averianov and Skutschas, 2001; 2009; Averianov et al, 2003; Skutschas, 2008). New data on fauna and palynology from the Mogoito locality make it possible to estimate the age of the formation as Late

Valanginian – Barremian (~133–125 Ma), although some of the data are quite contradictory and require further clarification (Averianov et al., 2022).

2. The Ubukun Fm. (K_1 ub) (analogous to the upper sub-formation of the Sanga Fm. according to Komarov (1962), (Fig. 3)) is 300-450 m thick and characterized by deep-lake sediment facies. Mudstones are widespread in the lower part of the formation, interbedded with siltstones and fine-grained sandstones higher-up in the section. Sandstones with small coal lenses dominate the upper part of the section. The fossil fauna (mostly ostracods) is exclusively limnophilic, characteristic of a lake at least 50 m deep (Skoblo et al., 2001). Sandy facies with coal lenses in the upper part of the formation indicate shallowing of the lake and development of swamps. The biostratigraphic age of the Ubukun Fm. is determined as Hauterivian (132.6–129.4 Ma) (Skoblo et al., 2001).

3. The Selenga Fm. (K_1sl) forms the lower part of the coal-bearing strata of the Gusinoozersk series, and shows the greatest regional distribution. It is characterized by transgression-regression cycles and divided into two sub-formations. The Lower Selenga sub-formation (K_1 sl_1) corresponds to the Selenga Fm., and the Upper Selenga sub-formation (K_1 sl_2) corresponds to the Bain-Zurkhen Fm. according to Komarov (1962), (Fig. 3)). The Lower Selenga Sfm., with a total thickness of up to 600 m is represented by interbedded gravelstones, sandstones, siltstones, mudstones, and coal. The grain size is decreasing up section. The sub-formation is characterized by three ostracod horizons. The Upper Selenga Sfm., up to 500 m thick, lacks gravelstones and is dominated by finer-grained sediments. The number and thickness of coal seams in the Upper Selenga Sfm. is greater than in the Lower Selenga Sfm. Different parts of the section display carbonaceous sandy shale layers (“paper” oil shale) with fish, pelecypod and ostracod horizons. The sub-formation is also characterized by various bivalves and gastropods. The biostratigraphic age of the entire Selenga Fm. is determined as Hauterivian-Barremian (~130 Ma) (Skoblo et al., 2001).

4. The Kholboldzhin Fm. (K_1 hl) forms the upper part of the Mesozoic deposits in the Gusinoozersk Basin (Fig. 3). It has a thickness of up to 1200 m and conformably overlies the Selenga Fm. The deposits are represented by polymictic arkose sandstones, siltstones and coal. The coal occurrence in this formation is the highest in the Gusinoozersk Basin, displaying more than 16 coal seams with a thickness of 2-4 to 53 m. The deposits contain ostracods and small bivalves. The biostratigraphic age of the Kholboldzhin Fm. is determined as Barremian-Aptian (~129.4–113 Ma) (Skoblo et al., 2001).

The Monostoy foothill series form a separate stratigraphic unit along the foot of the Monostoy Ridge and is represented by colluvions, conglomerates, breccias, gravelstones with sandstone interbeds. Drilling data show that sediments of this series are laterally correlated to fine-grained sediments in the basin, starting from the Lower Selenga Sfm. (Bulnaev, 2006; Skoblo et al., 2001) (Fig.3). This indicates that, starting from the time of the accumulation of the Lower Selenga Sfm., the Monostoy Fault played the main role in the subsidence of the basin.

The correlation of sections in several areas of the Gusinoozersk Basin is based on the complexes of fauna (especially ostracods and mollusks) and takes into account all the geological and structural data. Though numerous intra-formation erosion surfaces are exposed, the overall stratigraphy seems conformable, without major erosion lags. Biostratigraphically, this is confirmed by the succession of faunal complexes and the stability of the plant association throughout the Lower Cretaceous. The composition of the flora from individual formations and sub-formations indicates that they evolved under similar paleoenvironmental conditions (Skoblo, 1967; Skoblo et al., 2001). At the same time, the variations in sediment facies assemblages and depositional environments indicate different dynamics of basin subsidence.

The discussion above clearly shows that the age and stratigraphy of the deposits of the Gusinoozersk Basin have been debated for many decades. So far, no geochronological data have been published on the Late Mesozoic sedimentary deposits of the basin, nor data on the evolution of sediment sources. Such data are nonetheless necessary to fully constrain the onset of formation

of the Cretaceous basins in Transbaikalia and assess the morphostructural and paleoenvironmental evolution associated with the collapse of the Mongol-Okhotsk orogen.

3. Detrital zircon U-Pb (LA-ICP-MS) and igneous rocks $^{40}Ar/^{39}Ar$ dating

3.1. Sampling sites

In this study, we selected samples from three key formations of the Gusinoozersk Basin and performed U–Pb (LA-ICP-MS) analysis of detrital zircons to clarify the depositional age and determine the evolution of the source-to-sink pattern. The samples were taken from the basal Murtoi Fm., the Lower Selenga Sfm. and the Kholboldzhin Fm, covering the entire section of the Cretaceous deposits (Figs. 2, 3).

The Murtoi Fm. was sampled from an outcrop located near the Murtoi Valley (N51°09.745′; E106°13.630′) (Fig. 4, sample Gus-17-1, see Fig. 2 for location). The deposits are poorly sorted conglomerates composed of largely self-supported, moderately to well-rounded pebbles and cobbles up to 20 cm in size with a limited sandy matrix. Pebbles and cobbles consist mainly of intermediate and felsic volcanic rocks with mafic inclusions. The deposits are interpreted as proluvial-alluvial facies from braided rivers. Sample Gus-17-1, collected for U-Pb (LA-ICP-MS) detrital zircon dating was taken from the sandy matrix (Fig. 4C).

Within the studied outcrop, the conglomerates are intruded by the Murtoi dike belonging to the Khurai-Baiba dike complex (Komarov, 1962) (Fig. 4A, B). The apparent width of the dike is 9 m. The dike has a lamprophyric composition with inclusions of granitoid xenoliths (Khubanov et al., 2017). There are at least three magmatic intrusion phases, similar in composition but different in degree of crystallization (Andryushchenko et al., 2010). The dike was previously dated by Rb-Sr and K-Ar methods, which yielded ages of 117 ± 6 Ma and 122 Ma (without stated uncertainty), respectively (Litvinovsky et al., 1989). To clarify the age of the intrusion within the studied outcrop and to establish the upper limit of the age of the sampled sedimentary unit, a sample Mur-17-1 was taken from the dike for $^{40}Ar/^{39}Ar$ analysis.

The Lower Selenga Sfm. is represented by a 90-meter thick section in the undercut of a road, NW of the basin (N51°16.491′; E106°22.275′) (Fig. 5A, see position of sample Gus-14-6 on fig. 2 for location) (Jolivet et al., 2017). The deposits are tilted westward. The lower (eastern) part of the section is represented by medium- and fine-grained light grey sandstones alternating with siltstones and rare thin coal interlayers. In the upper part of the section, the coal layers become thicker (up to 1 m) and are interbedded with siltstones and fine-grained sandstones. According to Martinson (1961) and Jolivet et al. (2017) such deposits characterize a subsiding, wet, densely-vegetated alluvial plain environment. The change from coarse-grained to fine-grained deposits with an increase in the proportion of coals indicates a retrogradation trend and a transition to a lacustrine depositional environment. The fine-grained deposits and the occurrence of coal interlayers suggest a low-relief topography in the area of the basin and a relatively low input of clastic sediments. A sample for U-Pb (LA-ICP-MS) dating of detrital zircons (Gus-14-6) was collected from a medium-grained sandstone at 61 m from the base of the logged section (Fig. 5A).

The Kholboldzhin Fm. is represented by a 70-meter thick section within the Gusinoozersk coal deposit on the eastern shore of Lake Gusinoe (N51°09.284′; E106°25.795′) (see position of sample Gus-14-1 on fig. 2 for location) (Jolivet et al., 2017). The section displays interbedded grey siltstones with plant remains, rare interlayers of fine- to medium-grained sandstone, and coal seams up to 3 m thick (Fig. 5B, C). This facies assemblage is interpreted as lacustrine to marsh depositional environments. The upper ~20 m of the section are represented mainly by fine- to medium-grained sandstones with a calcareous and clay cement, interpreted as meandering river facies (Jolivet et al., 2017). A sample for detrital zircon dating (Gus-14-1) was collected from one of the fine-to-medium-grained sandstone interbeds in the lower part of the section (23 m from bottom) (Fig. 5B).

3.2. Analytical methods and results

Sample preparation for detrital zircons analysis was carried out at the Centre for Geodynamics and Geochronology of the Institute of the Earth's Crust SB RAS. U-Pb (LA-ICP-

MS) analysis was made at the Analytical center of mineralogical, geochemical and isotope studies at the Geological Institute, SB RAS. The sample preparation and analytical procedures are the same as described in Arzhannikova et al. (2020). The isotopic ratios measurement technique is described in detail in Khubanov et al. (2016) and Buyantuev et al. (2017). For this study, more than 100 zircon grains were selected from each sample, with no differentiation of size (the size of the analyzed grains varied from 60 μm to 180 μm) or morphology. U-Pb analysis was performed using an ICP-MS Element XR (ThermoFisher Scientific) coupled to an UP-213 laser (New Wave). Zircons 91500 (1065 Ma) (Wiedenbeck et al., 1995), Plešovice (337 Ma) (Slama et al., 2008), and GJ-1 (608.5 Ma) (Jackson et al., 2004) were used as external standards. The relative errors in the measurement for isotope ratios in the reference standards varied within ranges of 1%–2.3% for $^{208}Pb/^{232}Th$, 2.1%–2.6% for $^{207}Pb/^{206}Pb$, 1.1%–2.6% for $^{206}Pb/^{238}U$ and 2%–2.5% for $^{207}Pb/^{235}U$. Analytical results were processed using the GLITTER (Griffin et al., 2008) software. Only data with a concordance >90% were taken into account in the interpretation. The abundance histograms and probability density curves for each sample were plotted for $^{206}Pb/^{238}U$ ages with 2σ analytical uncertainty using the Dezirteer software (Powerman et al., 2021). Most U-Pb ages cluster below 400 Ma with few outliers showing older ages (Supplementary Data, Tables S1-S3). Therefore, we used only grains younger than 400 Ma to plot the diagrams (Fig. 6).

$^{40}Ar/^{39}Ar$ dating was carried out at the Centre for Geodynamics and Geochronology of the Institute of the Earth's Crust SB RAS using an ARGUS VI mass spectrometer coupled to a double-vacuum resistance oven. The age was calculated relative to the BERN4M standard with an age of 18.885 ± 0.097 Ma, which makes it possible to directly compare the $^{40}Ar/^{39}Ar$ and U-Pb ages (Ivanov et al., 2017).

Ninety-one concordant U-Pb zircon ages were obtained from the basal Murtoi Fm. (sample Gus-17-1). They are statistically distributed into the following populations: 150-165, 170-185, 215-245, 250-270 and 280–300 Ma. The youngest zircon has an age of 136 ± 4 Ma (Fig. 6A; Supplementary Data, Tables S1). In the Lower Selenga Sfm. (sample Gus-14-6), 76 concordant

U-Pb zircon ages were obtained. The main age population ranges 175–210 Ma, and is complemented by a minor group with ages of 225–245 Ma and few, scattered older ages. The youngest zircon present in the sample has an age of 116 ± 2 Ma (Fig. 6B; Supplementary Data, Tables S2). In the Kholboldzhin Fm. (sample Gus-14-1), 103 concordant U-Pb zircon ages were obtained. Zircon ages are distributed into one major population at 160–230 Ma with a main peak at 191 Ma. A few older outliers are also present as in the Lower Selenga sample. The youngest zircon in the sample is 160 ± 2 Ma (Fig. 6C; Supplementary Data, Tables S3).

The $^{40}Ar/^{39}Ar$ plateau age of lamprophyre sample Mur-17-1 lamprophyres collected from the Murtoi dike is 130 ± 1 Ma (Fig. 7A). The same plateau steps form an inverse isochron with age of 130 ± 1 Ma and initial $^{40}Ar/^{36}Ar$=285 ± 63. Because the initial argon isotope composition is equal to the atmospheric value (~300), the calculation of the plateau age, which assumes the atmospheric initial value, is justified. Further, we use the plateau age because it has lower analytical uncertainty.

4. Discussion

4.1. Age and evolution of provenance of the Gusinoozersk Basin deposits

In sample Gus-17-1 from the Murtoi Fm. the age population of 150–165 Ma forms a significant age peak (see Fig. 6A). This age range corresponds to that of the “Ichetui” bimodal volcanics identified in the southern part of the Khambin Ridge (see Fig. 2). The main age population of 215–270 Ma corresponds in age to the Sogotinsk igneous complex identified in the northern part of the Khambin Ridge (see Fig. 2). The small age population of 280–300 Ma zircons in this sample can be attributed to the Angara-Vitim batholith. Finally, tracing the provenance of the 170–185 Ma zircons is a challenge. Almost no igneous rocks of this age have been found in Western Transbaikalia or Northern Mongolia. The only dating of syenites in this range (178 ± 3 Ma) is situated in the Burgutuy massif of the Buteel metamorphic core complex (Mazukabzov et al., 2006) (see Fig. 1B for location).

In sample Gus-14-6 from the Lower Selenga Sfm., most zircons ages range 175–210 Ma (see fig. 6B), which can be attributed to the syenites of the Burgutuy massif, as well as to the Early Jurassic bimodal association, identified within the Monostoy Ridge. A small population with an age of 225–245 Ma matches the age of the Sogotinsk igneous complex.

In sample Gus-14-1 from the Kholboldzin Fm., almost all zircons ages are 160–230 Ma, with the maximum number occurring between 160 and 200 Ma (see Fig. 6C), as in the Selenga Sfm.

As evidenced by the histogram of the age distribution of detrital zircons from the Murtoi Fm. (Fig. 6A), the contribution of proximal sources located in the Khambin Ridge in the total amount of zircons is major. The mostly coarse-grained deposits suggest that most of the clastic material was transported by braided rivers draining the Khambin Rigde. The minor zircon population of 170–185 Ma indicates a small contribution to the sedimentation from more distant provinces located to the south in the area of the Burgutuy massif of the Buteel metamorphic core complex (see fig. 1B for location). In the overlying Selenga and Kholboldzhin Fms., zircons brought from the Khambin Ridge are practically absent, except for a small population with an age of 225–245 Ma. The main source of sediments in these formations appears to be the Monostoy Ridge and the Buteel metamorphic core complex. Syn-tectonic biotite $^{40}Ar/^{39}Ar$ age and U-Pb age of metamorphic zircon from the footwall of the Buteel metamorphic core complex indicate that its exhumation occurred between 138 Ma and 122 Ma (Mazukabzov et al., 2011), possibly exposing the 178 ± 3 Ma Burgutuy massif to erosion and providing a new sediment source for the Gusinoozersk Basin. A fine-grained lithology of the Selenga and Kholboldzhin Fms. sediments reflects a smoothing of the topography in the region, suggesting a low-intensity tectonic regime. The slow subsidence of the basin during the accumulation of the Selenga and Kholboldzhin Fms. was largely compensated by sedimentation mainly occurring in lacustrine-swamp depositional environments with an occasional supply of coarser alluvial material associated with erosion of the sides of the basin. All formations contain a few zircons with ages of 280–330 Ma that match the

age of the Angara-Vitim batholith (Litvinovsky et al., 2011) located to the north of the Gusinoozersk Basin. Judging by the significant occurrence of Late Carboniferous–Early Permian detrital U–Pb zircon ages in the Lower–Middle Jurassic deposits of the Verkhoyansk margin and the Irkutsk Basin (see fig. 1B for location), the Angara–Vitim batholith region represented an uplifted area up to the beginning of the Middle Jurassic (Prokopiev et al., 2008; Demonterova et al. , 2017; Mikheeva, 2017). Until that time, the rivers draining the southern part of the Angara-Vitim batholith transported the clastic material southward to the Mongol-Okhotsk continental margin. The closure of the Mongol-Okhotsk Ocean in the region of Western Transbaikalia at the Early and Middle Jurassic boundary led to a reorganization of the drainage network and a change in the direction of transport of sedimentary material to the north (Arzhannikova et al., 2020). The occurrence of zircon ages corresponding to sources both north and south of Western Transbaikalia in one sample indicates recycling of sediments from previous deposits (Yang et al., 2013), as it has been observed for the Middle Jurassic deposits of the neighboring Tugnui Basin (Arzhannikova et al., 2020) (see fig. 1B for location). The pre-existing cover sequence at the Mongol-Okhotsk continental margin, containing zircons derived from the Angara-Vitim batholith, was probably still largely preserved by the Early Cretaceous and participated to the clastic material source. Although the contribution of recycled zircons to the deposits of the Gusinoozersk Basin is not significant: in the Murtoi Fm., zircons with the age of the Angara-Vitim batholith do not exceed 7%, and only single grains of this age are found in the overlying formations.

Single zircon grains with ages ranging from 330 to 400 Ma are found in samples from the Lower Selenga Sfm. and Kholboldzhin Fm. There are no zircons of this age in the sample from the Murtoi Fm. In the adjacent areas, volcanic rocks with such ages are not known (Wang et al., 2022); therefore, the question of the provenance of these zircons remains open.

The youngest generations of zircons in the samples were found in the Murtoi Fm. and Lower Selenga Sfm. These are composed of a very few single grains with ages ranging from ~116 to 145 Ma (Fig. 6 A, B). These ages correspond to the ages of single paleovolcanoes of

trachybasaltic and trachyandesite composition in the Khambin Ridge (127–124 Ma) (Andryushchenko et al., 2010), large volcanoes of alkaline rhyolites (~140 Ma), including those within the Monostoy Ridge (Yarmolyuk et al., 2000), as well as two stages of magmatic activity that occurred in Western Transbaikalia at 143–135 Ma and 131–111 Ma (Vorontsov et al., 2016). In their study, Vorontsov et al. (2016) pointed out that after 135 Ma, the emitted volume of volcanic rocks sharply decreased and their composition changed from bimodal associations to basaltoid ones. The predominance of mafic rocks among the Early Cretaceous volcanics (up to 90%) (Donskaya et al., 2013; Sheldrick et al., 2020) possibly explains the small number of zircons of this age in the samples.

Thus, our geochronological studies made it possible to clarify the onset time of the formation of the Gusinoozersk Basin. While it was previously considered as Middle Jurassic to Early Cretaceous (Komarov, 1962; Martinson, 1961; Kolesnikov, 1964; Otchirov, 1964; Skoblo et al., 2001 and others), our detrital zircon U-Pb age data from the basal Murtoi Fm. indicate that the basin began to subside not earlier than ~136 million years ago (according to the age of the youngest zircon in the sample). However, this age of ~136 Ma relies on a single grain and is therefore statistically very weak. A more representative number of young zircons (3 grains) have an age of 150–153 Ma (Supplementary Data, Tables S1). However, the age of ~136 Ma is in better agreement with the biostratigraphic data. Based on freshwater mollusks, Kolesnikov (1980) estimated the age of the Murtoi Fm as Berriasian – Valanginian (~145–132.9 Ma). Based on the age of the ostracods, Scoblo et al. (2001) dated the Murtoi Fm. as Berriasian–Hauterivian (~145–129.4 Ma). The spore-pollen assemblages associated with the overlying Selenga and Kholboldzhin Fms. are characterized by Late Jurassic species, while the flora macro-remains in the same deposits are Early Cretaceous (see for example the Old Zagustay samples in Jolivet et al., 2017). Jolivet et al. (2017) also reported the occurrence of few Cretaceous spores and pollens from the Selenga Sfm., finally suggesting that the Selenga, Bainzorkhen and Kholboldshin Fms are of late Late Jurassic – Early Cretaceous age. Averianov et al. (2022) identified spore-pollen spectra from the

Murtoi Fm., which correspond to those that were widespread across Siberia in the Lower Cretaceous. For some species (*Foraminisporis asymmetricus* and *Rouuseisporites reticulatus*), the lower stratigraphic limit corresponds to the middle of the lower Valanginian (Averianov et al., 2022), which is in good agreement with the lower age limit of the formation at ~136 Ma obtained in our work from the dating of the youngest zircon. This result suggests that the Jurassic spore-pollen spectra found in the Selenga and Kholboldzhin Fms. (Jolivet et al., 2017) were indeed recycled from the Jurassic sediments widespread in the region in the Lower Cretaceous. This would explain the discrepancy between those Jurassic spore-pollen spectra and the Lower Cretaceous age of the flora macro-remains found in the same formations. Indeed, while spores and pollens are small and resistant enough to be recycled from older sediment deposits (Stanley, 1966), macro-remains, and especially soft parts such as leafs are impossible to recycled. Since the $^{40}Ar/^{39}Ar$ dating of the Khurai-Baiba dike complex, intruding the deposits of the Murtoi Fm., showed an upper age limit of 130 ± 1 Ma for the basal formation, we suggest that the formation of the Gusinoozersk Basin started at 136–130 Ma. These data are consistent with the biostratigraphic age of the Murtoi Fm. However, our new geochronological data narrows the age interval for the beginning of sedimentation in the Gusinoozersk Basin.

4.2. Taphonomy of the Mogoito locality series and paleoenvironmental application

Based on the fossils found at the Mogoito locality, we can model the paleoenvironment at the time of the onset of sedimentation in the Gusinoozersk Basin during deposition of the Murtoi Fm. It yielded the largest number of vertebrates remains from the Gusinoozersk Basin. The Mogoito locality consists of a series of natural outcrops in shallow ravines and scours on the western bank of Lake Gusinoe exposing sediments from the Murtoi Fm. The locality represents an important source of information about the Early Cretaceous vertebrate fauna of Central Asia. The lower alluvial-proluvial part of the Murtoi section in Mogoito locality is made of large and medium pebble conglomerates of varying rounding, gravelstone and sandstone containing rare fragmentary dinosaur fossils and remains of petrified wood. The upper alluvial part of the section

is composed of alluvial cross-bedded fine-to-coarse grain sandstone alternating with a thinner layer of shale and siltstone with remains of bivalve mollusks and vertebrates. The remains of fossil bones are randomly scattered in the sediments. There are no articulated skeletal elements here, and most of the bones are highly fragmented. Some bones were carried by water currents and rounded.

A major amount of fossils belongs to the sauropods *Tengrisaurus starkovi* (Averianov and Skutschas, 2017; Averianov et al., 2021) belonging to the titanosaurs group. Remains of another sauropod (Sauropoda indet.) are also present but yet under study (Averianov et al., 2022). Three theropod groups have been identified from the Mogoito locality based on the isolated bones and teeth: Ornithomimosauria, Therizinosauroidea, and Dromaeosauridae (Averianov et al., 2003; Averianov and Skutschas, 2009; Averianov et al., 2022). All available remains previously identified as Ornithopoda indet. as well as a *Psittacosaurus* sp. (Averianov and Skutschas, 2009) from Mogoito locality can be attributed to a representative of the basal ornithischian clade Jeholosauridae indet. (Averianov et al., 2022). Remains of other diapsid reptiles such as lizards, pterosaurs, turtles *Kirgizemys dmitrievi* and choristoderes *Khurendukhosaurus* sp. (Skutschas and Vitenko, 2017) are also found. The fossil crocodyliforms, another reptile group found in more southern Late Mesozoic vertebrate faunas in Mongolia, have not been recorded so far from there. This is most likely due to the cool climate, which is not suitable for crocodyliforms, although it is impossible to exclude the possibility that they simply did not get into the paleontological record. Fish remains *Stichopterus* sp., Paleonisciformes indet., cf. *Irenichthys* sp. (Averianov and Skutschas, 2009) are found in alluvial deposits. The discovery of the eutherian mammal *Murtoilestes abramovi* (Averianov and Skutschas, 2001) in one of the Mogoito gullies is noteworthy.

The Mogoito locality is largely similar to the Khuren Dukh locality of Mongolia, sharing the macrobaenid turtle *Kirgizemys* and the long-necked choristodere *Khurendukhosaurus* (Averianov and Skutschas, 2000). However, abundant remains of *Psittacosaurus* at the Khuren Dukh locality (Kalandadze and Kurzanov, 1974) are not known in the Mogoito locality. Apparently, this

indicates an older age of the sediments in Mogoito, because when present, *Psittacosaurus* is the most abundant dinosaur taxon in an assemblage (Averianov et al., 2022).

Dinosaurs cannot be used as good indicators of climate because some of them thrived and even bred in the cool temperate climate above the Arctic Circle, such as in Kakanaut locality (Chukotka, Russia). A CLAMP analysis of the Maastrichtian Kakanaut coastal paleoflora, using the Physg3brcAZ and the WorldClim2 calibration data sets, yielded a mean annual temperature of ~12 °C, the warmest month having a mean temperature of ~21 °C, and the coldest month a mean temperature of ~5 °C (Zolina et al., 2020). However, the absence of crocodyliforms and the presence of turtles and choristoderes in the Mogoito locality suggest a temperate climate, with an annual mean temperature well above freezing level but below 14°C (Markwick, 1998; Mannion et al., 2015; Amiot, 2011). The sedimentation age of the Murtoi Fm. (136–130 Ma, this study) coincides with the global cooling Weissert Event, which took place at ~133 Ma (Cavalheiro et al., 2021) during the earliest Cretaceous (Berriasian to Barremian) and can be characterized as something "in-between" a hothouse and an icehouse (Fig. 8). The average global temperature was about 17◦C (Scotese et al., 2021).

All palynological samples from the Mogoito locality revealed only rare palynomorphs including spores and pollen of terrestrial plants and freshwater microphytoplankton. The low counts in palynomorphs could be probably attributed to a taphonomic bias related to the coarse-grained character of the deposits less favorable to the accumulation of light-weighted organic material. Terrestrial palynomorphs are represented by spores of cyatheaceous/dipteridaceous, osmundaceous and schizaeaceous ferns, liverworts and lycopods, ginkgoalean pollen grains and saccate pollen of conifers. Stratigraphically important taxa include *Cicatricosisporites* sp., *Foraminisporis asymmetricus* and *Rouseisporites reticulatus*, which were widespread across Siberia in the Lower Cretaceous (Averianov et al., 2022).

Taking into account the data on ostracods and malacofauna, it can be assumed that in the Murtoi time there were no large deep lakes in the Gusinoozersk Basin. Water bodies rather

consisted in a series of small open lakes and oxbow lakes. The climate was cooler than in subsequent ages although absolute temperature ranges are difficult to estimate.

The overlying Ubukun Fm. is represented by lacustrine sediments. All fossil fauna found here is limnophilic. The morphological features of ostracods in the lower part of the formation indicate a depth of the paleolake of 50-100 m. The main representatives of ostracods here are *Mongolianella subexsortis*, *M. rocodi*, *M. substriata*, *Limnocypridea grammi* (Skoblo et al. 2001). In the upper part of the formation, the faunal complex changes. Forms characteristic of small marshy lakes appear. The complex of bivalves given by (Kolesnikov, 1977) contains forms characteristic of the entire Gusinoozersk Series. Vertebrate remains have not been found here, with the exception of one aquatic macrobaenid turtle *Kirgizemys* (similar to those found in the Murtoi Fm.), which, most likely, comes from the Ubukun Fm. (Danilov et al., 2006).

The Selenga and Kholboldzhin Fms. are represented by alluvial and lacustrine-alluvial deposits. The lakes were periodically swamped, and the lacustrine-swampy sediments were later repeatedly eroded by the river. In the Selenga Fm. several marker horizons contain (from bottom to top) *Limnocypridea defense, Darwinula murtoensis, Cypridea selenginensis*, which were living in large open lakes (Skoblo et al., 2001). Marking horizons containing *Cypridea zagustaica* and Ferganoconchidae correspond to the facies of shallow stagnant bodies (Skoblo et al. 2001). According to (Vakhrameev, 1964, 1982), plant remains, such as *Cyparissidium gracile, Pterophyllum sensovianum, Coniopteris (Birisia) onychioides, Sphenopteris (Ruffordia) goeppertii, Onychiopsis elongate, Scleropteris dahurica,* belong to typical Early Cretaceous forms.

A large number of fossils remains of flora and fauna thus make it possible to reconstruct the paleoenvironmental evolution of the basin. The onset of formation of the Gusinoozersk Basin coincided with the global cooling Weissert Event. During that period the temperate climate prevailing in Transbaikalia was favorable to the existence and reproduction of dinosaur, turtles and choristoderes, but not suitable for crocodiles. Following the small-scale open-water lakes and marshes of the Murtoi Fm., deep lakes (or a single, large lake) formed during the deposition time

of the Ubukun Fm. This is supported both by the sediment facies and the rich ostracod fauna. Later, in the early Selenga Sub-fm. time, the lakes periodically decreased in size, and in the late Selenga and Kholboldzhin times, there were again a series of small swampy lakes.

4.3. Tectonic evolution of the Gusinoozersk Basin

The vast majority of detrital zircon ages in the sample of the Murtoi Fm. correspond to the age of the volcanic rocks of the Khambin Ridge bordering the basin to the West. There are almost no zircons with ages corresponding to the volcanic rocks of the Monostoy Ridge in the sample. These two results suggest that most of the topographic relief was mainly localized to the West, further suggesting that the subsidence of the Gusinoozersk Basin at the initial stage was mainly controlled by the Khambin Fault. The basin thus initially developed as a west-tilted (actual reference frame) semi-graben (Fig. 9A). By this time, the predominant deposits were proximal deposits from braided rivers draining the Khambin Ridge. In the overlying formations, represented by fine-grained material, there is only minor amount of zircons with ages matching the Khambin volcanic rocks (see Fig. 6B, C). However, these samples contain a zircon age population consistent with the age range of the Early Jurassic bimodal association, identified within the Monostoy Ridge to the East (Yarmolyuk et al., 2000) (see Fig. 2). The absence of "monostoy" zircons in the basal Murtoi Fm. and their presence in the Lower Selenga Sfm. and Kholboldzhin Fm. indicate the formation of a positive relief to the East. This suggests an activation of the Monostoy normal fault later than the accumulation time of the Murtoi Fm. (Fig. 9B). The beginning of the subsidence of the eastern side of the basin was accompanied by simultaneous erosion of the Monostoy Ridge. This is also supported by the deposition of the coarse-grained "Monostoy" facies sediments, starting from the Lower Selenga Sfm. and higher along the section, which facially replaced coal-bearing deposits (Skoblo et al., 2001) (see fig. 3 and 9B). Since the age of the Lower Selenga Sfm., according to the youngest zircon in the sample, is younger than ~116 Ma, it can be argued that the Monostoy Fault began to control the subsidence of the basin not earlier than this time. As in the case of the Murtoi Fm., the age is estimated from a single grain and should be taken with caution.

The next young zircon has an age of ~171 Ma (Supplementary Data, Tables S2), which is obviously older than the age of the underlying Murtoi Fm. The absence of a sufficient amount of young zircons, corresponding to the age of sedimentation of the Selenga Fm., is possibly related to the mafic composition of volcanism characteristic of this time (Donskaya et al., 2013; Vorontsov et al., 2016; Sheldrick et al., 2020). Thus, we rely on the only obtained date of ~116 Ma to characterize the age of the Lower Selenga Sfm., but at the same time we assume that the beginning of its deposition may be older, but not older than ~130 Ma. Since the thickness of the sediments in the basin is not constant (there is a trend towards an increase in thickness from the western to the eastern side (Bulnaev, 2006)), the Monostoy Fault most probably played a major role in the second stage of the development of the basin, which started with the beginning of the accumulation of the Selenga Fm. (Fig. 9).

The Khambin and Monostoy faults are trending obliquely to the direction of the Buteel metamorphic core complex, and their activation is not directly related to its tectonic exposure. However, the coincidence in time between the onset of active subsidence in the Gusinoozersk Basin and the exhumation of the Buteel core complex suggest that they interacted structurally during a single process of crustal extension. The Khambin Fault participates to the Dzhida-Vitim structural suture (see fig. 1B for location), which is the boundary between the regions of Late Proterozoic Baikalian and Early Paleozoic Caledonian folding (Luchitsky, 1975). The Mesozoic reactivation of the Dzhida-Vitim structure has been evidenced along its entire length. It controlled the development of the Dzhida-Vitim depression zone, represented by a chain of Mesozoic depressions, which include the Gusinoozersk Basin. Cretaceous reactivation has also been recorded along the Primorsky structural suture in the neighbouring Baikal region (see fig. 1B for location). The apatite fission track data from the Primorsky Ridge and the Olkhon block show rapid exhumation at 140–120 Ma along the Primorsky suture (Van der Beek et al., 1996; Jolivet et al., 2009). Thus, during the Cretaceous extension, large inherited structures were activated. The basins of Transbaikalia were formed both in conjunction with the exhumation of metamorphic

core complexes and mainly located along reactivated structural sutures. While middle to lower crust was exhumed to the surface within the metamorphic core complexes, the probably Cretaceous basins developed along listric faults rooting in the ductile decollement zone at depth (Wernicke, 1981; Donskaya et al., 2008; Mazukabzov et al., 2011).

The basal Murtoi Fm. is composed mainly of poorly sorted conglomerates, which we interpret as representing rapid erosion linked to the active subsidence of the depression at the initial stage and the formation of alluvial fans at the foot of the Khambin Ridge (see fig. 9A). The remote provinces located to the south of the basin also took a small part in the sedimentation during that time – the rivers started transporting clastic material from the Buteel metamorphic core complex. A modern analogue of such rivers could be the Selenga River, whose catchment includes this region. The Selenga River flows to the northeast, passing near the Gusinoozersk Basin through the Monostoy Ridge, and flows into Lake Baikal (see fig. 1B). Among the detrital zircons extracted from modern deposits of the Selenga River Delta (Ivanov et al., 2016), some display U-Pb ages corresponding to the age of syenites of the Burgutuy massif of the Buteel metamorphic core complex. We thus assume that during the accumulation of the Gusinoozersk Basin such a river flowed through the basin towards the Siberian Craton, unloading sediments transported from the southern provinces within the basin. An increase in the contribution of the southern sources up the section indicates either that they have become more eroded or that local sources have decreased.

Fine-grained sediments of the Selenga and Kholboldzhin Fms. (sandstones, siltstones, mudstones with interlayers of coals) indicate that, starting from the middle Aptian (considering that the ~116 Ma zircon age corresponds to the lower limit of sedimentation), Western Transbaikalia evolved in a relatively calm tectonic regime, characterized by the slow subsidence in the various basins and the continuing denudation of not yet completely eroded ridges. At that time, the Monostoy Fault still played the main role in the subsidence of the depression. This is confirmed by the deposition of the "Monostoy" conglomerates at the foot of the Monostoy Ridge, laterally replacing the fine-grained sediments of the Selenga and Kholboldzhin fms, and by the

occurrence of zircons derived from volcanic rocks located in the Monostoy Ridge. The "Monostoy" facies corresponds to the proximal parts of the alluvial fans deposited by the rivers that were draining the Monostoy Ridge. In the central part of the basin, distal alluvial plain sediment facies accumulated in fluvial and lacustrine-swamp environments (see fig. 9B). The decrease in the subsidence rate of the depression and smoothing of the topography led to the overfilling of the depression with sediments, swamping and peat formation, which gave rise to the formation of coal.

Thus, by the end of the Early Cretaceous, the topography finally flattened out and the Gusinoozersk Basin ceases to be an area of sedimentation. However, it seems that the process of collapse of the Mongol-Okhotsk orogen does not end there, and the extension is shifted closer to the boundary of the Siberian Craton to the area of the Baikal rift system. For example, Van der Beek et al. (1996) and Jolivet et al. (2009) based on apatite fission track data showed the reactivation of the Primorsky and Barguzin faults of the Baikal rift system (see Fig. 1 for location) in the Late Cretaceous and interpreted it as a continuation of postorogenic extension in Transbaikalia.

5. Conclusions

Geochronological dating of sedimentary and igneous rocks of the Gusinoozersk Basin made it possible to clarify the age of paleogeographic events associated with the collapse of the Mongol-Okhotsk orogen in Western Transbaikalia. U/Pb (LA-ICP-MS) dating of detrital zircons from sedimentary deposits and $^{40}Ar/^{39}Ar$ dating of intruding volcanic rocks showed that the formation of the Cretaceous basins of Transbaikalia began around 136–130 Ma. It is related to the main episode of extension associated with the exhumation of metamorphic core complexes.

The lowest coarse-clastic Murtoi Fm. characterizes the rapid subsidence of the basin and the predominance of proximal sediment sources. The provinces located south of the Gusinoozersk

Basin also made a contribution to sedimentation indicating the rise of a positive topography associated with the exhumation of the metamorphic core complexes.

From the middle of the Aptian, Western Transbaikalia developed in a relatively calm tectonic regime, as evidenced by fine-grained deposits of the Selenga Sfm. and Kholboldzhin Fm. Within the general pattern of a significant smoothing of the topography, the exposed metamorphic cores complexes continued to be a source of sediments for the basins of Transbaikalia.

The subsidence of the Gusinoozersk Basin was controlled by two side faults: at an early stage, by the Khambin Fault, and at a later stage, by the Monostoy Fault. The Khambin Fault is an inherited Paleozoic structure reactivated during Cretaceous extension. The basins of Transbaikalia were formed both in conjunction with the exhumation of metamorphic cores complexes and reactivated structural sutures.

New data on dinosaur fauna and palynology, together with the dating of host deposits, made it possible to correct the age of faunal assemblages in Western Transbaikalia, which is very important for biostratigraphic correlations in various regions of Central Asia. The onset of formation of the Gusinoozersk Basin coincided with the global cooling Weissert Event. During that period the temperate climate prevailing in Transbaikalia was favorable to the existence and reproduction of dinosaur, turtles and choristoderes, but not suitable for crocodiles.

Acknowledgments

The study was conducted in the frame of the grant of the Ministry of Science and High Education of the Russian Federation No. 075-15-2022-1100. Detrital zircons were extracted from the bulk sample and prepared for U–Pb analysis at the Centre for Geodynamics and Geochronology of the Institute of the Earth's Crust SB RAS (Irkutsk, Russia). U–Pb isotope analysis of zircons was made at the "Analytical center of mineralogical, geochemical and isotope studies" at the Geological Institute, SB RAS (Ulan-Ude, Russia). After reduction of data in Glitter (Griffin, 2008), all calculations were conducted using Dezirteer program, specially designed for

the analysis of U-Pb detrital zircon data (Powerman et al., 2021). The latter can be downloaded for free at http://dezirteer.com/ or used online at https://dezirteer.crust.irk.ru/. We thank three anonymous reviewers for their valuable comments, which greatly improved the original manuscript.

References:

Amiot, R., Wang, X., Zhou, Zh., Wang, X., Buffetaut, E., Lécuyer, C., Ding, Zh., Fluteau, F., Hibino, T., Kusuhashi, N., Mo, J., Suteethorn, V., Wang, Y., Xu, X., Zhang, F., 2011. Oxygen isotopes of East Asian dinosaurs reveal exceptionally cold Early Cretaceous climates. PNAS 108(13), 5179–5183. https://doi.org/10.1073/pnas.1011369108

Andryushchenko, S.V., Vorontsov, A.A., Yarmolyuk, V.V., Sandimirov, I.V., 2010. Evolution of Jurassic-Cretaceous magmatism in the Khambin volcanotectonic complex (Western Transbaikalia). Russ. Geol. Geophys. 51 (7), 734–749. https://doi.org/10.1016/j.rgg.2010.06.002.

Arzhannikova, A.V., Demonterova, E.I., Jolivet, M., Arzhannikov, S.G., Mikheeva, E.A., Ivanov, A.V., Khubanov, V.B., Pavlova, L.A., 2020. Late Mesozoic topographic evolution of western Transbaikalia: Evidence for rapid geodynamic changes from the Mongol-Okhotsk collision to widespread rifting. Geosci. Front. 11, 1695-1709.

Arzhannikova, A.V., Demonterova, E.I., Jolivet, M., Mikheeva, E.A., Ivanov, A.V., Arzhannikov, S.S., Khubanov, V.B., Kamenetsky, V.S., 2022. Segmental closure of the Mongol-Okhotsk Ocean: insight from detrital geochronology in the East Transbaikalia Basin. Geosci. Front. 13(1), 101254. https://doi.org/10.1016/j.gsf.2021.101254

Arzhannikova, A.V., Frolov, A.O., Arzhannikov, S.G., Demonterova, E.I., Ivanov, A.V., Jolivet, M., Rubtsova, M.N., Dorozhko, A.L., 2018. On correlation between the Jurassic deposits

of the Irkutsk basin and Southwestern Transbaikalia from the paleobotanical and geochronological data. Russ. Geol. Geophys. 59 (6), 773–791.

Averianov, A.O., Sizov A.V., Grigoriev D.V., Pestchevitskaya, E.B., Vitenko D.D., Skutschas, P.P., 2022. New data on dinosaurs from the Lower Cretaceous Murtoi Formation of Transbaikalia, Russia. Cretaceous Res. 138, 105287. https://doi.org/10.1016/j.cretres.2022.105287

Averianov, A.O., Sizov, A.V., Skutschas, P.P., 2021. Gondwanan affinities of Tengrisaurus, Early Cretaceous titanosaur from Transbaikalia, Russia (Dinosauria, Sauropoda). Cretaceous Res., 104731.

Averianov, A.O., Skutschas, P.P., 2000. A eutherian mammal from the Early Cretaceous of Russia and biostratigraphy of the Asian Early Cretaceous vertebrate assemblages. Lethaia 33, 330-340.

Averianov, A.O., Skutschas, P.P., 2001. A new genus of eutherian mammal from the Early Cretaceous of Transbaikalia, Russia. Acta Palaeontol. Pol. 46, 431-436.

Averianov, A.O., Skutschas, P.P., 2009. Additions to the Early Cretaceous dinosaur fauna of Transbaikalia, eastern Russia. Proceedings ZIN 313, 363-378.

Averianov, A.O., Skutschas, P.P., 2017. A new lithostrotian titanosaur (Dinosauria, Sauropoda) from the Early Cretaceous of Transbaikalia, Russia. Biol. Commun. 62, 6–18.

Averianov, A.O., Starkov, A. I., Skutschas, P.P., 2003. Dinosaurs from the Early Cretaceous Murtoi Formation in Buryatia, Eastern Russia. J. Vertebr. Paleontol. 23, 586–594.

Bulnaev, K.B., 2006. The formation of "Transbaikal type" depressions. Russ. J. Pac. Geol. 25, 18-30.

Buyantuev, M.D., Khubanov, V.B. and Vrublevskaya, T.T., 2017. U-Pb LA-ICP-MS dating of zircons from subvolcanics of the bimodal dyke series of the Western Transbaikalia: technique, and evidence of the Late Paleozoic extension of the crust. Geodyn. Tectonophys. 8(2), 369-384 (in Russian).

Cavalheiro, L., Wagner, T., Steinig, S., Bottini, C., Dummann, W., Esegbue, O., Gambacorta, G., Giraldo-Gómez, V., Farnsworth, A., Flögel, S., Hofmann, P., Lunt, D.J., Rethemeyer, J., Torricelli, S., Erba, E, 2021. Impact of global cooling on Early Cretaceous high pCO_2 world during the Weissert Event. Nat. Commun. 12, 5411. https://doi.org/10.1038/s41467-021-25706-0

Cramer, B.D., Jarvis, I. 2020. Chapter 11 - Carbon Isotope Stratigraphy. In: Gradstein, F.M., Ogg, J.G., Schmitz, M.D., Ogg, G.M. (Eds.), Geologic Time Scale 2020. Elsevier, pp. 309-343. https://doi.org/10.1016/B978-0-12-824360-2.00011-5.

Danilov, I.G., Averianov, A.O., Skutschas, P.P., Rezvyi, A.S., 2006. *Kirgizemys* (Testudines, 'Macrobaenidae'): New material from the Lower Cretaceous of Buryatia (Russia) and taxonomic revision. Fossil Turtle Research 1, 46–62.

Daoudene, Y., Gapais, D., Cogn_e, J.-P., Ruffet, G., 2017. Late Mesozoic continental extension in northeast Asia – relationship to plate kinematics. BSGF-Earth Sci. B. 188 (1–2), 10.

Daoudene, Y., Ruffet, G., Cocherie, A., Ledru, P., Gapais, D., 2013. Timing of exhumation of the Ereendavaa metamorphic core complex (northeastern Mongolia) – U-Pb and 40Ar/39Ar constraints. J. Asian Earth Sci. 62, 98–116.

Darby, B.J., Davis, G.A., Zheng, Y., 2001. Structural evolution of the southwestern Daqing Shan, Yinshan belt, Inner Mongolia, China. In: Hendrix, M.S., Davis, G.A. (Eds.), Paleozoic and Mesozoic Tectonic Evolution of Central Asia: from Continental Assembly to Intracontinental Deformation. Mem. Geol. Soc. Am., Boulder, Colorado, p. 194.

Davis, G.A., Wang, C., Zheng, Y.D., Zhang, J.J., Zhang, C.H., Gehrels, G.E., 1998. The enigmatic Yinshan fold-and-thrust belt of northern China: new views on its intraplate contractional styles. Geology 26, 43–46.

Demonterova, E.I., Ivanov, A.V., Mikheeva, E.A., Arzhannikova, A.V., Frolov, A.O., Arzhannikov, S.G., Bryanskiy, N.V., Pavlova, L.A., 2017. Early to Middle Jurassic history

of the southern Siberian continent (Transbaikalia) recorded in sediments of the Siberian Craton: Sm-Nd and U-Pb provenance study. BSGF-Earth Sci. B. 188 (1–2), 8.

Dmitriev, G.A., 1960. New finds of dinosaurs in Buryatia. Paleontol. J. 1, 148 (in Russian).

Donskaya, T.V., Gladkochub, D.P., Mazukabzov, A.M., Ivanov, A.V., 2013. Late Paleozoic-Mesozoic subduction-related magmatism at the southern margin of the Siberian continent and the 150 million-year history of the Mongol-Okhotsk Ocean. J. Asian Earth Sci. 62, 79–97.

Donskaya, T.V., Windley, B.F., Mazukabzov, A.M., Kr€oner, A., Sklyarov, E.V., Gladkochub, D.P., Ponomarchuk, V.A., Badarch, G., Reichow, M.K., Hegner, E., 2008. Age and evolution of late Mesozoic metamorphic core complexes in southern Siberia and northern Mongolia. J. Geol. Soc. 165, 405–421.

Gordienko, I.V., Klimuk, V.S., Ivanov, V.G., Posokhov, V.F., 1997. New data on composition and age of bimodal volcanic series of the Tugnui riftogenic depression, Trans-Baikal Region. Dokl. Earth Sci. 353 (2), 273–276.

Gordienko, I.V., Kuz'min, M.I., 1999. Geodynamics and metallogeny of the Mongolo-Transbaikalian region. Russ. Geol. Geophys. 40 (11), 1545–1562 (in Russian).

Griffin, W.L., Powell, W.J., Pearson, N.J., O'Reilly, S.Y., 2008. GLITTER: Data reduction software for laser ablation ICP–MS. In: Sylvester, P.J. (Ed.), Laser Ablation ICPMS in the Earth Sciences. MAC Short-Course series Association, 40, 307-311.

Grossman, E.L., Joachimski, M.M., 2020. Chapter 10 - Oxygen Isotope Stratigraphy. In: Gradstein, F.M., Ogg, J.G., Schmitz, M.D., Ogg, G.M. (Eds.), Geologic Time Scale 2020. Elsevier, pp. 279-307. https://doi.org/10.1016/B978-0-12-824360-2.00010-3.

Guo, Z.H., Yang, Y.T., Zyabrev, S., Hou, Z.H., 2017. Tectonostratigraphic evolution of the Mohe-Upper Amur Basin reflects the final closure of the Mongol-Okhotsk Ocean in the latest Jurassic–earliest Cretaceous. J. Asian Earth Sci. 145 (B), 494–511.

Ivanov, A.V., Demonterova, E.I., Reznitskii, L.Z., Barash, I.G., Arzhannikov, S.G., Arzhannikova, A.V., Hung, C.-H., Chung, S.-L., Iizuka, Y., 2016. Catastrophic outburst and tsunami flooding of Lake Baikal: U-Pb detrital zircon provenance study of the Paleo-Manzurka megaflood sediments. Int. Geol. Rev. 58 (14), 1818-1830. Doi:10.1080/00206814.2015.1064329.

Ivanov, A.V., Meffre, S., Thompson, J., Corfu, F., Kamenetsky, V.S., Kamenetsky, M.B., Demonterova, E.I., 2017. Timing and genesis of the Karoo-Ferrar large igneous province: New high precision U-Pb data for Tasmania confirm short duration of the major magmatic pulse. Chem. Geol. 455, 32-43.

Ivanov, A.V., Demonterova, E.I., He, H.Y., Perepelov, A.B., Travin, A.V., Lebedev, V.A., 2015. Volcanism in the Baikal rift: 40 years of active-versus-passive model discussion. Earth Sci. Rev. 148, 18-43.

Ivanov, V.G., Yarmolyuk, V.V., Smirnov, V.N., 1995. New data on the age of volcanism evidence in West-Zabaikalian Late Mesozoic-Cenozoic volcanic domain. Dokl. Earth Sci. 345 (5), 648–652 (in Russian).

Jackson, S.E., Pearson, N.J., Griffin, W.L., Belousova, E.A., 2004. The application of laser ablation-inductively coupled plasma-mass spectrometry to in situ U-Pb zircon geochronology. Chem. Geol. 211, 47–69.

Jolivet, M., Arzhannikov, S., Chauvet, A., Arzhannikova, A., Vassallo, R., Kulagina, N., Akulova, V., 2013. Accomodating large-scale intracontinental extension and compression in a single stress-field: A key example from the Baikal Rift System. Gondwana Res. 24(3-4), 918-935. Doi: 10.1016/j.gr.2012.07.017

Jolivet, M., Arzhannikova, A., Frolov, A., Arzhannikov, S., Kulagina, N., Akulova, V., Vassallo, R., 2017. Late Jurassic – Early Cretaceous paleoenvironment evolution of the Transbaikal basins (SE Siberia): implications for the Mongol-Okhotsk orogeny. BSGF-Earth Sci. B. 188(1-2), 9. DOI: 10.1051/bsgf/2017010

Jolivet, M., De Boisgrollier, T., Petit, C., Fournier, M., Sankov, V.A., Ringenbach, J.-C., Byzov, L., Miroshnichenko, A.I., Kovalenko, S.N. & Anisimova, S.V., 2009. How old is the Baikal Rift Zone? Insight from apatite fission track thermochronology. Tectonics 28, Tc3008.

Kalandadze, N.N., Kurzanov, S.M., 1974. Lower Cretaceous localities of terrestrial vertebrates in Mongolia. In: Kramarenko, N.N. (Ed.), Trudy Sovmestnoi Sovetsko-Mongol'skoi Paleontologicheskoi Ekspeditsii (Proceedings of the Joint Soviet–Mongolian Paleontological Expedition), 1. Nauka, Moscow, pp. 288-295 (in Russian).

Khubanov, V.B., Vrublevskaya, T.T., Tsygankov, A.A., Vladimirov, A.G., Buyantuev, M.D., Sokolova, E.N., Posokhov, V.F., Khromova, E.A., 2017. Melting conditions of granitoid xenoliths in contact with alkaline mafic magma (Gusinoozerskaya dyke, Western Transbaikalia): to the problem of the origin of ultrapotassic acid melts. Geodyn. Tectonophys. 8(2), 347–368. Doi:10.5800/GT-2017-8-2-0245.

Khubanov, V.B., Buyantuev, M.D. and Tsygankov, A.A., 2016. U-Pb dating of zircons from PZ(3)-MZ igneous complexes of Transbaikalia by sector-field mass spectrometry with laser sampling: technique and comparison with SHRIMP. Russ. Geol. Geophys. 57, 1, 190-205.

Kolesnikov, Ch.M., 1961. Stratigraphy of the Mesozoic continental deposits in the Buryat ASSR (Western Zabaikalye). Izv. Akad. Nauk SSSR Ser. Geol. 4, 59-73 (in Russian).

Kolesnikov, Ch.M., 1964. The continental Mesozoic stratigraphy of Zabaikalye. In: Stratigraphy and paleontology of the Mesozoic and Cenozoic deposits in the East Siberia and the Far East. Izd-vo Akademii Nauk SSSR, Moscow-Leningrad, pp. 5-138 (in Russian).

Kolesnikov, Ch.M., 1977. Mesozoic limnic bivalves of USSR. Synopsis of the M.S. thesis, Leningrad, 38 pp. (in Russian).

Kolesnikov, Ch.M., 1980. System, stratigraphic distribution, and zoogeography of the Mesozoic limnic bivalves of the USSR. In: Martinson, G.G. (Ed.), Limnobios of ancient lacustrine basins of Eurasia. Nauka, Leningrad, pp. 9-65 (in Russian).

Komarov, I.V. (ed.), 1962. Geological map of the USSR, scale 1:200,000. West-Zabaikalskaya series, sheet M-48-XI. VSEGEI, Leningrad (in Russian).

Leonov, Yu.G., 1983. Mesozoic tectonics and magmatism of East Asia (Correlation between time of manifestation of tectonic movements and magmatism). Nauka, Moscow, 232 pp. (in Russian).

Litvinovsky B.A., Posokhov V.F., Shadaev M.G., Shalagin V.L., 1989. New data on the age of the Early Cretaceous volcanic rocks of the Western Transbaikalia (Rb–Sr and K–Ar datings). Dokl. Akad. Nauk SSSR 308 (4), 946–949 (in Russian).

Litvinovsky, B.A., Tsygankov, A.A., Jahn, B.M., Katzir, Y., Be'eri-Shlevin, Y., 2011. Origin and evolution of overlapping calc-alkaline and alkaline magmas: The Late Palaeozoic post-collisional igneous province of Transbaikalia (Russia). Lithos 125, 845-874.

Litvinovsky, B.A., Yarmolyuk, V.V., Vorontsov, A.A., Zhuravlev, D.Z., Posokhov, B.F., Sandimirova, G.P., Kuzmin, D.V., 2001. Late Triassic stage of formation of the Mongolian–Transbaikalian alkaline-granitoid province: data of isotope geochemical studies. Russ. Geol. Geophys. 42 (3), 445–455.

Luchitsky I.V., 1975. Mesozoic tectonics of Transbaikalia. Novosibirsk: Nauka, Sib. Dept., 206 pp. (in Russian).

Mannion, P.D., Benson, R.B.J., Carrano, M.T., Tennant, J.P., Judd, J., Butler, R.J., 2015. Climate constrains the evolutionary history and biodiversity of crocodilians. Nat. Commun. 6, 8438. https://doi.org/10.1038/ncomms9438 PMID: 26399170

Markwick, P.J., 1998. Fossil crocodilians as indicators of Late Cretaceous and Cenozoic climates: implications for using palaeontological data in reconstructing palaeoclimate. Palaeogeogr. Palaeoclimatol. Palaeoecol. 137, 205-71.

Martinson, G.G., 1955. About stratigraphy of the Mesozoic continental deposits in Zabaikalye. Dokl. Akad. Nauk SSSR 105 (2), 335-338 (in Russian).

Martinson, G.G., 1961. Mesozoic and Cenozoic mollusks of the continental deposits in the Siberian platform, Zabaikalye and Mongolia. In: Tr. Baikal limnological station, issue 19. Izd-vo Akademii Nauk SSSR, Moscow-Leningrad, 332 pp. (in Russian).

Mazukabzov, A.M., Donskaya, T.V., Gladkochub, D.P., Sklyarov, E.V., Ponomarchuk, V.A. and Salnikova, E.B., 2006. Structure and age of the metamorphic core complex of the Burgutui ridge (southwestern Transbaikal region). Dokl. Earth Sci. 407, 179-183.

Mazukabzov, A.M., Sklyarov, E.V., Donskaya, T.V., Gladkochub, D.P., Fedorovsky, V.S., 2011. Metamorphic core complexes of the Transbaikalia: review. Geodyn. Tectonophys. 2(2), 95-125.

Metelkin, D.V., Vernikovsky, V.A., Kazansky, A.Y., and Wingate, M.T.D., 2010. Late Mesozoic tectonics of Central Asia based on paleomagnetic evidence. Gondwana Research 18, 400-419.

Metelkin, D. V., Gordienko, I. V. and Zhao, X., 2004. Paleomagnetism of Early Cretaceous volcanic rocks from Transbaikalia: argument for Mesozoic strike-slip motions in Central Asian structure. Russ. Geol. Geophys. 45(12), 1349-1363.

Mikheeva, E.A., 2017. Age Limits, Correlation and Source Areas of the Jurassic Sediments in the Irkutsk Basin. Synopsis of the M.S. thesis, IEC SB RAS, Irkutsk, 16 pp. (in Russian).

Nesov, L.A., Starkov, A.I., 1992. Cretaceous vertebrates of Gusinoe Lake depression in Transbaikalia and their contribution into dating and determination of sedimentation conditions. Russ. Geol. Geophys. 6 (378), 10-19 (in Russian).

Nie, S., 1991. Paleoclimatic and paleomagnetic constraints on the Paleozoic Reconstructions of south China, north China and Tarim. Tectonophysics 196, 279–308.

Nie, S., Rowley, D.B., Ziegler, A.M., 1990. Constraints on the location of Asian microcontinents in Paleo-Tethys during late Palaeozoic. In: McKerrow, W.S., Scotese, C.R. (Eds.), Palaeozoic Palaeogeography and Biogeography, vol. 12. Geol. Soc. Mem. Am., pp. 12397–12409.

Otchirov, Ts.O., 1964. Geology of the Gusino-Ivolginsk part of Buryatia. Buryat Publ. House, Ulan-Ude, 155 pp. (in Russian).

Parfenov, L.M., Berzin, N.A., Khanchuk, A.I., Badarch, G., Belichenko, V.G., Bulgatov, A.N., Dril, S.I., Kirillova, G.L., Kuzmin, M.I., Nockleberg, W., Prokopyev, A.V., Timofeev, V.F., Tomurtogoo, O., Yan, X., 2003. A model for the formation of orogenic belts in Central and NE Asia. Russ. J. Pac. Geol. 22 (6), 7–41.

Parfenov, L.M., Popeko, L.I., Tomurtogoo, O., 2001. Problems of tectonics of the Mongol-Okhotsk orogenic belt. Russian Journal of Pacific Geology 16, 797–830.

Platov V.S., Tereshchenkov V.G., Savchenko A.A., Busuek S.M., Anosova G.B., Polyansky S.A., 2013. State geological map of the Russian Federation, scale 1:200,000. Sheet M-48-V. Selenga series. Explanatory note. MF VSEGEI, Moscow.

Powerman, V.I., Buyantuev, M.D., Ivanov, A.V., 2021. A review of detrital zircon data treatment, and launch of a new tool 'Dezirteer' along with the suggested universal workflow. Chem. Geol. 583, 120437 DOI: 10.1016/j.chemgeo.2021.120437

Prokopiev, A.V., Toro, J., Miller, E.L., Gehrels, G.E., 2008. The paleo-Lena River – 200 m.y. of transcontinental zircon transport in Siberia. Geology 36 (9), 699–702.

Qi, X., and Wang, Z. (Eds.), 2008. Geological map of Central Asia and adjacent areas 1:2500000. Geological Publishing House, Beijing.

Reichow, M.K., Litvinovsky, B.A., Parrish, R.R., Saunders, A.D., 2010. Multi-stage emplacement of alkaline and peralkaline syenite-granite suites in the Mongolian-Transbaikalian Belt, Russia: Evidence from U-Pb geochronology and whole rock geochemistry. Chem. Geol. 273(1–2), 120–135. http://dx.doi.org/10.1016/j.chemgeo.2010.02.017

Scotese, C.R., Song, H., Mills, B.J.W., van der Meer, D.G., 2021. Phanerozoic paleotemperatures: The Earth's changing climate during the last 540 million years. Earth-Sci. Rev 215, 103503. https://doi.org/10.1016/j.earscirev.2021.103503.

Sengör, A.M.C., Natal'in, B.A., 1996. Paleotectonics of Asia: fragments of a synthesis. In: Yin, A., Harrison, T.M. (Eds.), The Tectonics of Asia. Cambridge Univ. Press, New York, pp. 486–640.

Serdobolskaya, I.N. and Kozubova, L.A., 1976. On the age of the Ichetui suite in West Transbaikaliya. Russ. Geol. Geophys. 7, 90-93 (in Russian).

Sheldrick, T.C., Barry, T.L., Dash, B. et al., 2020. Simultaneous and extensive removal of the East Asian lithospheric root. Sci Rep 10, 4128. https://doi.org/10.1038/s41598-020-60925-3

Sklyarov, E.V., Mazukabzov, A.M., Mel'nikov, A.I., 1997. Metamorphic Core Complexes of the Cordilleran Type. SPC UIGGM Siberian Branch of the RAS, Novosibirsk, pp. 176 (in Russian).

Skoblo, V.M., 1967. The biostratigraphic scheme of the Lower Cretaceous in the western Zabaikalye. In: The problems of geology of Pribaikalye and Zabaikalye, issue 2(4). Chita (in Russian).

Skoblo, V.M., Lyamina, N.A., Rudnev, A.F., Luzina, I.V., 2001. Continental Upper Mesozoic of Pribaikalia and Transbaikalia (Stratigraphy, Sedimentation Conditions, Correlations). Izd-vo SB RAS, Novosibirsk, pp. 332 (in Russian).

Skutschas, P.P., 2008. A choristoderan reptile from the Lower Cretaceous of Transbaikalia, Russia. Neues Jahrb. fur Geol. Palaontol. - Abh. 247, 63-78.

Skutschas, P.P., Vitenko, D.D., 2017. Early Cretaceous choristoderes (Diapsida, Choristodera) from Siberia, Russia. Cretac. Res. 77, 79-92.

Sláma, J., Košler, J., Condon, D.J., Crowley, J.L., Gerdes, A., Hanchar, J.M., Horstwood, M.S.A., Morris, G.A., Nasdala, L., Norberg, N., Schaltegger, U., Schoene, B., Tubrett, M.N., Whitehouse, M.J., 2008. Plesovice zircon - A new natural reference material for U-Pb and Hf isotopic microanalysis. Chem. Geol. 249, 1–35.

Sorokin, A.A., Zaika, V.A., Kovach, V.P., Kotov, A.B., Xu W.L., Yang, H., 2020. Timing of closure of the eastern Mongol-Okhotsk Ocean: Constraints from U-Pb and Hf isotopic data of detrital zircons from metasediments along the Dzhagdy Transect. GR. 81, 58-78.

Stanley, E.A., 1966. The problem of reworked pollen and spores in marine sediments. Marine Geology 4(6), 397-408.

Vakhrameev, V.A., 1964. Jurassic and early Cretaceous floras of Eurasia and the paleofloristic provinces of this period. Moscow, 263 pp. (in Russian).

Vakhrameev, V.A., 1982. Division and correlation of continental deposits according to paleobotanical data // Soviet Geology 1, 58-67 (in Russian).

Van der Beek, P., Delvaux, D., Andriessen, P.A.M., and Levi, K.G., 1996. Early Cretaceous denudation related to convergent tectonics in the Baikal Region, SE Siberia // J Geol Soc, London 153, 515-523.

Vorontsov, A.A., Ivanov, V.G., Yarmolyuk, V.V., Kuzmin, M.I., Sandimirova, G.P., Smirnov, V.N., 1999. Late Mesozoic bimodal alkaline volcanic association of Western Transbaikalia and the age of its formation: geological and geochronological (Rb-Sr and K-Ar) data. Dokl. Earth Sci. 369(2), 220-224 (in Russian).

Vorontsov, A.A., Yarmolyuk, V.V., Komaritsyna, T.Yu., 2016. Late Mesozoic-Early Cenozoic rifting magmatism in the Uda sector of Western Transbaikalia. Russ. Geol. Geophys. 57(5), 723-744.

Wang, T., Guo, L., Zheng, Y., Donskaya, T., Gladkochub, D., Zeng, L., Li, J., Wang, Y., Mazukabzov, A., 2012. Timing and processes of late Mesozoic mid-lower-crustal extension in continental NE Asia and implications for the tectonic setting of the destruction of the North China Craton: mainly constrained by zircon U-Pb ages from metamorphic core complexes. Lithos 154, 315–345.

Wang, T., Tong, Y., Xiao, W.J., Guo, L., Windley, B.F., Donskaya, T., Li, S., Narantsetseg, T. and Zhang, J.J., 2022. Rollback, scissor-like closure of the Mongol-Okhotsk Ocean and

formation of an orocline: magmatic migration based on a large archive of age data. Natl. Sci. Rev. 9(5), nwab210.

Wang, T., Zheng, Y.D., Zhang, J.J., Zeng, L.S., Donskaya, T.V., Guo, L., Li, J.B., 2011. Pattern and kinematic polarity of late Mesozoic extension in continental NE Asia: perspectives from metamorphic core complexes. Tectonics 30, TC6007. https://doi.org/10.1029/2011TC002896.

Wernicke, B., 1981. Low-angle normal faults in the Basin and Range Province: nappe tectonics in an extending orogen. Nature 291, 645-648

Wiedenbeck, M., Allé, P., Corfu, F., Griffin, W.L., Meier, M., Oberli, F., Van Quadt, A., Roddick, J.C., Spiegel, W., 1995. Three natural zircon standards for U-Th-Pb, Lu-Hf, trace element and REE analyses. Geostandards Newslett. 19, 1–23.

Yang, W., Jolivet, M., Dupont-Nivet, G., Guo, Z., Zhang, Z., Zhang, Z., 2013. Source to sink relations between the Tian Shan and Junggar Basin (northwest China) from Late Palaeozoic to Quaternary: evidence from detrital U-Pb zircon geochronology. Basin Res. 25, 219–240.

Yang, Y.-T., Guo, Z.-X., Song, C.-C., Li, X.-B., and He, S., 2015. A short-lived but significant Mongol–Okhotsk collisional orogeny in latest Jurassic–earliest Cretaceous. Gondwana Research 28(3), 1096-1116.

Yarmolyuk, V.V., Kozlovsky, A.M., Savatenkov, V.M., Kovach, V.P., Kozakov, I.K., Kotov, A.B., Lebedev, V.I. and Eenjin, G., 2016. Composition, Sources, and Geodynamic Nature of Giant Batholiths in Central Asia: Evidence from the Geochemistry and Nd Isotopic Characteristics of Granitoids in the Khangai Zonal Magmatic Area. Petrology 24(5), 433–461.

Yarmolyuk, V.V., Vorontsov, A.A., Ivanov, V.G., Kovalenko, V.I., Baikin, D.N. and Sandimirova, G.P. 2000. Stages of Bimodal and Alkaline Granite Magmatism in the Western Transbaikal Region: Geochronological Data on Rocks from the Tugnui Depression. Dokl. Earth Sci. 373, 811-815.

Yin, A., Nie, S., 1993. An indention model for North and South China collision and the development of the Tan Lu and Honam fault systems, eastern Asia. Tectonics 12, 801–813.

Yin, A., Nie, S., 1996. A Phanerozoic plinspatic reconstruction of China and its neighbouring regions. In: Yin, A., Harrison, T.M. (Eds.), The Tectonic Evolution of Asia. Cambridge University Press, Cambridge, pp. 442–485.

Zhang, K.-J., Yan, L.-L., and Ji, C., 2019. Switch of NE Asia from extension to contraction at the mid-Cretaceous: A tale of the Okhotsk oceanic plateau from initiation by the Perm Anomaly to extrusion in the Mongol–Okhotsk ocean? Earth-Science Reviews 198, 102941.

Zheng, Y., Wang, S., Wang, Y., 1991. An enormous thrust nappe and extensional metamorphic core complex in Sino-Mongolian boundary area. Science in China, ser. B 34, 1145–1152.

Zonenshain, L.P., Kuzmin, M.I., Natapov, L.M., 1990. Geology of the USSR: A Plate tectonic synthesis. American Geophysical Union. Geodyn. 21 https://doi.org/10.1029/GD021.

Zorin, Yu.A., 1999. Geodynamics of the western part of the Mongolia–Okhotsk collisional belt, Trans-Baikal region (Russia) and Mongolia. Tectonophysics 306, 33–56.

Zorin, Yu.A., Belichenko, V.G., Turutanov, E.Kh, Kozhevnikov, V.M., Sklyarov, E.V., Tomurtogoo, O., Khosbayar, P., Arvisbaatar, N., Byambaa, Ch, 1998. Terranes in east Mongolia and central Transbaikalia and evolution of the Okhotsk-Mongolian fold belt. Russ. Geol. Geophys. 39(1), 11–25.

Zorin, Yu.A., Sklyarov, E.V., Mazukabzov, A.M., Belichenko, V.G., 1997. Metamorphic core complexes and Early Cretaceous rifting in the Trans-Baikal region. Russ. Geol. Geophys. 38, 1574–1584.

al., 2020).

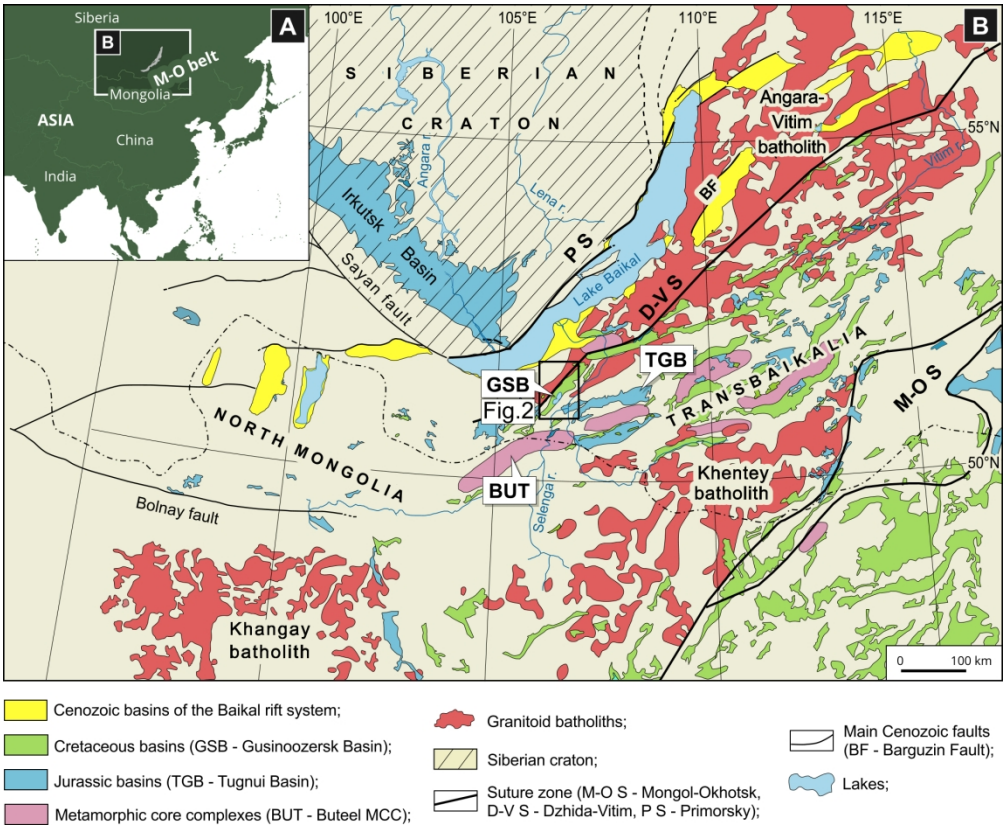

Fig. 1. A - Location of the Mongol-Okhotsk orogenic belt (M-O belt) on the map of Asia; B - Geological setting of Transbaikalia and adjacent areas (Qi and Wang, 2008; Jolivet et al., 2013; Yarmolyuk et al., 2016): 1 - Siberian craton, 2 - Lakes, 3 - Jurassic basins (TGB - Tugnui Basin), 4 - Cretaceous basins (GSB - Gusinoozersk Basin), 5 - Cenozoic basins of the Baikal rift system, 6 - Metamorphic core complexes (BUT - Buteel MCC), 7 - Granitoid batholiths, 8 - Suture zone: M-O S - Mongol-Okhotsk, D-V S - Dzhida-Vitim, P S - Primorsky, 9 - Main Cenozoic faults: BF - Barguzin Fault.

175x144mm (300 x 300 DPI)

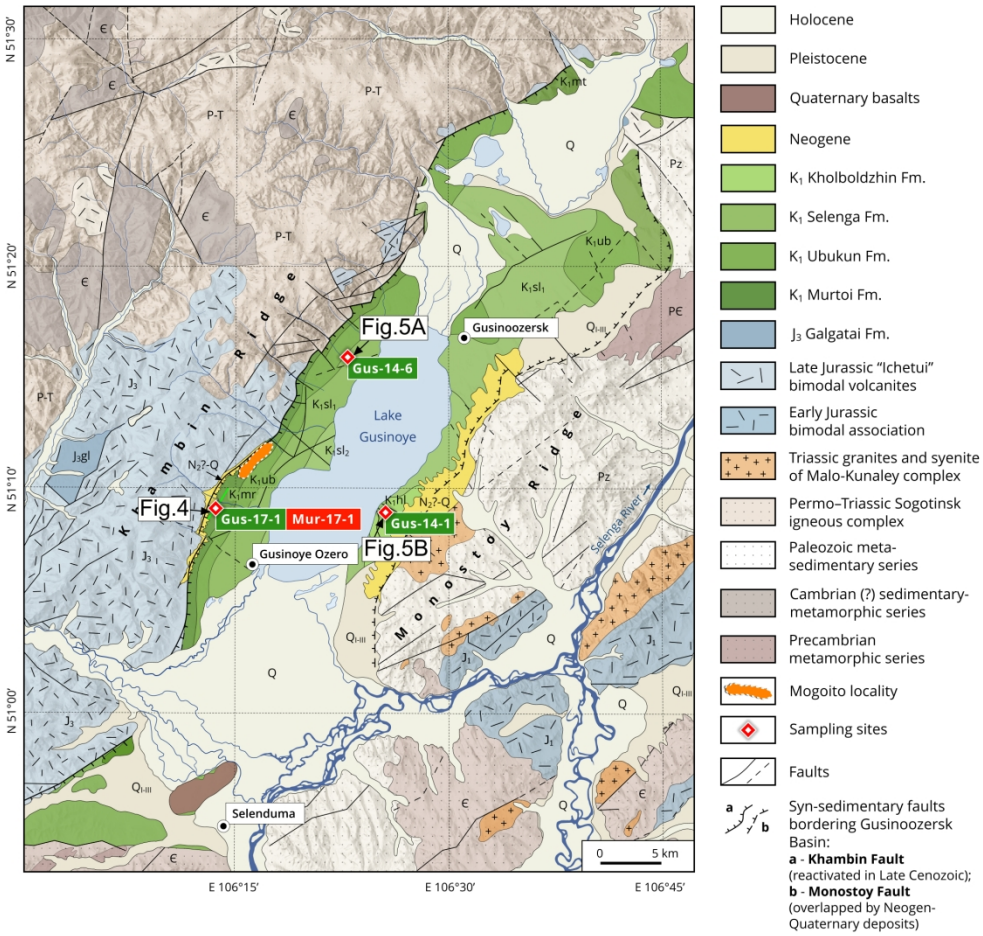

Fig. 2. Simplified geological map of the Gusinoozersk Basin and surrounding area showing the outcrops of Mesozoic deposits based on the Russian geological map (Komarov, 1962) with modifications and additions after Jolivet et al. (2017) with the refinement of some rock ages after Yarmolyuk et al. (2000); Andryushchenko et al. (2010), Platov et al. (2013) and Bulnaev (2006). Here and below, the sample numbers are indicated in the rectangles. Samples dated 40Ar/39Ar (volcanites) are marked in red, and U-Pb (detrital zircons) are marked in green.

180x171mm (300 x 300 DPI)

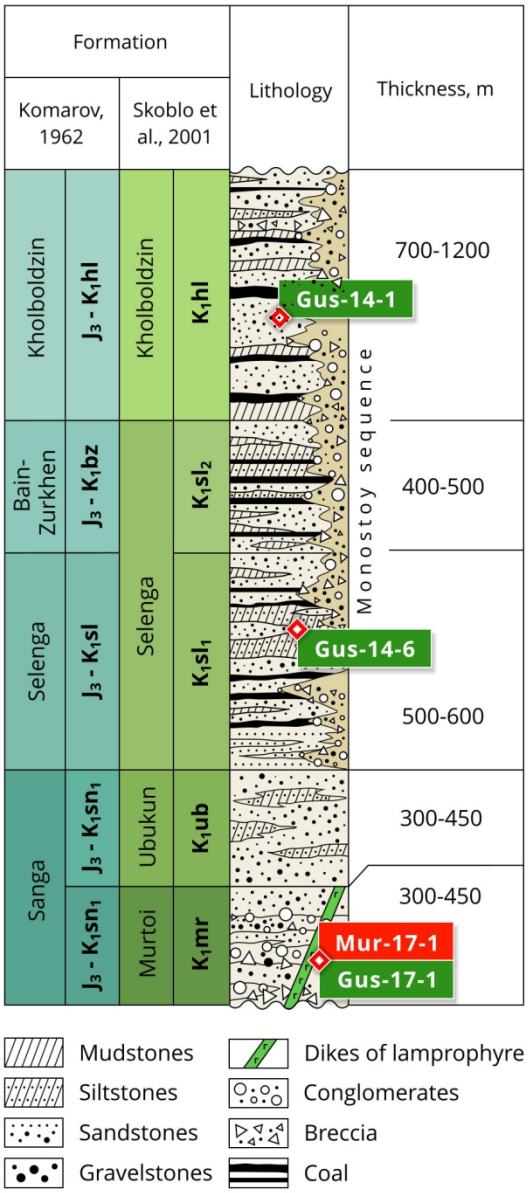

Fig. 3 Stratigraphy of the Early Cretaceous deposits of the Gusinoozersk Basin after Komarov (1962), modified after Skoblo et al. (2001). Red square indicates samples position (schematically, without reference to depth and upper/lower parts of fms.).

77x172mm (300 x 300 DPI)

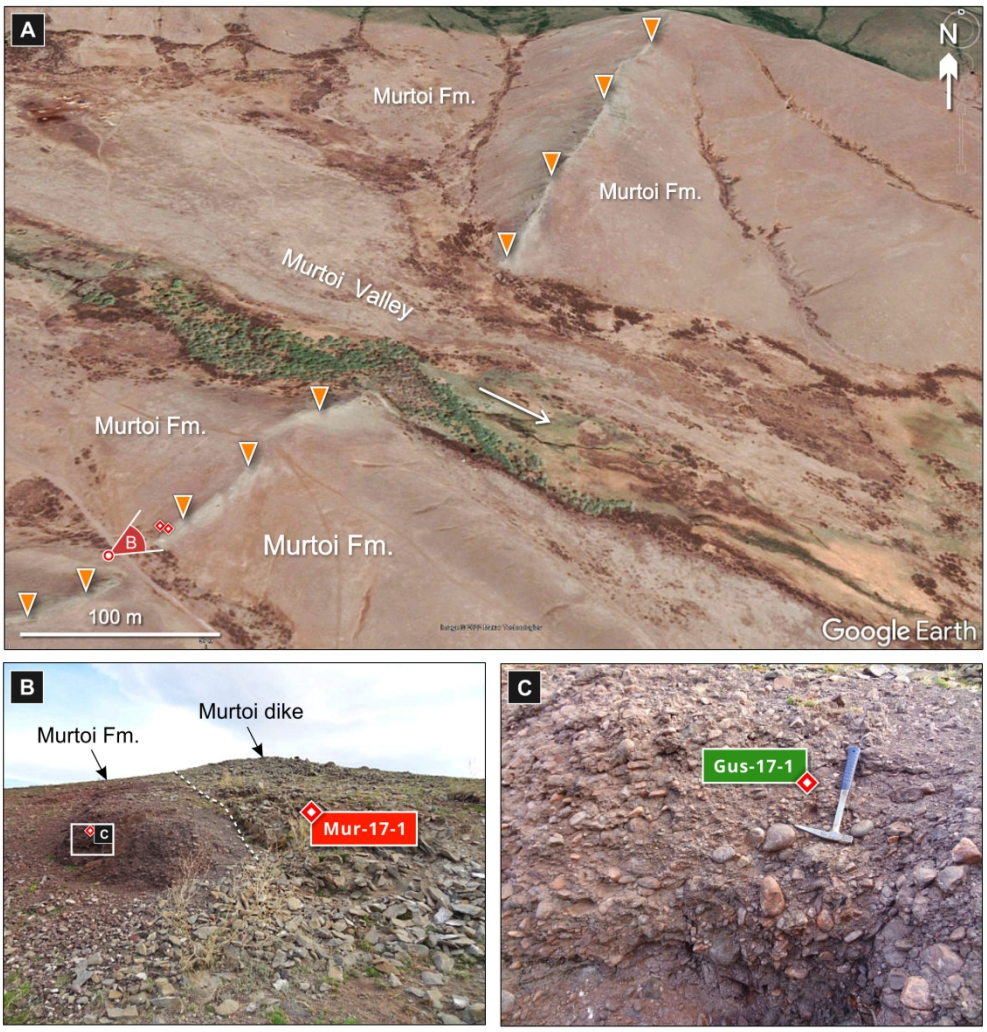

Fig. 4. (A) Google Earth satellite image of the Murtoi Fm. intruded by the Murtoi dike (indicated by orange triangles). Field view (B) and zoom (C) of the sampling site.

180x186mm (300 x 300 DPI)

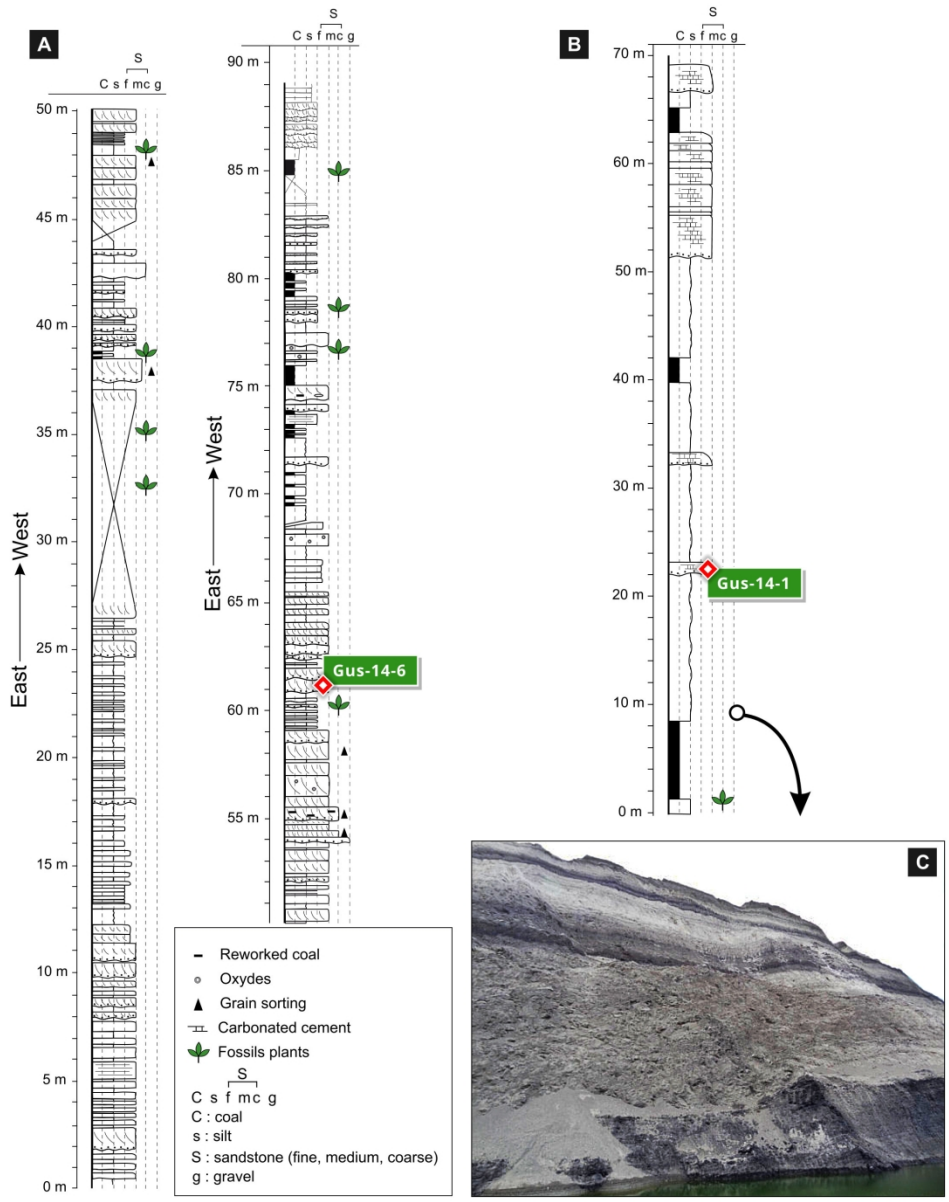

Fig. 5. Sections of sedimentary deposits of the Selenga Fm. (A) and Kholboldzhin Fm. (B) at sampling sites for U-Pb dating of detrital zircons (modified after Jolivet et al. (2017)). Red squares indicate sampling locations within the section. C - Field view of the Kholboldzhin Fm. section.

187x237mm (300 x 300 DPI)

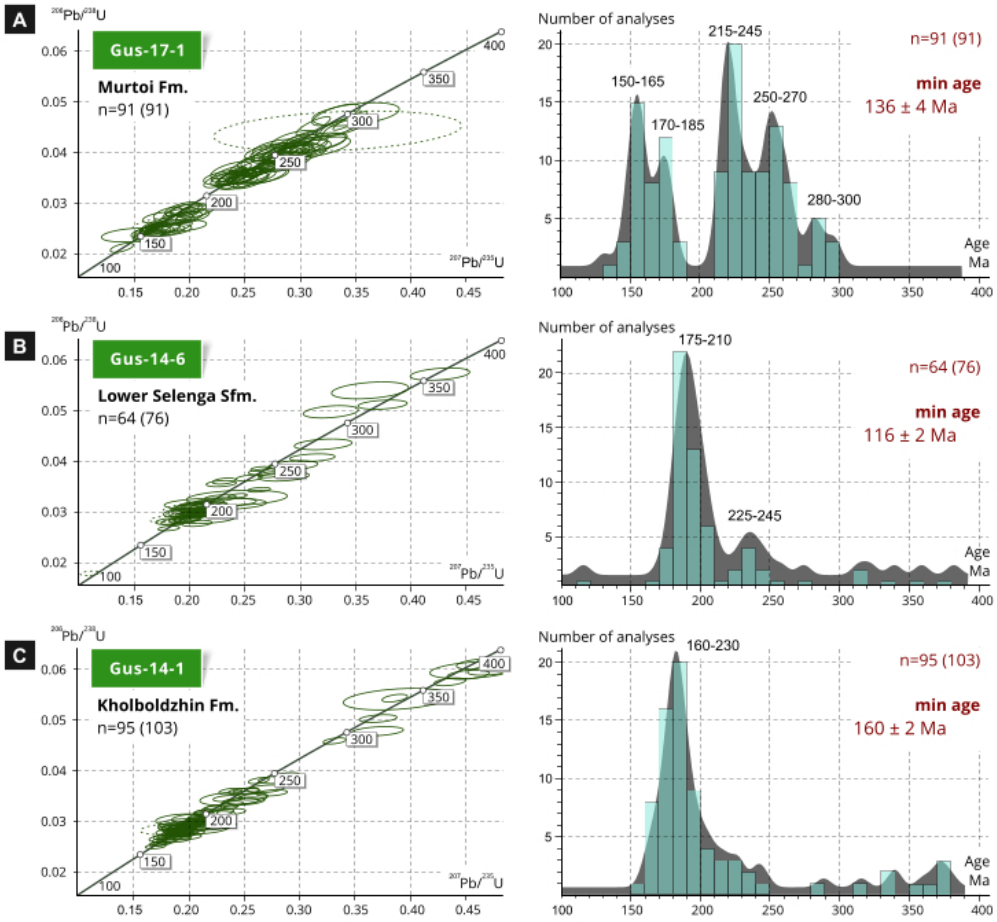

Fig. 6. U-Pb concordia diagrams and histograms coupled with kernel density estimates (grey area) for zircons from A – Murtoi Fm., B – Lower Selenga Sfm., C – Kholboldzhin Fm. n – number of grains younger than 400 Ma, in brackets - the number of all concordant ages.

192x177mm (96 x 96 DPI)

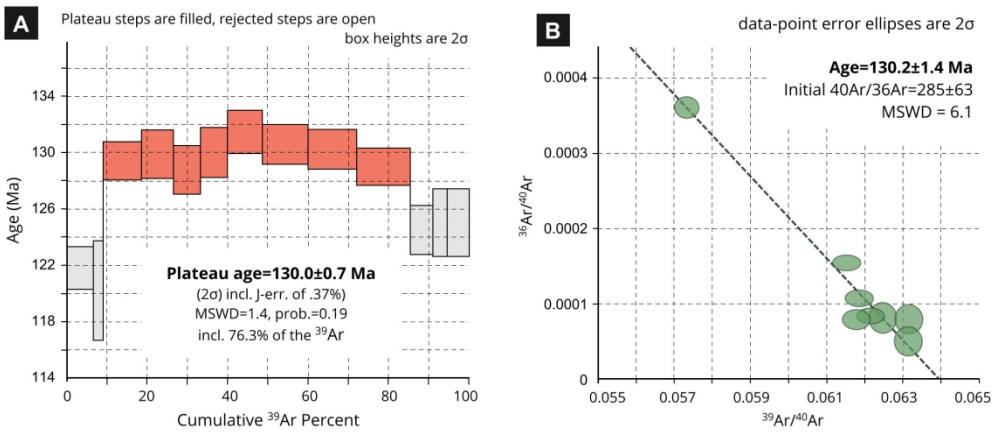

Fig. 7. Stepwise heating (A) and inverse isochrone (B) plots for volcanic sample Mur-17-1 from the Murtoi dike.

172x75mm (300 x 300 DPI)

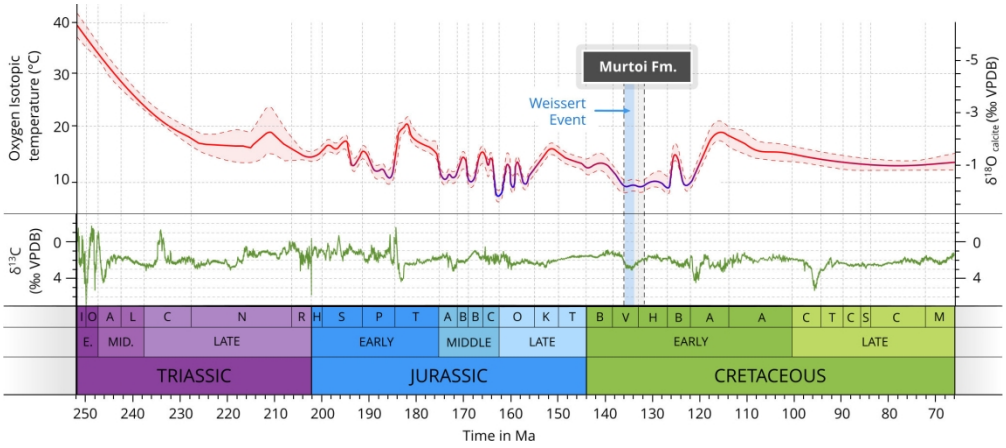

Fig. 8. A Mesozoic Oxygen and Carbon isotope records with the addition of the time of deposition of the Murtoi Fm. and the Weissert Event. For Oxygen isotopic red-blue bold line represents Locfit regression and dashed lines show ±95% confidence interval (Grossman et al., 2020). Green line represents variation in δ13Ccarb through the Mesozoic (Cramer et al., 2020).

173x75mm (300 x 300 DPI)

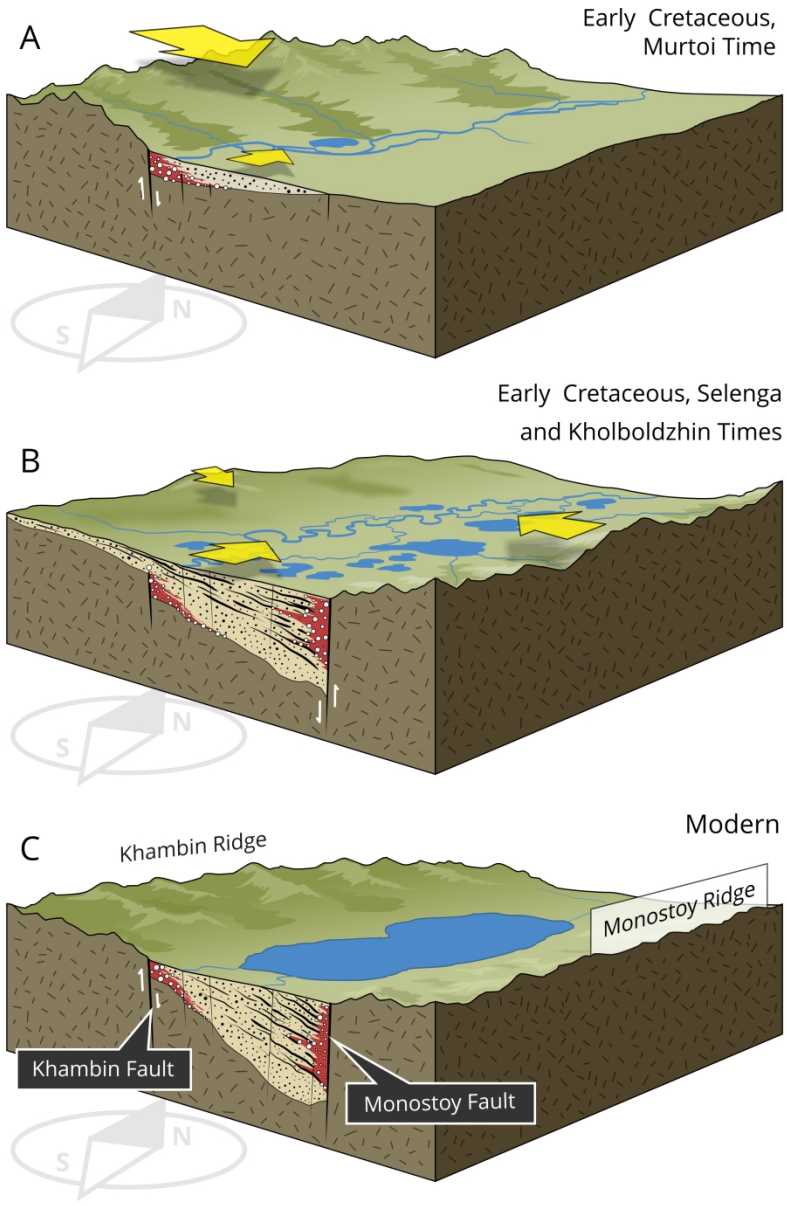

Fig. 9. Paleogeographical models of the Gusinoozersk Basin for the Murtoi (A), Selenga and Kholboldzin (B) and modern (C) time showing tectonic control of the basin subsidence and evolution of provenance of the deposits (for Lower Cretaceous stages). Yellow arrows show the direction of sediment transport. The size of the arrows indicates the contribution of sediments from different provinces.

90x135mm (600 x 600 DPI)

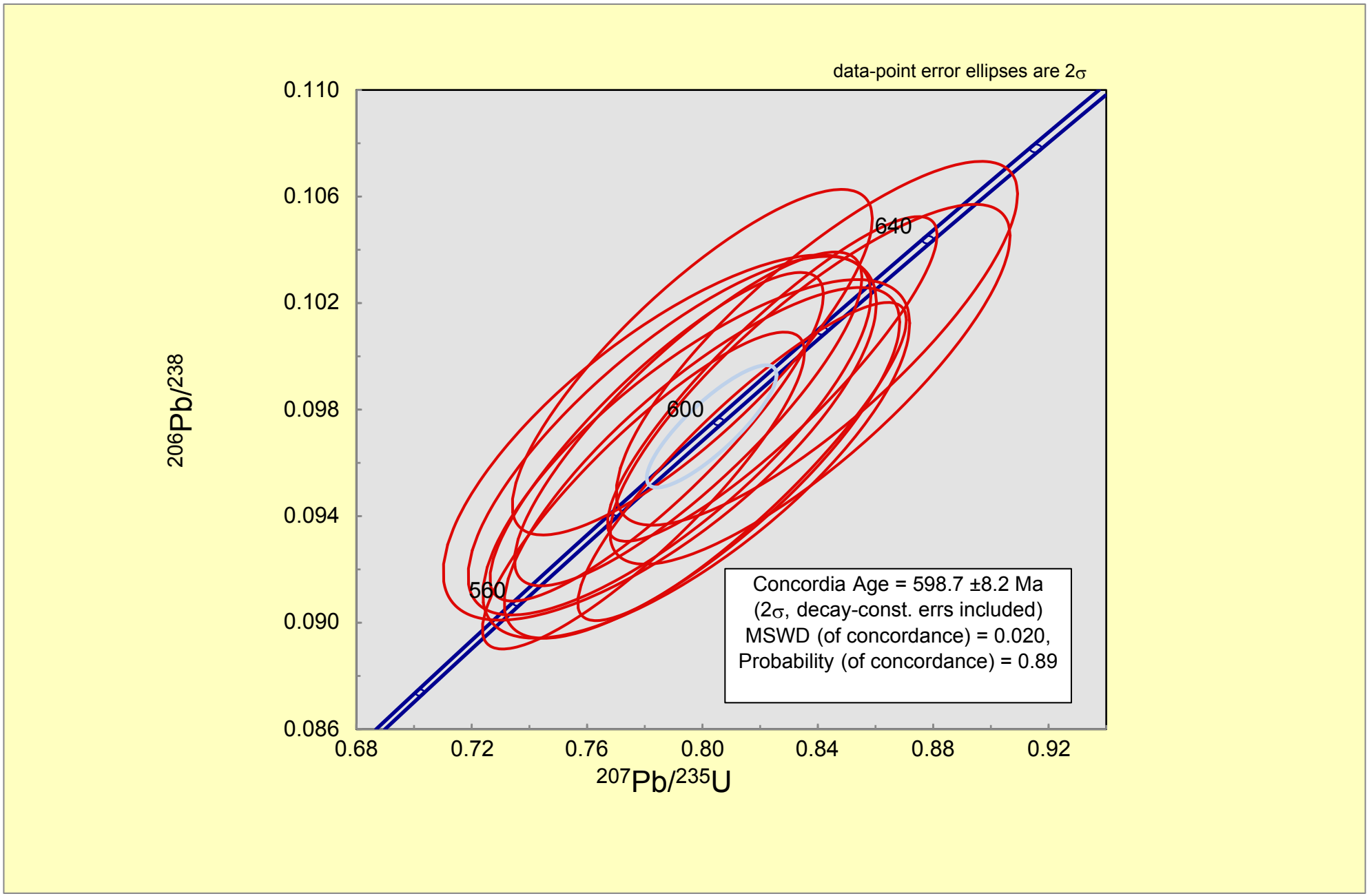
data-point error ellipses are 2σ
0.110
0.106
0.102
0.098
0.094
0.090
0.086
206Pb/238
0.68
0.72
0.76
0.80
0.84
0.88
0.92
207Pb/235U
640
600
560
Concordia Age = 598.7 ±8.2 Ma
(2σ, decay-const. errs included)
MSWD (of concordance) = 0.020,
Probability (of concordance) = 0.89

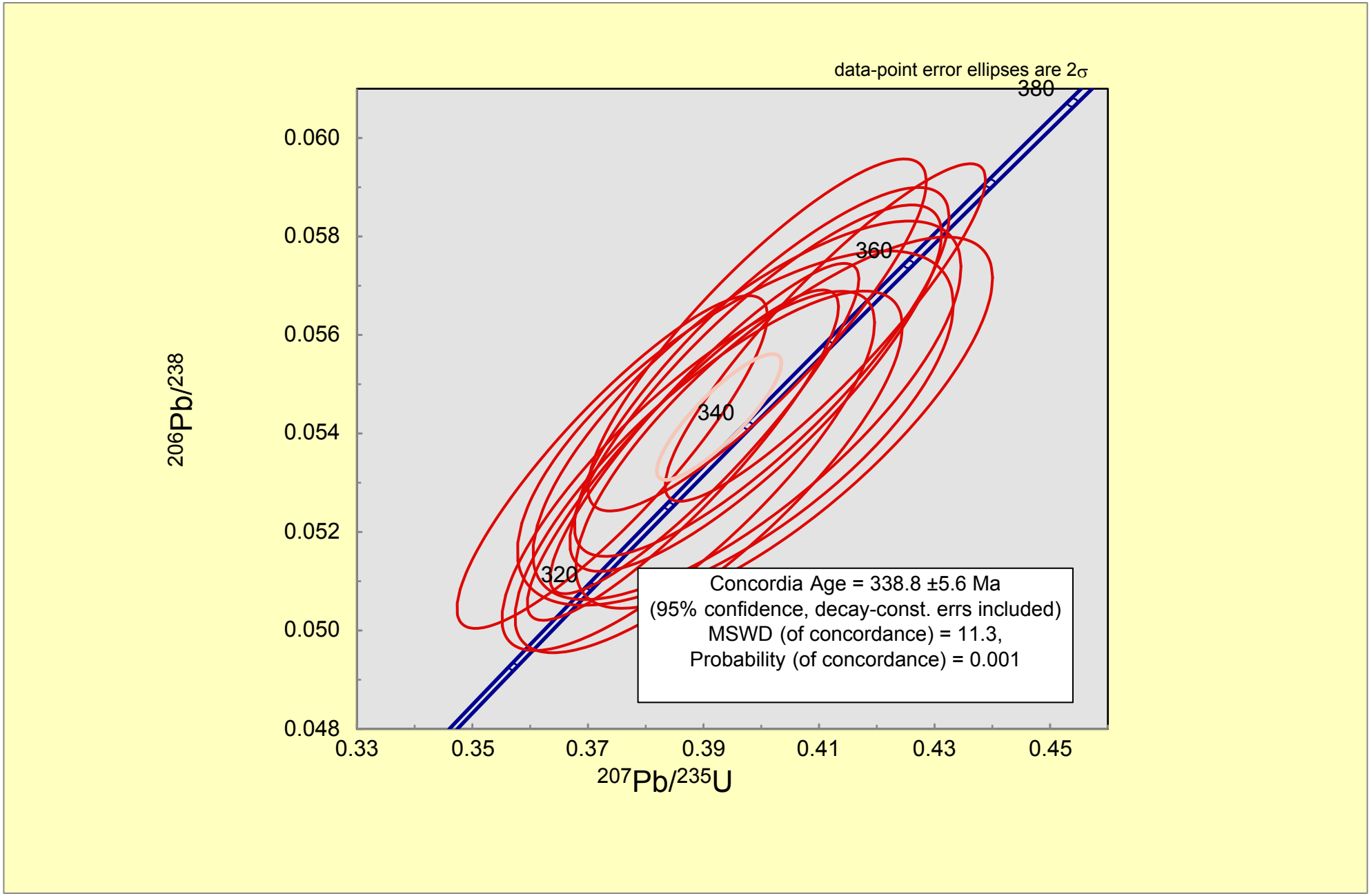
data-point error ellipses are 2σ
380
360
340
320
0.060
0.058
0.056
0.054
0.052
0.050
0.048
0.33
0.35
0.37
0.39
0.41
0.43
0.45
206Pb/238
207Pb/235U
Concordia Age = 338.8 ±5.6 Ma
(95% confidence, decay-const. errs included)
MSWD (of concordance) = 11.3,
Probability (of concordance) = 0.001

#	Изотопные отношения							
	$\frac{Th}{U}$	1σ (abs)	$\frac{^{207}Pb}{^{206}Pb}$	1σ (abs)	$\frac{^{208}Pb}{^{232}Th}$	1σ (abs)	$\frac{^{207}Pb}{^{235}U}$	1σ (abs)
GUS-17-1	**number of sample**		**91 zircons**					
PRB57	1.04	0.0395	0.0486	0.0024	0.0067	0.0002	0.1428	0.0068
PRB68	1.36	0.0526	0.0512	0.0029	0.0075	0.0002	0.1664	0.0091
PRB58	0.94	0.0362	0.0463	0.0056	0.0080	0.0004	0.1521	0.0181
PRB107	1.75	0.0715	0.0507	0.0030	0.0072	0.0003	0.1679	0.0096
PRB86	2.36	0.0932	0.0502	0.0035	0.0075	0.0003	0.1685	0.0115
PRB83	1.70	0.0666	0.0520	0.0029	0.0075	0.0002	0.1753	0.0094
PRB79	1.17	0.0458	0.0484	0.0022	0.0078	0.0002	0.1643	0.0070
PRB34	0.86	0.0324	0.0532	0.0036	0.0077	0.0003	0.1811	0.0119
PRB84	1.24	0.0492	0.0533	0.0046	0.0081	0.0003	0.1819	0.0153
PRB29	1.24	0.0465	0.0512	0.0022	0.0072	0.0002	0.1763	0.0071
PRB41	0.92	0.0347	0.0514	0.0036	0.0067	0.0003	0.1770	0.0118
PRB18	1.28	0.0482	0.0491	0.0023	0.0072	0.0002	0.1695	0.0072
PRB48	2.16	0.0813	0.0488	0.0020	0.0073	0.0002	0.1695	0.0063
PRB7	1.26	0.0474	0.0518	0.0029	0.0082	0.0002	0.1811	0.0094
PRB14	1.20	0.0451	0.0546	0.0028	0.0073	0.0002	0.1919	0.0090
PRB101	1.86	0.0750	0.0481	0.0019	0.0076	0.0002	0.1696	0.0063
PRB33	1.03	0.0386	0.0494	0.0017	0.0074	0.0002	0.1744	0.0054
PRB9	0.90	0.0342	0.0542	0.0052	0.0086	0.0004	0.1913	0.0179
PRB27	1.10	0.0414	0.0461	0.0023	0.0074	0.0002	0.1635	0.0074
PRB98	1.00	0.0403	0.0512	0.0028	0.0080	0.0003	0.1910	0.0102
PRB15	1.31	0.0493	0.0470	0.0027	0.0082	0.0002	0.1759	0.0096
PRB97	1.28	0.0513	0.0528	0.0030	0.0086	0.0003	0.1982	0.0107
PRB62	1.16	0.0443	0.0544	0.0028	0.0083	0.0003	0.2058	0.0100
PRB65	0.99	0.0380	0.0534	0.0025	0.0089	0.0003	0.2051	0.0090
PRB67	0.87	0.0336	0.0508	0.0029	0.0091	0.0003	0.1953	0.0106
PRB75	0.65	0.0254	0.0474	0.0023	0.0087	0.0003	0.1836	0.0083
PRB21	0.82	0.0309	0.0534	0.0028	0.0090	0.0003	0.2092	0.0104
PRB47	1.78	0.0673	0.0490	0.0020	0.0083	0.0002	0.1931	0.0073
PRB78	1.07	0.0416	0.0515	0.0021	0.0085	0.0002	0.2035	0.0077
PRB1a	1.52	0.0617	0.0479	0.0021	0.0086	0.0003	0.1894	0.0081
PRB64	0.70	0.0270	0.0510	0.0028	0.0086	0.0003	0.2023	0.0106
PRB82	1.23	0.0484	0.0494	0.0027	0.0086	0.0003	0.1968	0.0103
PRB42	0.95	0.0360	0.0523	0.0027	0.0096	0.0003	0.2459	0.0119
PRB59	1.73	0.0657	0.0518	0.0021	0.0108	0.0003	0.2454	0.0093
PRB63	1.16	0.0445	0.0544	0.0023	0.0110	0.0003	0.2579	0.0105
PRB108	1.19	0.0486	0.0485	0.0022	0.0107	0.0004	0.2314	0.0102
PRB80	1.93	0.0754	0.0534	0.0025	0.0109	0.0003	0.2557	0.0114
PRB56	1.68	0.0639	0.0500	0.0021	0.0108	0.0003	0.2400	0.0093
PRB51	2.11	0.0795	0.0490	0.0020	0.0102	0.0003	0.2356	0.0090
PRB92	1.66	0.0661	0.0508	0.0025	0.0106	0.0003	0.2459	0.0114
PRB11	1.42	0.0538	0.0495	0.0034	0.0112	0.0003	0.2396	0.0158
PRB22	0.77	0.0290	0.0544	0.0024	0.0106	0.0003	0.2641	0.0106
PRB77	0.36	0.0140	0.0496	0.0020	0.0108	0.0003	0.2408	0.0090
PRB43	1.46	0.0551	0.0517	0.0022	0.0104	0.0003	0.2516	0.0097
PRB66	1.47	0.0566	0.0523	0.0021	0.0104	0.0003	0.2546	0.0094
PRB61	1.88	0.0718	0.0560	0.0024	0.0112	0.0003	0.2732	0.0109
PRB72	1.31	0.0507	0.0523	0.0028	0.0114	0.0004	0.2554	0.0133

PRB30	2.19	0.0825	0.0509	0.0018	0.0104	0.0002	0.2490	0.0077
PRB26	1.68	0.0634	0.0555	0.0029	0.0107	0.0003	0.2716	0.0133
PRB36	1.16	0.0439	0.0516	0.0023	0.0099	0.0003	0.2524	0.0103
PRB54	1.36	0.0512	0.0492	0.0017	0.0099	0.0003	0.2417	0.0078
PRB53	1.03	0.0390	0.0482	0.0021	0.0103	0.0003	0.2371	0.0095
PRB2	1.67	0.0628	0.0529	0.0019	0.0110	0.0002	0.2662	0.0085
PRB60	1.26	0.0482	0.0477	0.0025	0.0109	0.0003	0.2401	0.0119
PRB6	1.94	0.0732	0.0528	0.0021	0.0111	0.0003	0.2683	0.0095
PRB24	2.54	0.0955	0.0520	0.0018	0.0110	0.0002	0.2647	0.0080
PRB38	1.88	0.0709	0.0505	0.0020	0.0103	0.0002	0.2574	0.0090
PRB69	0.68	0.0261	0.0494	0.0021	0.0111	0.0003	0.2540	0.0102
PRB1	3.26	0.1224	0.0526	0.0019	0.0115	0.0002	0.2728	0.0084
PRB16	0.95	0.0357	0.0551	0.0027	0.0109	0.0003	0.2863	0.0130
PRB102	1.53	0.0618	0.0548	0.0029	0.0114	0.0004	0.2889	0.0149
PRB31	1.09	0.0412	0.0502	0.0025	0.0117	0.0003	0.2646	0.0122
PRB89	1.12	0.0447	0.0510	0.0028	0.0117	0.0004	0.2710	0.0144
PRB87	0.59	0.0235	0.0529	0.0023	0.0127	0.0004	0.2861	0.0117
PRB99	0.77	0.0312	0.0536	0.0028	0.0122	0.0005	0.2924	0.0146
PRB109	0.97	0.0398	0.0509	0.0026	0.0120	0.0004	0.2790	0.0135
PRB91	0.68	0.0273	0.0540	0.0035	0.0118	0.0005	0.2964	0.0188
PRB74	1.01	0.0392	0.0531	0.0024	0.0125	0.0004	0.2917	0.0123
PRB17	0.55	0.0205	0.0506	0.0018	0.0117	0.0003	0.2782	0.0086
PRB111	0.73	0.0301	0.0521	0.0038	0.0121	0.0006	0.2884	0.0204
PRB52	1.76	0.0665	0.0498	0.0019	0.0114	0.0003	0.2752	0.0098
PRB94	0.83	0.0331	0.0526	0.0027	0.0120	0.0004	0.2910	0.0144
PRB40	0.89	0.0340	0.0506	0.0034	0.0114	0.0004	0.2797	0.0179
PRB112	0.98	0.0402	0.0545	0.0030	0.0119	0.0005	0.3052	0.0160
PRB50	0.78	0.0294	0.0497	0.0026	0.0113	0.0004	0.2799	0.0136
PRB73	1.03	0.0400	0.0537	0.0027	0.0125	0.0004	0.3040	0.0148
PRB110	1.05	0.0432	0.0565	0.0032	0.0124	0.0005	0.3202	0.0175
PRB32	1.13	0.0426	0.0522	0.0019	0.0122	0.0003	0.2978	0.0100
PRB5	1.07	0.0405	0.0540	0.0022	0.0125	0.0003	0.3096	0.0112
PRB44	0.89	0.0337	0.0522	0.0026	0.0117	0.0004	0.2996	0.0139
PRB103	0.84	0.0342	0.0545	0.0033	0.0127	0.0005	0.3149	0.0184
PRB8	1.06	0.0401	0.0558	0.0025	0.0134	0.0003	0.3241	0.0130
PRB35	0.91	0.0343	0.0505	0.0025	0.0126	0.0004	0.2960	0.0135
PRB10	0.80	0.0300	0.0516	0.0020	0.0130	0.0003	0.3025	0.0103
PRB70	1.00	0.0435	0.0550	0.0123	0.0130	0.0015	0.3353	0.0730
PRB3	0.69	0.0260	0.0548	0.0020	0.0142	0.0003	0.3388	0.0109
PRB96	0.43	0.0172	0.0548	0.0024	0.0139	0.0005	0.3414	0.0143
PRB46	1.43	0.0541	0.0503	0.0018	0.0127	0.0003	0.3135	0.0101
PRB13	0.36	0.0137	0.0544	0.0018	0.0119	0.0003	0.3465	0.0101
PRB95	0.80	0.0319	0.0511	0.0023	0.0144	0.0005	0.3339	0.0141
PRB55	0.69	0.0264	0.0537	0.0041	0.0148	0.0007	0.3515	0.0256
GJ-1								
GJ1	0.03	0.0011	0.0603	0.0020	0.0328	0.0013	0.8242	0.0234
GJ10	0.03	0.0012	0.0589	0.0023	0.0291	0.0017	0.7886	0.0285
GJ11	0.03	0.0011	0.0602	0.0024	0.0351	0.0021	0.7978	0.0302
GJ12	0.03	0.0013	0.0587	0.0024	0.0300	0.0017	0.7852	0.0307
GJ2	0.03	0.0011	0.0614	0.0020	0.0282	0.0012	0.8137	0.0233
GJ3	0.03	0.0011	0.0595	0.0020	0.0306	0.0013	0.7795	0.0228
GJ4	0.03	0.0011	0.0586	0.0020	0.0274	0.0013	0.7841	0.0236
GJ5	0.03	0.0011	0.0591	0.0020	0.0283	0.0014	0.7951	0.0246

GJ6	0.03	0.0011	0.0579	0.0021	0.0284	0.0014	0.7965	0.0255
GJ7	0.03	0.0011	0.0606	0.0022	0.0299	0.0016	0.8397	0.0284
GJ8	0.03	0.0011	0.0614	0.0022	0.0345	0.0017	0.8373	0.0283
GJ9	0.03	0.0011	0.0604	0.0023	0.0338	0.0018	0.7998	0.0280
Plesovice								
PL1	0.10	0.0037	0.0532	0.0017	0.0169	0.0004	0.4111	0.0113
PL10	0.10	0.0038	0.0533	0.0020	0.0173	0.0006	0.3909	0.0137
PL11	0.10	0.0041	0.0540	0.0021	0.0165	0.0006	0.4040	0.0147
PL12	0.10	0.0043	0.0529	0.0021	0.0152	0.0006	0.3975	0.0151
PL2	0.10	0.0037	0.0523	0.0017	0.0165	0.0004	0.3902	0.0109
PL3	0.10	0.0037	0.0523	0.0017	0.0160	0.0004	0.3864	0.0110
PL4	0.10	0.0038	0.0508	0.0017	0.0153	0.0004	0.3742	0.0110
PL5	0.10	0.0037	0.0517	0.0017	0.0156	0.0004	0.3993	0.0120
PL6	0.10	0.0037	0.0530	0.0022	0.0143	0.0007	0.3955	0.0154
PL7	0.10	0.0038	0.0527	0.0019	0.0175	0.0005	0.3990	0.0132
PL8	0.10	0.0039	0.0525	0.0019	0.0166	0.0005	0.4001	0.0133
PL9	0.10	0.0038	0.0528	0.0019	0.0161	0.0005	0.3874	0.0132

			Возраст, млн лет					
$^{206}Pb/^{238}U$	1σ (abs)	Rho	$^{207}Pb/^{206}Pb$	1σ	$^{208}Pb/^{232}Th$	1σ	$^{207}Pb/^{235}U$	1σ
0.0213	0.0006	0.6	127.6	112.8	135.6	4.0	135.6	6.0
0.0236	0.0007	0.5	250.3	125.5	150.7	4.6	156.3	7.9
0.0238	0.0009	0.3	15.3	268.7	161.8	8.8	143.7	15.9
0.0240	0.0007	0.5	228.9	131.3	144.2	5.2	157.6	8.4
0.0243	0.0008	0.5	205.6	155.9	151.1	5.0	158.1	10.0
0.0244	0.0007	0.5	286.6	122.8	150.7	4.7	164.0	8.1
0.0246	0.0007	0.7	118.8	102.5	156.2	4.5	154.5	6.1
0.0247	0.0007	0.4	338.1	147.4	154.5	5.8	169.0	10.2
0.0248	0.0008	0.4	340.6	184.3	162.3	6.8	169.7	13.1
0.0250	0.0007	0.7	247.4	97.8	144.0	3.6	164.8	6.1
0.0250	0.0007	0.4	258.2	152.6	135.2	5.3	165.5	10.2
0.0250	0.0007	0.6	153.8	104.1	144.2	3.6	159.0	6.2
0.0252	0.0007	0.7	136.2	92.6	146.5	3.6	159.0	5.5
0.0253	0.0007	0.5	277.8	122.3	164.7	4.6	169.0	8.0
0.0255	0.0007	0.6	396.6	108.7	146.2	4.1	178.2	7.7
0.0256	0.0007	0.8	103.2	89.4	152.1	4.7	159.0	5.4
0.0256	0.0007	0.8	166.9	79.4	149.0	3.4	163.3	4.7
0.0256	0.0008	0.3	377.6	204.4	172.9	8.4	177.8	15.3
0.0257	0.0007	0.6	1.9	113.5	148.5	4.0	153.8	6.5
0.0270	0.0008	0.6	250.8	122.3	161.2	5.8	177.5	8.7
0.0272	0.0007	0.5	46.5	132.9	165.5	4.7	164.5	8.3
0.0272	0.0008	0.6	318.3	122.6	172.9	6.0	183.6	9.1
0.0274	0.0008	0.6	388.8	110.4	167.4	5.0	190.0	8.4
0.0278	0.0008	0.6	347.1	101.2	178.2	5.1	189.4	7.6
0.0279	0.0008	0.5	230.9	125.6	182.9	6.1	181.1	9.0
0.0281	0.0008	0.6	69.8	109.9	175.1	5.5	171.1	7.1
0.0284	0.0008	0.5	345.7	115.0	181.7	5.6	192.9	8.7
0.0286	0.0008	0.7	146.4	93.8	167.0	4.2	179.2	6.3
0.0286	0.0008	0.7	264.9	89.9	170.4	4.8	188.0	6.5
0.0287	0.0008	0.7	91.0	103.1	172.4	5.7	176.1	6.9
0.0288	0.0008	0.6	240.4	120.9	172.7	6.0	187.1	8.9
0.0289	0.0009	0.6	167.7	122.8	173.1	5.6	182.4	8.8
0.0341	0.0009	0.6	299.8	113.0	192.3	5.8	223.3	9.7
0.0344	0.0010	0.7	274.7	90.0	216.7	5.6	222.8	7.6
0.0344	0.0010	0.7	386.5	93.1	221.7	6.0	233.0	8.4
0.0346	0.0010	0.7	123.9	104.4	214.6	7.3	211.3	8.4
0.0347	0.0010	0.6	345.1	101.9	218.8	6.2	231.2	9.2
0.0348	0.0010	0.7	195.2	92.8	217.3	5.6	218.4	7.6
0.0349	0.0009	0.7	146.8	94.2	205.0	5.2	214.8	7.4
0.0351	0.0010	0.6	230.2	107.9	212.5	6.6	223.3	9.3
0.0351	0.0010	0.4	169.5	153.4	224.1	6.8	218.1	12.9
0.0352	0.0009	0.7	388.2	94.4	212.1	5.7	237.9	8.5
0.0352	0.0010	0.8	176.8	90.3	216.4	6.6	219.0	7.4
0.0353	0.0010	0.7	273.7	92.9	208.2	5.2	227.9	7.9
0.0353	0.0010	0.8	298.7	87.0	209.7	5.5	230.3	7.6
0.0354	0.0010	0.7	450.2	91.0	224.7	5.8	245.2	8.7
0.0354	0.0010	0.6	298.7	119.1	229.2	7.0	231.0	10.7

0.0355	0.0009	0.8	236.8	78.9	210.0	4.6	225.7	6.3
0.0355	0.0010	0.6	431.7	112.5	215.5	5.7	243.9	10.6
0.0355	0.0010	0.7	267.0	97.9	198.8	5.2	228.5	8.3
0.0357	0.0010	0.8	155.5	80.8	199.3	4.9	219.8	6.4
0.0357	0.0010	0.7	107.7	98.9	206.4	5.6	216.0	7.8
0.0365	0.0009	0.8	323.4	80.7	221.8	4.8	239.7	6.8
0.0365	0.0011	0.6	83.4	119.9	218.1	6.4	218.5	9.8
0.0368	0.0010	0.7	321.5	87.4	223.3	4.9	241.3	7.6
0.0369	0.0010	0.9	285.4	76.3	221.1	4.8	238.5	6.4
0.0370	0.0010	0.8	219.3	86.8	206.7	4.9	232.6	7.3
0.0373	0.0011	0.7	166.6	96.4	223.9	6.5	229.8	8.3
0.0377	0.0010	0.8	309.9	78.8	231.9	4.9	244.9	6.7
0.0377	0.0010	0.6	417.2	105.7	219.0	6.2	255.6	10.3
0.0382	0.0011	0.6	402.7	115.4	228.6	7.9	257.7	11.7
0.0383	0.0010	0.6	202.3	110.8	234.5	6.5	238.4	9.8
0.0385	0.0011	0.6	242.6	122.6	235.7	8.0	243.5	11.5
0.0393	0.0011	0.7	322.2	94.7	255.7	8.1	255.5	9.2
0.0396	0.0012	0.6	352.4	112.3	245.5	8.9	260.4	11.4
0.0397	0.0012	0.6	238.0	111.5	240.6	8.7	249.9	10.7
0.0398	0.0012	0.5	370.6	141.1	236.3	10.3	263.6	14.7
0.0398	0.0011	0.7	332.5	97.6	250.9	7.2	259.9	9.7
0.0399	0.0010	0.8	220.8	79.6	234.9	5.5	249.2	6.9
0.0401	0.0013	0.5	291.1	157.8	243.5	11.8	257.3	16.1
0.0401	0.0011	0.8	185.0	88.0	229.7	5.8	246.8	7.8
0.0401	0.0012	0.6	311.6	113.5	240.1	8.4	259.3	11.3
0.0401	0.0012	0.5	220.1	147.4	230.0	8.5	250.4	14.2
0.0406	0.0012	0.6	391.6	116.9	239.5	9.2	270.5	12.4
0.0409	0.0011	0.6	180.6	115.3	227.3	7.3	250.6	10.8
0.0411	0.0012	0.6	358.2	110.5	250.4	7.8	269.5	11.5
0.0411	0.0013	0.6	469.5	121.5	249.1	9.6	282.1	13.5
0.0414	0.0011	0.8	293.0	82.7	245.2	5.8	264.6	7.8
0.0416	0.0011	0.7	370.2	88.2	251.1	6.0	273.9	8.7
0.0417	0.0012	0.6	293.0	108.7	235.1	7.1	266.1	10.8
0.0419	0.0013	0.5	392.0	130.3	254.5	10.3	277.9	14.2
0.0421	0.0011	0.6	444.7	94.9	269.4	6.8	285.0	10.0
0.0425	0.0012	0.6	219.2	109.0	252.8	7.2	263.2	10.6
0.0425	0.0011	0.7	266.5	85.7	261.4	6.2	268.4	8.1
0.0442	0.0026	0.3	411.3	433.8	261.5	29.1	293.6	55.5
0.0449	0.0011	0.8	402.3	79.6	284.2	6.6	296.3	8.3
0.0452	0.0013	0.7	402.3	95.1	279.2	9.8	298.3	10.9
0.0452	0.0012	0.8	207.4	80.3	254.5	6.1	276.9	7.8
0.0462	0.0012	0.9	387.4	73.0	238.3	5.6	302.1	7.6
0.0474	0.0014	0.7	246.7	98.5	288.3	9.2	292.6	10.7
0.0475	0.0015	0.4	359.0	162.0	297.8	13.5	305.8	19.2

0.0992	0.0025	0.9	614.2	70.2	651.3	26.3	610.4	13.0
0.0970	0.0028	0.8	564.5	81.5	579.9	32.9	590.4	16.2
0.0962	0.0028	0.8	609.2	84.1	696.3	40.2	595.6	17.1
0.0970	0.0028	0.7	556.5	86.9	598.0	34.0	588.4	17.5
0.0961	0.0024	0.9	654.6	69.7	561.8	24.2	604.5	13.0
0.0950	0.0024	0.9	586.5	71.3	608.3	26.1	585.2	13.0
0.0970	0.0025	0.9	553.4	72.7	545.4	25.4	587.8	13.4
0.0977	0.0026	0.8	569.2	73.6	563.9	26.7	594.0	13.9

0.0998	0.0027	0.8	526.4	75.9	565.4	27.7	594.8	14.4
0.1005	0.0028	0.8	625.7	76.8	595.0	30.8	619.0	15.7
0.0990	0.0028	0.8	652.2	76.2	685.8	33.3	617.7	15.7
0.0960	0.0027	0.8	618.3	78.7	670.8	35.4	596.7	15.8

0.0561	0.0014	0.9	337.5	72.1	337.9	8.4	349.7	8.2
0.0532	0.0015	0.8	339.5	82.2	346.2	11.6	335.0	10.0
0.0542	0.0015	0.8	371.5	84.3	331.6	11.8	344.5	10.7
0.0545	0.0016	0.8	324.9	88.3	305.0	11.5	339.8	11.0
0.0541	0.0014	0.9	298.6	72.8	331.3	8.4	334.5	8.0
0.0536	0.0014	0.9	299.3	73.2	321.0	8.4	331.8	8.1
0.0534	0.0014	0.9	231.6	75.3	307.3	8.4	322.8	8.1
0.0560	0.0015	0.9	273.0	75.4	312.1	8.7	341.1	8.7
0.0541	0.0015	0.7	330.4	92.5	285.9	14.2	338.4	11.2
0.0549	0.0015	0.8	316.3	79.0	350.6	10.5	340.9	9.5
0.0553	0.0015	0.8	308.1	79.2	332.0	10.1	341.7	9.6
0.0532	0.0015	0.8	318.2	80.7	322.5	10.5	332.4	9.6

$\frac{^{206}Pb}{^{238}U}$	1σ	D, %
136.1	3.9	-0.4
150.2	4.4	4.1
151.7	5.4	-5.3
152.8	4.6	3.1
154.9	4.8	2.1
155.6	4.6	5.4
156.8	4.4	-1.5
157.1	4.5	7.6
157.7	5.1	7.6
159.1	4.2	3.6
159.1	4.6	4.0
159.3	4.2	-0.2
160.6	4.3	-1.0
161.3	4.3	4.8
162.2	4.3	9.9
162.7	4.6	-2.3
163.0	4.2	0.2
163.1	5.1	9.0
163.8	4.3	-6.1
172.0	5.1	3.2
172.8	4.6	-4.8
173.3	5.1	5.9
174.4	5.0	8.9
177.0	5.0	7.0
177.3	5.1	2.1
178.5	5.0	-4.1
180.6	4.9	6.8
181.8	4.8	-1.4
181.9	5.1	3.4
182.4	5.2	-3.5
182.9	5.3	2.3
183.5	5.3	-0.6
216.1	5.9	3.3
218.0	6.0	2.2
218.1	6.1	6.8
219.2	6.3	-3.6
220.1	6.2	5.0
220.6	6.1	-1.0
221.2	5.9	-2.9
222.5	6.4	0.4
222.6	6.2	-2.0
222.9	5.8	6.7
222.9	6.2	-1.7
223.5	5.9	2.0
223.6	6.2	3.0
224.3	6.2	9.3
224.3	6.5	3.0

224.6	5.7	0.5
224.8	6.1	8.5
224.8	5.9	1.6
225.9	5.9	-2.7
226.2	6.0	-4.5
231.2	5.8	3.7
231.2	6.5	-5.5
233.2	5.9	3.5
233.7	5.9	2.1
233.9	6.1	-0.6
236.0	6.6	-2.6
238.2	5.9	2.8
238.3	6.3	7.3
241.9	7.1	6.5
242.0	6.5	-1.5
243.5	7.1	0.0
248.2	7.0	2.9
250.2	7.3	4.1
251.0	7.3	-0.4
251.6	7.6	4.8
251.9	7.0	3.2
252.2	6.3	-1.2
253.5	8.0	1.5
253.5	6.7	-2.6
253.5	7.3	2.3
253.7	7.2	-1.3
256.6	7.6	5.4
258.2	7.0	-2.9
259.4	7.4	3.9
259.8	7.7	8.6
261.4	6.7	1.2
262.7	6.6	4.3
263.1	7.1	1.1
264.5	7.9	5.1
265.9	6.8	7.2
268.2	7.1	-1.9
268.6	6.7	-0.1
279.0	15.7	5.2
283.0	7.0	4.7
285.0	8.1	4.7
285.2	7.4	-2.9
291.1	7.2	3.8
298.2	8.4	-1.9
299.1	9.0	2.2

609.4	14.6	0.2
596.9	16.1	-1.1
591.8	16.2	0.6
596.5	16.5	-1.4
591.2	14.3	2.2
584.8	14.3	0.1
596.7	14.8	-1.5
600.6	15.1	-1.1

613.1	15.6	-3.0
617.3	16.3	0.3
608.3	16.2	1.5
590.9	15.9	1.0

351.5	8.6	-0.5
334.3	9.2	0.2
340.4	9.4	1.2
341.9	9.6	-0.6
339.6	8.4	-1.5
336.3	8.4	-1.3
335.5	8.4	-3.8
351.2	8.9	-2.9
339.7	9.0	-0.4
344.7	9.3	-1.1
346.7	9.4	-1.4
334.4	9.1	-0.6

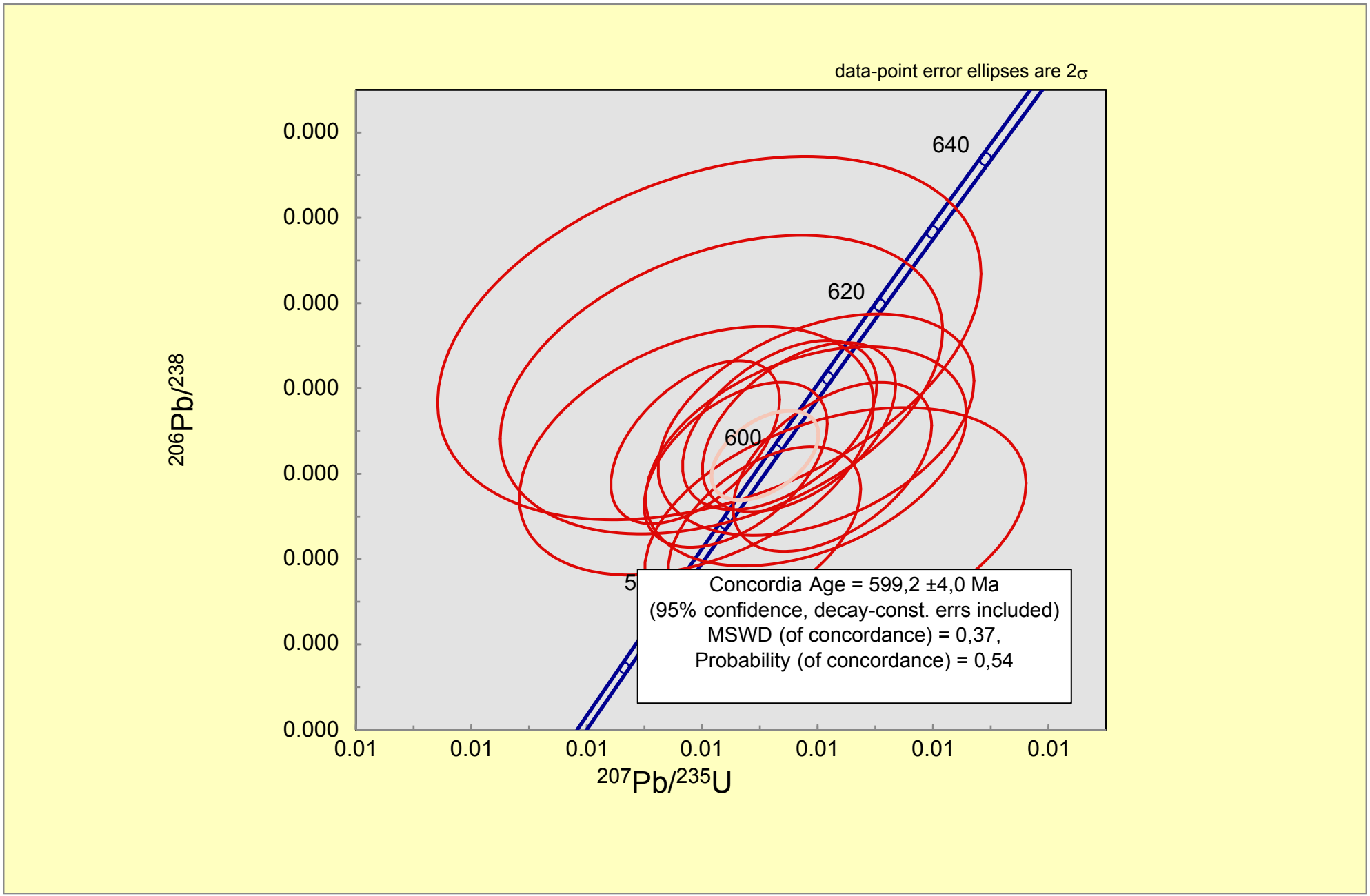
data-point error ellipses are 2σ
640
620
600
0.000
0.000
0.000
0.000
0.000
0.000
0.01
0.01
0.01
0.01
0.01
0.01
0.01
206Pb/238
207Pb/235U
Concordia Age = 599,2 ±4,0 Ma
(95% confidence, decay-const. errs included)
MSWD (of concordance) = 0,37,
Probability (of concordance) = 0,54

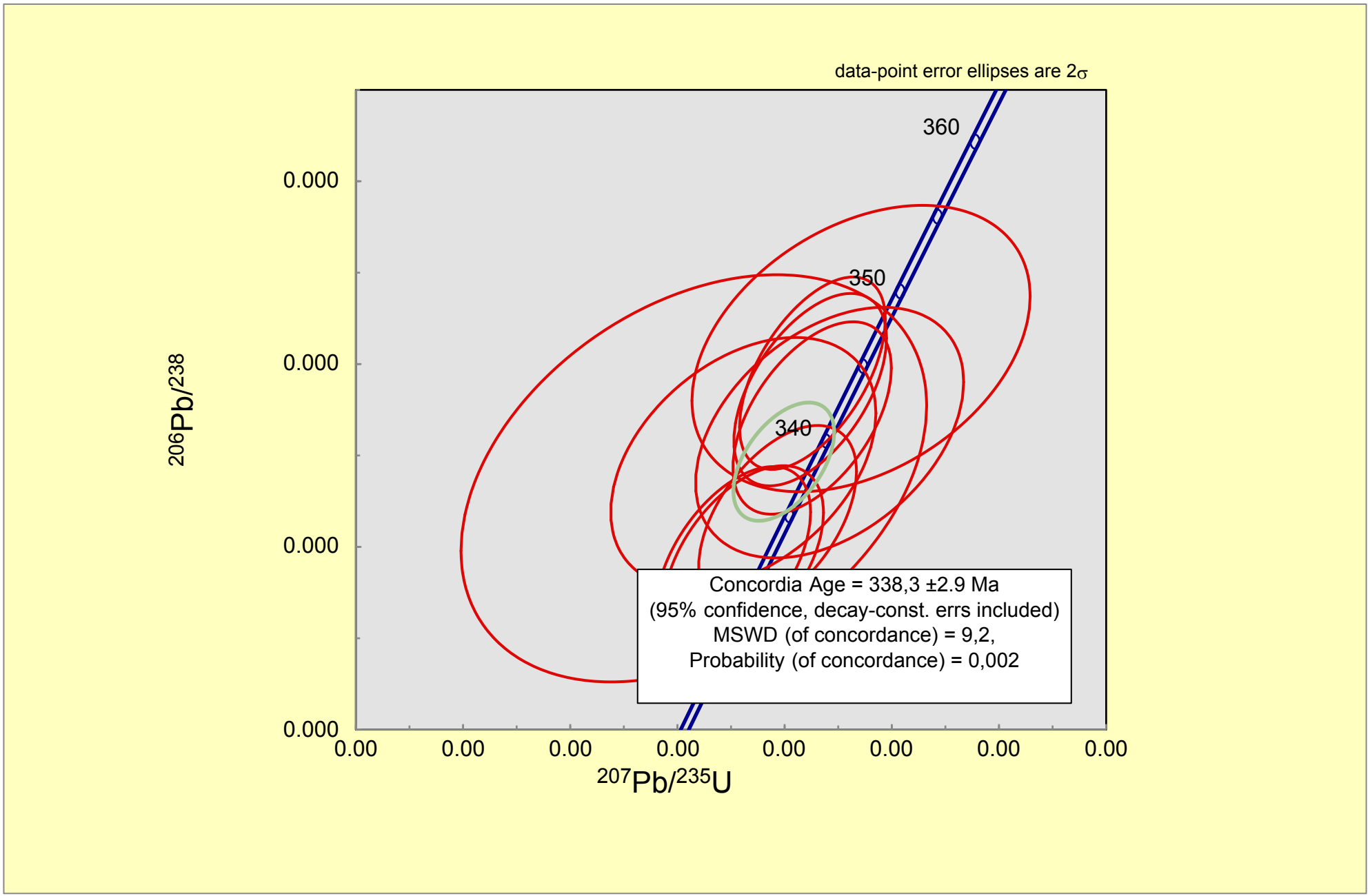
data-point error ellipses are 2σ
360
350
340
0.000
0.000
0.000
0.000
0.00
0.00
0.00
0.00
0.00
0.00
0.00
0.00
206Pb/238
207Pb/235U
Concordia Age = 338,3 ±2.9 Ma
(95% confidence, decay-const. errs included)
MSWD (of concordance) = 9,2,
Probability (of concordance) = 0,002

#	Isotope ratio							
	$\frac{Th}{U}$	1σ (abs)	$\frac{^{207}Pb}{^{206}Pb}$	1σ (abs)	$\frac{^{208}Pb}{^{232}Th}$	1σ (abs)	$\frac{^{207}Pb}{^{235}U}$	1σ (abs)
GUS-14-6	number of sample		76 zircons					
PRB91	0.72	0.0153	0.0458	0.0023	0.0055	0.0002	0.1146	0.0056
PRB43	0.72	0.0102	0.0499	0.0018	0.0079	0.0002	0.1850	0.0063
PRB33	0.32	0.0045	0.0501	0.0010	0.0084	0.0001	0.1922	0.0033
PRB62	0.33	0.0057	0.0547	0.0024	0.0101	0.0004	0.2102	0.0088
PRB88	0.87	0.0176	0.0486	0.0019	0.0088	0.0003	0.1888	0.0071
PRB86	0.49	0.0099	0.0471	0.0019	0.0085	0.0003	0.1843	0.0073
PRB102	0.56	0.0146	0.0504	0.0025	0.0090	0.0004	0.1995	0.0096
PRB94	0.82	0.0182	0.0454	0.0020	0.0087	0.0003	0.1798	0.0076
PRB54	0.98	0.0138	0.0499	0.0014	0.0083	0.0001	0.1975	0.0053
PRB60	0.32	0.0054	0.0506	0.0022	0.0092	0.0003	0.2005	0.0082
PRB55	0.66	0.0093	0.0519	0.0010	0.0086	0.0001	0.2060	0.0037
PRB98	0.32	0.0086	0.0545	0.0045	0.0097	0.0007	0.2167	0.0176
PRB15	0.10	0.0014	0.0498	0.0010	0.0090	0.0002	0.2000	0.0037
PRB45	0.43	0.0060	0.0497	0.0011	0.0090	0.0002	0.2004	0.0042
PRB22	0.50	0.0072	0.0516	0.0017	0.0083	0.0002	0.2085	0.0067
PRB49	0.50	0.0072	0.0509	0.0014	0.0090	0.0002	0.2066	0.0052
PRB56	0.72	0.0122	0.0501	0.0022	0.0095	0.0003	0.2042	0.0086
PRB59	0.85	0.0144	0.0508	0.0019	0.0097	0.0003	0.2073	0.0076
PRB74	0.36	0.0062	0.0495	0.0016	0.0091	0.0003	0.2033	0.0064
PRB9	0.56	0.0079	0.0514	0.0014	0.0098	0.0002	0.2108	0.0056
PRB70	0.39	0.0067	0.0527	0.0025	0.0093	0.0004	0.2165	0.0099
PRB57	0.50	0.0086	0.0545	0.0025	0.0095	0.0003	0.2237	0.0099
PRB52	0.42	0.0059	0.0505	0.0011	0.0091	0.0002	0.2077	0.0042
PRB41	0.05	0.0008	0.0558	0.0011	0.0160	0.0004	0.2332	0.0041
PRB96	1.57	0.0369	0.0466	0.0021	0.0088	0.0004	0.1929	0.0085
PRB21	0.30	0.0043	0.0521	0.0012	0.0100	0.0002	0.2156	0.0047
PRB63	0.41	0.0067	0.0507	0.0015	0.0101	0.0003	0.2102	0.0059
PRB99	0.28	0.0069	0.0477	0.0022	0.0092	0.0004	0.1980	0.0089
PRB17	0.39	0.0056	0.0506	0.0013	0.0096	0.0002	0.2107	0.0051
PRB71	0.62	0.0106	0.0475	0.0018	0.0096	0.0003	0.1989	0.0074
PRB69	0.37	0.0062	0.0488	0.0017	0.0100	0.0003	0.2054	0.0068
PRB44	0.74	0.0106	0.0553	0.0017	0.0090	0.0002	0.2325	0.0067
PRB107	0.46	0.0133	0.0461	0.0025	0.0093	0.0005	0.1953	0.0102
PRB78	0.46	0.0084	0.0472	0.0021	0.0102	0.0003	0.2000	0.0088
PRB104	0.59	0.0156	0.0479	0.0023	0.0093	0.0004	0.2045	0.0095
PRB80	0.43	0.0078	0.0495	0.0014	0.0099	0.0003	0.2122	0.0059
PRB100	0.98	0.0244	0.0486	0.0022	0.0098	0.0004	0.2095	0.0094
PRB108	0.72	0.0212	0.0483	0.0025	0.0097	0.0005	0.2079	0.0107
PRB37	0.56	0.0085	0.0498	0.0031	0.0096	0.0004	0.2163	0.0129
PRB73	0.36	0.0061	0.0495	0.0013	0.0101	0.0002	0.2157	0.0056
PRB64	0.48	0.0080	0.0522	0.0016	0.0107	0.0003	0.2273	0.0066
PRB47	0.49	0.0103	0.0518	0.0069	0.0101	0.0009	0.2263	0.0299
PRB4	0.43	0.0061	0.0515	0.0011	0.0095	0.0002	0.2273	0.0047
PRB39	0.45	0.0074	0.0532	0.0042	0.0099	0.0005	0.2354	0.0183
PRB25	0.04	0.0006	0.0493	0.0009	0.0098	0.0004	0.2182	0.0035
PRB7	0.37	0.0055	0.0510	0.0021	0.0101	0.0003	0.2311	0.0093
PRB92	0.28	0.0091	0.0541	0.0067	0.0149	0.0015	0.2457	0.0297
PRB53	0.52	0.0074	0.0537	0.0013	0.0098	0.0002	0.2464	0.0056

PRB20	0.29	0.0043	0.0558	0.0015	0.0145	0.0003	0.2655	0.0067
PRB77	0.38	0.0069	0.0471	0.0019	0.0110	0.0004	0.2318	0.0089
PRB27	0.26	0.0038	0.0470	0.0014	0.0112	0.0003	0.2343	0.0069
PRB79	0.31	0.0056	0.0506	0.0016	0.0120	0.0003	0.2566	0.0077
PRB95	0.83	0.0189	0.0563	0.0030	0.0113	0.0005	0.2877	0.0149
PRB26	1.11	0.0157	0.0534	0.0015	0.0114	0.0002	0.2760	0.0075
PRB29	0.80	0.0116	0.0519	0.0021	0.0123	0.0003	0.2717	0.0104
PRB23	0.72	0.0102	0.0502	0.0012	0.0117	0.0002	0.2667	0.0057
PRB85	0.64	0.0126	0.0545	0.0028	0.0124	0.0005	0.2959	0.0145
PRB76	0.54	0.0097	0.0557	0.0025	0.0133	0.0004	0.3131	0.0133
PRB97	0.90	0.0217	0.0539	0.0029	0.0133	0.0006	0.3227	0.0170
PRB101	0.51	0.0130	0.0480	0.0024	0.0165	0.0008	0.3295	0.0162
PRB61	0.37	0.0064	0.0532	0.0021	0.0166	0.0006	0.3757	0.0145
PRB109	0.75	0.0224	0.0490	0.0031	0.0160	0.0009	0.3645	0.0227
PRB93	1.65	0.0361	0.0541	0.0023	0.0172	0.0006	0.4269	0.0175
PRB24	0.60	0.0088	0.0602	0.0019	0.0205	0.0004	0.5061	0.0151
PRB50	0.25	0.0035	0.0569	0.0012	0.0191	0.0004	0.5411	0.0100
PRB67	0.36	0.0061	0.0556	0.0015	0.0231	0.0006	0.5628	0.0139
PRB87	0.83	0.0171	0.0572	0.0025	0.0236	0.0008	0.5824	0.0244
PRB84	0.24	0.0046	0.0537	0.0016	0.0219	0.0006	0.5649	0.0159
PRB42	0.43	0.0061	0.0581	0.0010	0.0212	0.0003	0.6278	0.0094
PRB103	0.77	0.0203	0.0543	0.0025	0.0239	0.0011	0.6162	0.0281
PRB34	0.82	0.0118	0.0668	0.0013	0.0411	0.0006	1.2616	0.0228
PRB110	0.97	0.0297	0.0663	0.0038	0.0421	0.0023	1.2739	0.0713
PRB14	0.86	0.0129	0.0702	0.0019	0.0427	0.0008	1.4308	0.0363
PRB16	0.35	0.0054	0.0755	0.0016	0.0505	0.0011	1.8130	0.0364
PRB51	0.58	0.0099	0.1096	0.0025	0.0888	0.0019	4.7380	0.0990
PRB90	0.25	0.0053	0.1427	0.0047	0.1568	0.0052	6.6377	0.2097
Standart	**GJ-1**							
GJ1	0.03	0.0005	0.0577	0.0010	0.0330	0.0013	0.7776	0.0120
GJ10	0.03	0.0007	0.0578	0.0019	0.0303	0.0018	0.7780	0.0251
GJ11	0.03	0.0008	0.0576	0.0024	0.0335	0.0021	0.7867	0.0313
GJ12	0.03	0.0010	0.0567	0.0028	0.0292	0.0021	0.7825	0.0385
GJ2	0.03	0.0005	0.0591	0.0011	0.0301	0.0013	0.7916	0.0130
GJ3	0.03	0.0006	0.0608	0.0011	0.0050	0.0016	0.8016	0.0136
GJ4	0.03	0.0006	0.0602	0.0011	0.0310	0.0014	0.8136	0.0137
GJ5	0.03	0.0006	0.0616	0.0012	0.0290	0.0015	0.8251	0.0141
GJ6	0.03	0.0006	0.0597	0.0011	0.0334	0.0015	0.8069	0.0138
GJ7	0.02	0.0006	0.0626	0.0022	0.0306	0.0019	0.8261	0.0270
GJ8	0.02	0.0006	0.0608	0.0018	0.0349	0.0021	0.8160	0.0227
GJ9	0.03	0.0006	0.0605	0.0017	0.0327	0.0018	0.8194	0.0224
Standart	**Plesovice**							
PL1	0.10	0.0015	0.0522	0.0008	0.0160	0.0003	0.3952	0.0056
PL10	0.10	0.0019	0.0488	0.0016	0.0152	0.0006	~~0.3604~~	~~0.0112~~
PL11	0.10	0.0024	0.0494	0.0020	0.0154	0.0007	~~0.3756~~	~~0.0144~~
PL12	0.10	0.0029	0.0504	0.0024	0.0167	0.0009	0.3731	0.0178
PL2	0.10	0.0015	0.0524	0.0009	0.0166	0.0003	0.3948	0.0058
PL3	0.10	0.0015	0.0527	0.0009	0.0151	0.0003	0.3951	0.0060
PL4	0.10	0.0015	0.0523	0.0009	0.0150	0.0003	0.3804	0.0059
PL5	0.10	0.0015	0.0529	0.0009	0.0154	0.0003	0.3887	0.0060
PL6	0.10	0.0015	0.0525	0.0009	0.0156	0.0003	0.3824	0.0061
PL7	0.09	0.0015	0.0532	0.0018	0.0169	0.0006	0.4043	0.0129

PL8	0.08	0.0014	0.0514	0.0014	0.0185	0.0006	0.3823	0.0101
PL9	0.09	0.0016	0.0533	0.0014	0.0164	0.0005	0.3984	0.0102

			Age, Ma					
$^{206}Pb/^{238}U$	1σ (abs)	Rho	$^{207}Pb/^{206}Pb$	1σ	$^{208}Pb/^{232}Th$	1σ	$^{207}Pb/^{235}U$	1σ
0.0181	0.0003	0.3	0.1	103.9	111	4.3	110.2	5.1
0.0269	0.0003	0.3	190.7	80.5	158.3	3.3	172.4	5.4
0.0278	0.0002	0.5	201.2	43.7	169.4	2.6	178.5	2.8
0.0279	0.0004	0.3	401	94.2	202.7	7.2	193.7	7.4
0.0282	0.0004	0.4	128.6	88.7	177.5	5.8	175.6	6.1
0.0283	0.0004	0.3	56.1	94.6	171.4	5.9	171.7	6.2
0.0287	0.0005	0.3	214.8	110.0	180.4	8.3	184.7	8.1
0.0287	0.0004	0.3	0.1	65.1	175.5	6.6	167.8	6.6
0.0288	0.0003	0.3	187.9	64.6	167.1	2.7	183	4.5
0.0287	0.0004	0.3	222.2	95.6	185.7	6.7	185.5	6.9
0.0288	0.0002	0.5	282.5	44.6	172.9	2.3	190.2	3.1
0.0288	0.0006	0.3	392.9	176.2	194.8	14.4	199.2	14.7
0.0292	0.0002	0.5	184.1	45.8	180.4	4.6	185.1	3.1
0.0292	0.0003	0.4	182.1	51.4	181.9	3.0	185.4	3.5
0.0293	0.0003	0.3	268.5	75.2	167.6	4.2	192.3	5.6
0.0295	0.0003	0.4	234.1	60.0	180.1	3.3	190.7	4.3
0.0296	0.0004	0.3	199.9	98.1	191.4	6.3	188.7	7.2
0.0296	0.0004	0.3	230	85.6	194.1	5.7	191.3	6.4
0.0298	0.0003	0.4	171.1	74.5	183.2	5.1	187.9	5.4
0.0298	0.0003	0.4	256.4	62.7	196.2	3.5	194.2	4.7
0.0298	0.0004	0.3	317.2	103.7	187.8	7.0	199	8.3
0.0298	0.0004	0.3	391.2	99.2	191.2	6.9	205	8.2
0.0299	0.0003	0.4	216.6	49.8	182.6	3.0	191.6	3.5
0.0303	0.0003	0.5	444.6	42.2	320.8	8.4	212.9	3.4
0.0300	0.0005	0.3	30.4	105.0	177.8	7.0	179.1	7.2
0.0300	0.0003	0.4	290.5	52.1	201.4	3.8	198.3	3.9
0.0301	0.0003	0.4	227.5	66.5	202.1	5.3	193.7	4.9
0.0301	0.0005	0.3	82.3	106.9	185.8	8.4	183.4	7.6
0.0302	0.0003	0.4	223.4	58.2	192.4	3.7	194.2	4.3
0.0304	0.0004	0.3	71.4	90.1	193.2	5.3	184.2	6.3
0.0305	0.0003	0.3	137.8	79.5	201.5	5.7	189.7	5.8
0.0305	0.0003	0.3	422.9	65.6	182	3.4	212.3	5.5
0.0307	0.0006	0.3	1.6	123.6	186.2	9.7	181.1	8.7
0.0308	0.0004	0.3	56.6	104.8	205.4	6.9	185.1	7.4
0.0310	0.0005	0.4	93.6	109.2	187.7	8.7	188.9	8.0
0.0311	0.0003	0.4	172.7	66.6	199.5	5.2	195.4	5.0
0.0312	0.0005	0.3	130.7	104.9	197	8.4	193.1	7.9
0.0313	0.0006	0.3	111.5	119.3	196	10.1	191.8	9.0
0.0315	0.0004	0.2	187.5	136.6	193.1	7.1	198.8	10.8
0.0316	0.0003	0.4	172.3	62.1	202.1	4.8	198.3	4.6
0.0316	0.0003	0.4	294.2	67.9	215.1	5.6	208	5.4
0.0317	0.0008	0.2	274.5	281.2	203.6	17.7	207.2	24.7
0.0320	0.0003	0.4	264.7	50.1	191.3	3.2	208	3.9
0.0321	0.0005	0.2	338.5	170.2	199.3	10.3	214.6	15.1
0.0321	0.0003	0.5	162.6	41.2	197.9	7.2	200.4	2.9
0.0329	0.0004	0.3	239.8	92.9	203.3	6.6	211.1	7.6
0.0329	0.0010	0.2	375.6	256.8	299.2	29.7	223.1	24.2
0.0333	0.0003	0.4	356.6	53.6	197.7	3.4	223.6	4.5

0.0345	0.0003	0.4	445.4	58.1	290.8	6.0	239.1	5.4
0.0357	0.0004	0.3	51.4	93.0	220	7.1	211.7	7.4
0.0362	0.0004	0.3	47.4	72.0	225.8	6.1	213.7	5.6
0.0368	0.0004	0.4	222.9	70.7	240.6	6.7	231.9	6.2
0.0371	0.0006	0.3	463.2	114.5	226.6	9.5	256.7	11.7
0.0375	0.0004	0.4	345.8	63.6	229.2	3.5	247.5	6.0
0.0380	0.0004	0.3	281.4	88.5	247.3	5.4	244	8.3
0.0386	0.0003	0.4	202.9	52.7	235.8	3.4	240.1	4.6
0.0393	0.0006	0.3	393	108.8	249.2	9.2	263.2	11.3
0.0408	0.0005	0.3	440.9	94.9	266.7	8.7	276.6	10.3
0.0434	0.0007	0.3	365.9	116.5	266	11.7	284	13.0
0.0498	0.0008	0.3	98.3	115.9	331	15.3	289.1	12.4
0.0512	0.0006	0.3	337.6	88.4	332.5	11.0	323.9	10.7
0.0540	0.0011	0.3	147.7	142.4	321.6	17.9	315.5	16.9
0.0572	0.0008	0.3	375.1	91.6	344.8	12.2	360.9	12.4
0.0610	0.0006	0.3	610.6	66.2	410.8	8.5	415.8	10.2
0.0690	0.0006	0.5	487.4	44.0	381.9	7.7	439.2	6.6
0.0734	0.0008	0.4	435.6	57.0	461.3	10.8	453.3	9.0
0.0739	0.0010	0.3	497.3	92.9	471.8	16.0	466	15.6
0.0763	0.0009	0.4	358.4	64.7	437.5	12.3	454.7	10.3
0.0784	0.0006	0.5	534.5	37.0	423.7	5.6	494.7	5.9
0.0824	0.0013	0.4	381.9	100.8	477.9	21.5	487.5	17.6
0.1371	0.0012	0.5	831.7	40.6	814.9	10.8	828.6	10.2
0.1395	0.0027	0.3	814.3	114.5	833	44.3	834.1	31.8
0.1480	0.0015	0.4	933.3	54.2	844.5	14.8	901.9	15.1
0.1744	0.0016	0.5	1081	42.9	994.8	20.3	1050.2	13.1
0.3137	0.0033	0.5	1793.1	40.2	1720	35.4	1774	17.5
0.3374	0.0042	0.4	2259.6	55.4	2943.9	90.1	2064.4	27.9
0.0977	0.0008	0.5	519.6	37.6	656.5	24.9	584.1	6.8
0.0975	0.0012	0.4	523.1	71.6	602.7	35.4	584.3	14.3
0.0991	0.0014	0.4	513.1	87.7	666.4	40.1	589.3	17.8
0.1002	0.0017	0.4	477.5	107.7	581.8	41.9	586.9	21.9
0.0972	0.0008	0.5	570.8	39.0	599	26.3	592.1	7.4
0.0957	0.0008	0.5	631.8	39.9	100.8	31.3	597.7	7.7
0.0981	0.0008	0.5	610.6	39.6	616.4	27.5	604.4	7.7
0.0972	0.0008	0.5	661.4	39.8	578.5	29.6	610.9	7.8
0.0981	0.0008	0.5	591.5	40.2	663.8	29.7	600.7	7.7
0.0958	0.0011	0.4	694.4	71.7	610	37.3	611.5	15.0
0.0974	0.0011	0.4	630.3	61.9	693.7	40.7	605.8	12.7
0.0982	0.0011	0.4	622.8	60.6	650.9	35.8	607.7	12.5
0.0549	0.0004	0.6	296.1	36.1	320.7	5.6	338.2	4.0
~~0.0535~~	~~0.0006~~	~~0.4~~	139.2	74.3	304.3	11.0	312.5	8.4
~~0.0552~~	~~0.0008~~	~~0.4~~	165.1	89.6	308.9	13.1	323.8	10.6
0.0538	0.0009	0.4	211	108.6	334.7	17.3	321.9	13.1
0.0547	0.0004	0.5	301.2	37.4	332.2	6.2	337.9	4.2
0.0544	0.0004	0.5	316.2	38.4	302.8	6.2	338.1	4.4
0.0529	0.0004	0.5	296.2	39.0	301.6	6.3	327.4	4.3
0.0533	0.0004	0.5	325.5	38.8	309.3	6.4	333.4	4.4
0.0529	0.0004	0.5	306.9	39.8	313.8	6.7	328.8	4.5
0.0552	0.0006	0.4	335.8	74.5	338	12.1	344.7	9.3

0.0539	0.0006	0.4	259.6	62.9	369.7	11.4	328.7	7.4
0.0543	0.0006	0.4	339.4	60.7	328.2	9.9	340.5	7.4

$\frac{^{206}Pb}{^{238}U}$	1σ	D, %
115.9	1.7	-4.9
171.1	1.8	0.8
176.9	1.4	0.9
177.1	2.3	9.4
179	2.3	-1.9
180.1	2.3	-4.7
182.3	3.0	1.3
182.7	2.6	-8.2
182.7	1.7	0.2
182.7	2.3	1.5
183	1.5	3.9
183.2	4.0	8.7
185.3	1.5	-0.1
185.8	1.6	-0.2
186.3	1.9	3.2
187.3	1.7	1.8
187.8	2.4	0.5
188.2	2.2	1.6
189.2	2.1	-0.7
189.2	1.7	2.6
189.2	2.5	5.2
189.2	2.5	8.4
189.7	1.6	1.0
192.6	1.6	10.5
190.6	2.8	-6.0
190.7	1.6	4.0
191	2.0	1.4
191.3	2.9	-4.1
191.9	1.7	1.2
193	2.3	-4.6
193.9	2.2	-2.2
193.9	1.9	9.5
195.2	3.5	-7.2
195.2	2.5	-5.2
196.5	3.2	-3.9
197.2	2.1	-0.9
198.3	3.1	-2.6
198.4	3.5	-3.3
199.9	2.8	-0.6
200.4	2.0	-1.0
200.4	2.1	3.8
201.4	5.1	2.9
203.1	1.7	2.4
203.6	3.4	5.4
203.8	1.6	-1.7
208.7	2.3	1.1
208.8	6.1	6.8
211.3	1.8	5.8

218.7	2.0	9.3
226.2	2.7	-6.4
229.2	2.2	-6.8
232.7	2.5	-0.3
234.6	3.8	9.4
237.4	2.2	4.3
240.3	2.7	1.5
244	2.1	-1.6
248.8	3.6	5.8
257.5	3.4	7.4
274.1	4.5	3.6
313.1	5.0	-7.7
322	3.9	0.6
338.8	6.6	-6.9
358.6	4.9	0.6
381.8	3.8	8.9
430.2	3.5	2.1
456.7	4.5	-0.7
459.4	6.2	1.4
473.8	5.1	-4.0
486.4	3.7	1.7
510.2	8.0	-4.4
828	6.7	0.1
841.8	15.4	-0.9
889.7	8.4	1.4
1036	8.8	1.4
1758.8	16.3	0.9
1874.1	20.3	10.2

601.1	4.6	-2.8
600	7.0	-2.6
609.1	8.4	-3.3
615.5	10.2	-4.6
598	4.7	-1.0
589.1	4.7	1.5
603.2	4.7	0.2
597.7	4.7	2.2
603.5	4.8	-0.5
589.5	6.7	3.7
599.2	6.2	1.1
603.5	6.2	0.7

344.5	2.6	-1.8
336.1	3.9	-7.0
346.2	4.7	-6.5
337.5	5.6	-4.6
343.4	2.6	-1.6
341.5	2.6	-1.0
332	2.6	-1.4
334.7	2.6	-0.4
332.1	2.6	-1.0
346.2	3.9	-0.4

338.5	3.4	-2.9
340.5	3.5	0.0

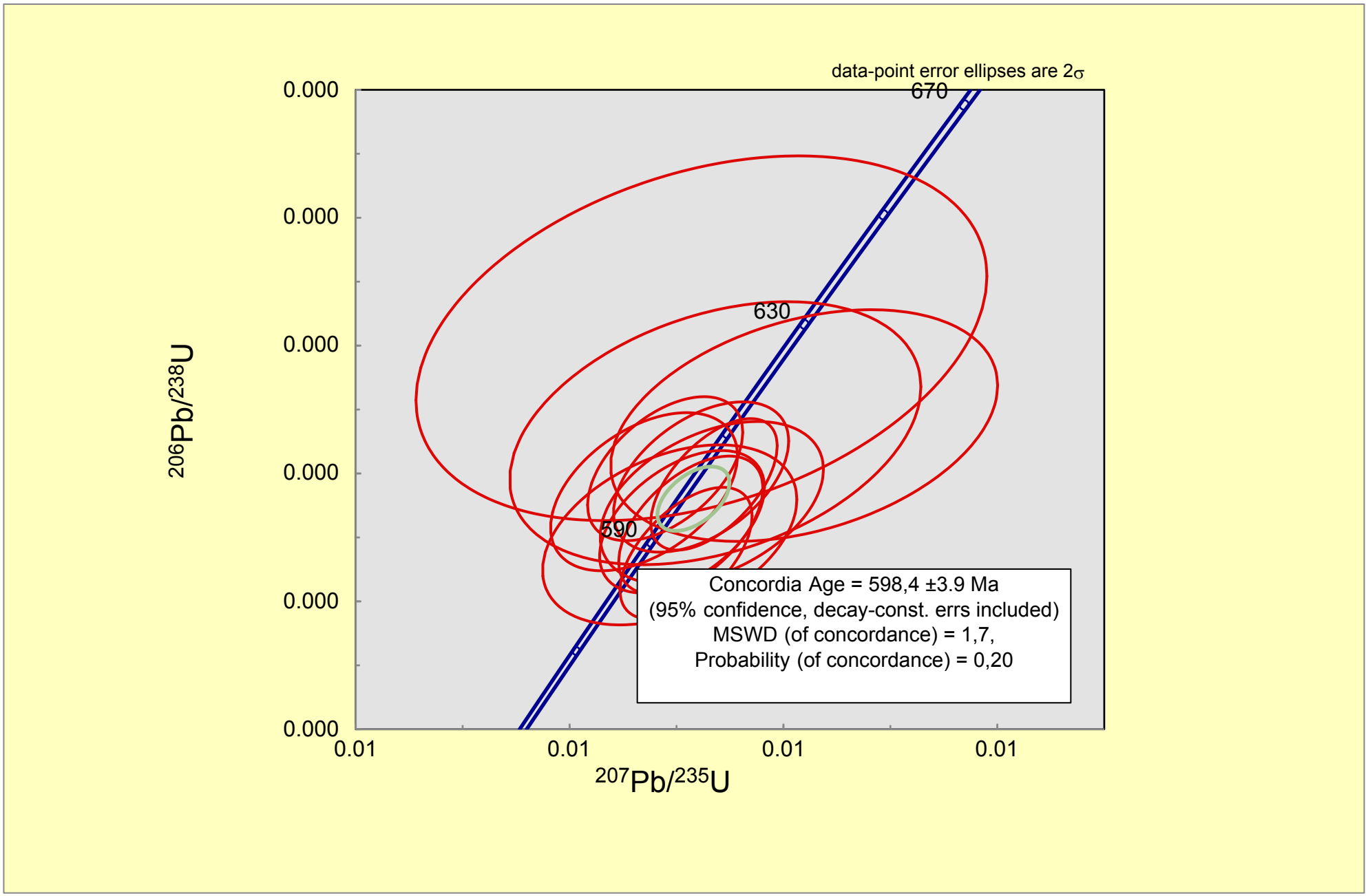
data-point error ellipses are 2σ
670
630
590
0.000
0.000
0.000
0.000
0.000
0.01
0.01
0.01
0.01
206Pb/238U
207Pb/235U
Concordia Age = 598,4 ±3.9 Ma
(95% confidence, decay-const. errs included)
MSWD (of concordance) = 1,7,
Probability (of concordance) = 0,20

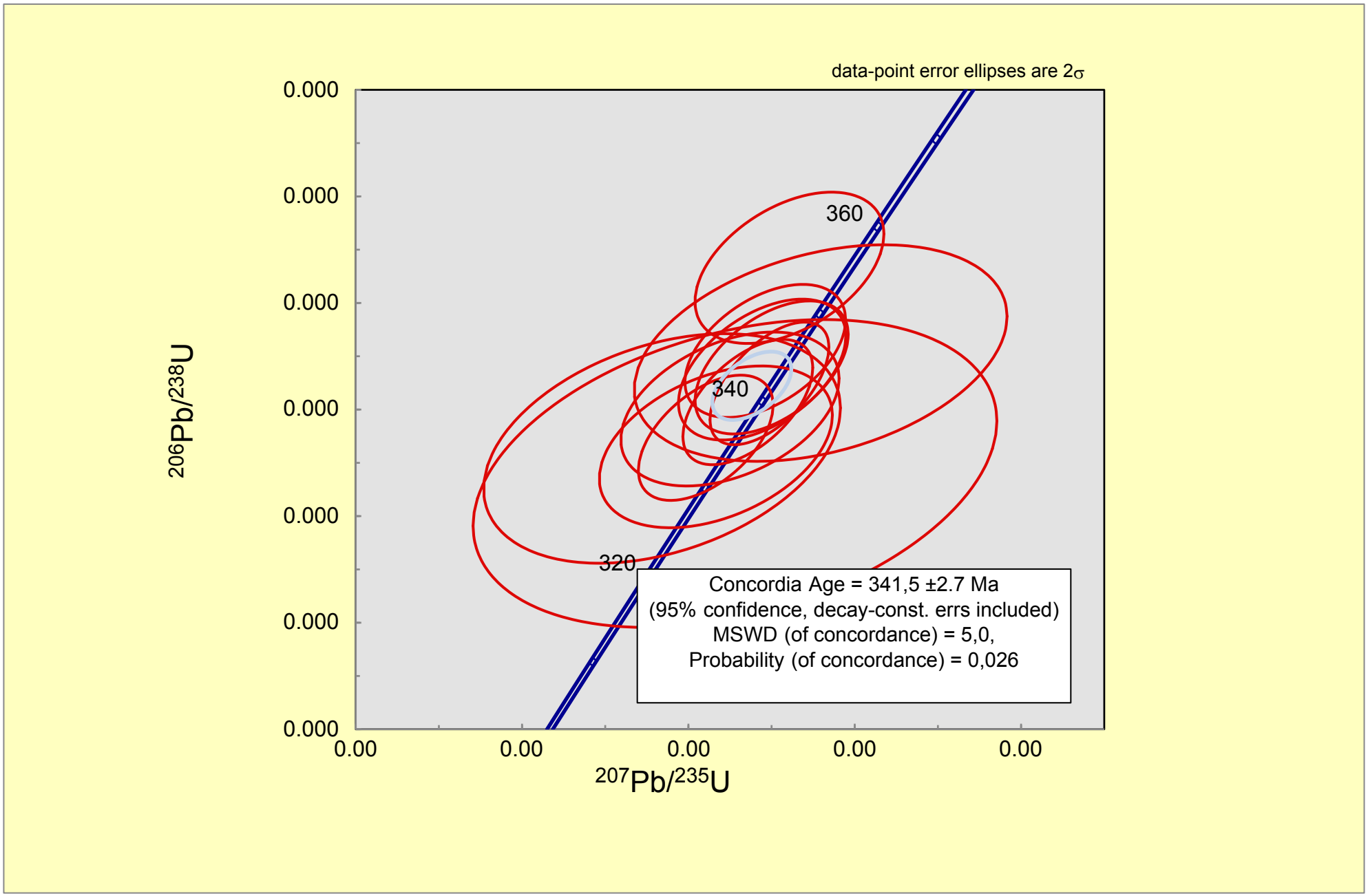
data-point error ellipses are 2σ
0.000
0.000
0.000
0.000
0.000
0.000
360
340
320
Concordia Age = 341,5 ±2.7 Ma
(95% confidence, decay-const. errs included)
MSWD (of concordance) = 5,0,
Probability (of concordance) = 0,026
0.00
0.00
0.00
0.00
0.00
206Pb/238U
207Pb/235U

#	Isotope ratio							
	$\frac{Th}{U}$	1σ (abs)	$\frac{^{207}Pb}{^{206}Pb}$	1σ (abs)	$\frac{^{208}Pb}{^{232}Th}$	1σ (abs)	$\frac{^{207}Pb}{^{235}U}$	1σ (abs)
GUS-14-1	number of sample		103 zircons					
PRB72	1.1555	0.0190	0.0500	0.0018	0.0082	0.0002	0.1731	0.0060
PRB57	2.1293	0.0350	0.0496	0.0015	0.0080	0.0001	0.1750	0.0051
PRB22	0.1512	0.0027	0.0503	0.0016	0.0086	0.0003	0.1786	0.0054
PRB90	0.4214	0.0071	0.0507	0.0018	0.0089	0.0002	0.1824	0.0062
PRB19	0.5837	0.0100	0.0489	0.0013	0.0084	0.0002	0.1769	0.0044
PRB5	0.7865	0.0160	0.0525	0.0025	0.0092	0.0004	0.1916	0.0085
PRB42	0.7710	0.0211	0.0494	0.0027	0.0079	0.0004	0.1820	0.0097
PRB80	0.6123	0.0100	0.0491	0.0011	0.0088	0.0002	0.1813	0.0039
PRB78	1.2360	0.0203	0.0530	0.0015	0.0087	0.0002	0.1965	0.0054
PRB103	0.6125	0.0106	0.0538	0.0026	0.0082	0.0003	0.1999	0.0093
PRB83	0.6243	0.0103	0.0483	0.0011	0.0088	0.0002	0.1799	0.0037
PRB31	0.6244	0.0129	0.0489	0.0020	0.0084	0.0003	0.1820	0.0072
PRB26	0.5240	0.0096	0.0528	0.0017	0.0086	0.0002	0.1985	0.0059
PRB87	0.6243	0.0104	0.0503	0.0015	0.0090	0.0002	0.1898	0.0055
PRB4	0.7588	0.0156	0.0512	0.0023	0.0093	0.0004	0.1942	0.0083
PRB39	0.8900	0.0216	0.0503	0.0025	0.0083	0.0004	0.1921	0.0092
PRB35	0.9537	0.0210	0.0505	0.0020	0.0085	0.0003	0.1930	0.0076
PRB71	0.6742	0.0111	0.0519	0.0014	0.0088	0.0002	0.1986	0.0052
PRB29	0.8749	0.0167	0.0533	0.0023	0.0085	0.0003	0.2040	0.0085
PRB2	0.4028	0.0085	0.0515	0.0024	0.0095	0.0004	0.1984	0.0087
PRB13	0.4246	0.0075	0.0516	0.0014	0.0090	0.0002	0.1988	0.0050
PRB40	0.7503	0.0186	0.0484	0.0024	0.0083	0.0004	0.1871	0.0091
PRB77	0.6807	0.0111	0.0503	0.0010	0.0088	0.0001	0.1953	0.0036
PRB37	0.1087	0.0026	0.0491	0.0021	0.0084	0.0004	0.1918	0.0079
PRB59	0.3126	0.0052	0.0495	0.0012	0.0090	0.0002	0.1937	0.0044
PRB36	0.4416	0.0101	0.0505	0.0021	0.0088	0.0004	0.1977	0.0079
PRB30	0.8557	0.0164	0.0492	0.0015	0.0088	0.0002	0.1929	0.0056
PRB92	0.3366	0.0056	0.0509	0.0014	0.0099	0.0002	0.1997	0.0053
PRB25	0.5354	0.0096	0.0495	0.0014	0.0090	0.0002	0.1947	0.0054
PRB55	0.7384	0.0277	0.0460	0.0036	0.0079	0.0006	0.1808	0.0141
PRB49	0.3659	0.0118	0.0547	0.0040	0.0084	0.0006	0.2156	0.0154
PRB48	0.2792	0.0088	0.0511	0.0033	0.0083	0.0005	0.2018	0.0129
PRB91	0.4262	0.0071	0.0502	0.0013	0.0099	0.0002	0.1986	0.0050
PRB43	0.5882	0.0164	0.0490	0.0027	0.0083	0.0004	0.1943	0.0106
PRB8	1.0195	0.0195	0.0489	0.0019	0.0097	0.0003	0.1939	0.0070
PRB24	0.4552	0.0082	0.0477	0.0018	0.0094	0.0003	0.1898	0.0071
PRB73	0.3299	0.0054	0.0513	0.0012	0.0092	0.0002	0.2044	0.0044
PRB110	0.8839	0.0152	0.0482	0.0013	0.0092	0.0002	0.1924	0.0052
PRB53	0.7311	0.0265	0.0500	0.0038	0.0081	0.0006	0.1994	0.0150
PRB50	0.4886	0.0158	0.0483	0.0031	0.0083	0.0005	0.1935	0.0122
PRB21	0.6680	0.0115	0.0516	0.0013	0.0094	0.0002	0.2073	0.0048
PRB65	0.8271	0.0136	0.0509	0.0014	0.0095	0.0002	0.2049	0.0054
PRB23	1.2473	0.0219	0.0531	0.0018	0.0091	0.0002	0.2136	0.0070
PRB18	0.5525	0.0095	0.0518	0.0018	0.0092	0.0002	0.2084	0.0069
PRB17	0.7132	0.0122	0.0547	0.0015	0.0097	0.0002	0.2203	0.0058
PRB45	0.4725	0.0139	0.0548	0.0041	0.0097	0.0006	0.2206	0.0160
PRB84	0.3867	0.0064	0.0487	0.0010	0.0093	0.0002	0.1964	0.0037
PRB79	0.5262	0.0086	0.0491	0.0009	0.0095	0.0001	0.1986	0.0034

PRB58	0.5913	0.0097	0.0510	0.0011	0.0095	0.0001	0.2072	0.0042
PRB70	0.5597	0.0092	0.0521	0.0016	0.0096	0.0002	0.2115	0.0061
PRB47	0.5005	0.0154	0.0477	0.0032	0.0088	0.0006	0.1948	0.0128
PRB86	0.5701	0.0095	0.0505	0.0015	0.0096	0.0002	0.2076	0.0060
PRB3	0.4479	0.0094	0.0524	0.0023	0.0104	0.0005	0.2160	0.0091
PRB82	0.7329	0.0120	0.0496	0.0012	0.0098	0.0002	0.2057	0.0045
PRB81	0.7405	0.0122	0.0533	0.0013	0.0100	0.0002	0.2214	0.0053
PRB101	0.8361	0.0141	0.0499	0.0012	0.0100	0.0002	0.2076	0.0049
PRB102	0.2546	0.0044	0.0503	0.0015	0.0104	0.0003	0.2098	0.0061
PRB61	0.4714	0.0079	0.0544	0.0020	0.0101	0.0003	0.2272	0.0080
PRB14	0.2424	0.0043	0.0497	0.0015	0.0104	0.0003	0.2078	0.0059
PRB51	0.6696	0.0234	0.0465	0.0034	0.0085	0.0006	0.1945	0.0141
PRB46	0.4986	0.0150	0.0487	0.0029	0.0087	0.0005	0.2057	0.0121
PRB105	0.4605	0.0078	0.0495	0.0013	0.0100	0.0002	0.2091	0.0055
PRB109	0.4608	0.0080	0.0501	0.0018	0.0101	0.0003	0.2131	0.0073
PRB1	0.3950	0.0086	0.0528	0.0027	0.0107	0.0005	0.2276	0.0109
PRB89	0.4008	0.0067	0.0497	0.0014	0.0100	0.0002	0.2161	0.0059
PRB99	0.5015	0.0089	0.0514	0.0028	0.0113	0.0004	0.2250	0.0118
PRB106	0.6877	0.0117	0.0493	0.0014	0.0102	0.0003	0.2159	0.0057
PRB60	0.4029	0.0068	0.0547	0.0020	0.0103	0.0003	0.2405	0.0085
PRB108	0.2673	0.0046	0.0498	0.0013	0.0097	0.0003	0.2231	0.0057
PRB107	0.4130	0.0071	0.0503	0.0014	0.0109	0.0003	0.2258	0.0062
PRB56	0.4362	0.0072	0.0530	0.0010	0.0104	0.0002	0.2400	0.0043
PRB93	0.9444	0.0158	0.0522	0.0016	0.0111	0.0002	0.2407	0.0069
PRB98	0.9959	0.0170	0.0532	0.0023	0.0107	0.0003	0.2493	0.0105
PRB27	1.2138	0.0227	0.0541	0.0024	0.0104	0.0003	0.2539	0.0109
PRB10	0.4799	0.0090	0.0500	0.0019	0.0114	0.0004	0.2374	0.0086
PRB52	0.8075	0.0289	0.0511	0.0042	0.0096	0.0007	0.2427	0.0199
PRB97	1.2397	0.0209	0.0542	0.0018	0.0109	0.0003	0.2600	0.0085
PRB76	0.5244	0.0088	0.0564	0.0020	0.0128	0.0003	0.2767	0.0092
PRB74	0.8484	0.0141	0.0509	0.0019	0.0113	0.0002	0.2520	0.0092
PRB104	0.5237	0.0089	0.0484	0.0014	0.0119	0.0003	0.2397	0.0067
PRB68	0.7953	0.0131	0.0512	0.0016	0.0114	0.0002	0.2540	0.0075
PRB100	0.8421	0.0144	0.0541	0.0022	0.0120	0.0003	0.2713	0.0108
PRB85	0.5675	0.0094	0.0506	0.0012	0.0127	0.0002	0.2651	0.0061
PRB20	0.6194	0.0109	0.0536	0.0023	0.0116	0.0003	0.2822	0.0115
PRB64	0.8573	0.0141	0.0539	0.0015	0.0123	0.0002	0.2899	0.0075
PRB62	0.4843	0.0080	0.0527	0.0011	0.0137	0.0002	0.3328	0.0068
PRB9	0.4231	0.0082	0.0564	0.0024	0.0159	0.0006	0.3711	0.0152
PRB75	0.9673	0.0160	0.0537	0.0017	0.0160	0.0003	0.3716	0.0111
PRB54	0.7295	0.0271	0.0522	0.0043	0.0151	0.0011	0.3884	0.0316
PRB63	0.6364	0.0105	0.0517	0.0011	0.0167	0.0002	0.3864	0.0075
PRB67	0.7552	0.0124	0.0550	0.0013	0.0179	0.0003	0.4355	0.0093
PRB88	0.7582	0.0127	0.0557	0.0016	0.0190	0.0004	0.4520	0.0124
PRB69	0.8243	0.0137	0.0573	0.0016	0.0188	0.0003	0.4709	0.0129
PRB44	0.8507	0.0242	0.0554	0.0031	0.0168	0.0009	0.4562	0.0254
PRB94	0.6201	0.0106	0.0552	0.0018	0.0204	0.0005	0.4634	0.0145
PRB66	0.9359	0.0154	0.0579	0.0014	0.0199	0.0003	0.4948	0.0112
PRB16	0.3939	0.0068	0.0565	0.0014	0.0212	0.0005	0.5105	0.0118
PRB96	0.6416	0.0108	0.0543	0.0013	0.0236	0.0005	0.5481	0.0126
PRB41	0.6459	0.0174	0.0584	0.0030	0.0242	0.0012	0.6829	0.0348
PRB11	0.3084	0.0057	0.0605	0.0019	0.0305	0.0009	0.7416	0.0216
PRB28	0.6276	0.0118	0.0647	0.0018	0.0385	0.0010	1.0978	0.0284

PRB12	0.5093	0.0096	0.0712	0.0024	0.0442	0.0013	1.3733	0.0436
PRB7	0.6658	0.0131	0.1092	0.0037	0.0920	0.0032	4.5354	0.1448
Standart	**GJ-1**							
GJ1	0.0268	0.0007	0.0627	0.0028	0.0361	0.0021	0.8597	0.0370
GJ10	0.0272	0.0005	0.0587	0.0012	0.0344	0.0012	0.7947	0.0148
GJ11	0.0268	0.0005	0.0601	0.0013	0.0347	0.0013	0.8115	0.0167
GJ12	0.0272	0.0005	0.0584	0.0014	0.0324	0.0012	0.7848	0.0179
GJ2	0.0269	0.0006	0.0610	0.0017	0.0312	0.0014	0.8165	0.0213
GJ3	0.0268	0.0006	0.0603	0.0013	0.0307	0.0013	0.8026	0.0157
GJ4	0.0295	0.0007	0.0601	0.0019	0.0291	0.0014	0.7968	0.0243
GJ5	0.0299	0.0009	0.0598	0.0029	0.0319	0.0019	0.8181	0.0393
GJ6	0.0314	0.0011	0.0576	0.0039	0.0283	0.0022	0.8117	0.0545
GJ7	0.0275	0.0005	0.0607	0.0010	0.0329	0.0010	0.8175	0.0121
GJ8	0.0268	0.0005	0.0611	0.0010	0.0312	0.0011	0.8045	0.0126
GJ9	0.0280	0.0005	0.0607	0.0011	0.0316	0.0011	0.8067	0.0138
Standart	**Plesovice**							
PL1	0.0865	0.0019	0.0543	0.0026	0.0179	0.0010	0.4118	0.0183
PL10	0.0892	0.0015	0.0529	0.0011	0.0166	0.0004	0.4000	0.0075
PL11	0.0892	0.0015	0.0527	0.0012	0.0164	0.0004	0.3977	0.0082
PL12	0.0890	0.0015	0.0518	0.0012	0.0174	0.0005	0.4043	0.0093
PL2	0.0862	0.0016	0.0524	0.0015	0.0169	0.0006	0.3900	0.0107
PL3	0.0881	0.0015	0.0524	0.0011	0.0165	0.0004	0.3985	0.0079
PL4	0.0900	0.0018	0.0526	0.0016	0.0152	0.0005	0.3866	0.0115
PL5	0.0952	0.0025	0.0509	0.0024	0.0144	0.0007	0.3737	0.0175
PL6	0.0981	0.0033	0.0538	0.0036	0.0155	0.0011	0.3912	0.0257
PL7	0.0938	0.0016	0.0531	0.0009	0.0159	0.0003	0.3995	0.0058
PL8	0.0882	0.0015	0.0528	0.0009	0.0164	0.0004	0.3943	0.0064
PL9	0.0899	0.0015	0.0521	0.0010	0.0167	0.0004	0.3842	0.0066

			Age, Ma					
$^{206}Pb/^{238}U$	1σ (abs)	Rho	$^{207}Pb/^{206}Pb$	1σ	$^{208}Pb/^{232}Th$	1σ	$^{207}Pb/^{235}U$	1σ
0.0251	0.0003	0.3	194.6	81.75	164.4	3.03	162.1	5.22
0.0256	0.0003	0.4	175.3	69.01	161.6	2.17	163.7	4.38
0.0257	0.0003	0.3	209.7	70.96	173.3	5.95	166.9	4.62
0.0261	0.0003	0.3	226.6	78.88	179.7	4.81	170.1	5.29
0.0263	0.0003	0.4	142.3	59.74	169.7	3.32	165.4	3.75
0.0265	0.0004	0.3	307.7	102.68	185.6	7.75	178	7.28
0.0267	0.0005	0.3	165.4	121.69	158.5	8.17	169.7	8.33
0.0268	0.0003	0.4	150.8	52.2	177.3	2.98	169.2	3.34
0.0269	0.0003	0.4	328.5	63.38	174.9	2.96	182.2	4.55
0.0270	0.0004	0.3	362.2	104.26	164.6	5.69	185	7.9
0.0270	0.0003	0.5	115.9	50.25	176.6	2.96	167.9	3.16
0.0270	0.0004	0.3	140.5	93.07	169.9	5.82	169.7	6.19
0.0273	0.0003	0.4	320.4	69.32	172.6	4.41	183.8	5.03
0.0274	0.0003	0.4	207.6	68.8	180.7	3.91	176.5	4.72
0.0275	0.0004	0.3	251.3	99.39	186.5	7.93	180.2	7.03
0.0277	0.0005	0.3	208.3	109.54	167.8	7.41	178.5	7.83
0.0277	0.0004	0.4	218.9	90.9	170.5	6.28	179.2	6.46
0.0277	0.0003	0.4	281.5	61.77	177.7	3.21	184	4.43
0.0278	0.0004	0.3	339.6	94	171.4	5.16	188.5	7.14
0.0279	0.0004	0.3	264.3	102.11	190.7	8.88	183.7	7.36
0.0280	0.0003	0.4	266.9	60.23	180.3	4.37	184.1	4.26
0.0280	0.0005	0.3	117.9	112.38	167.6	7.62	174.1	7.74
0.0281	0.0003	0.5	209.1	44.91	177.3	2.67	181.1	3.05
0.0283	0.0004	0.4	153	96.31	169.6	7.73	178.1	6.76
0.0284	0.0003	0.4	170.9	54.49	180	3.48	179.8	3.7
0.0284	0.0004	0.4	218.1	92	176.7	7.01	183.1	6.69
0.0284	0.0003	0.4	158	68.63	177.3	4.69	179.1	4.73
0.0285	0.0003	0.4	234.8	62.2	198.8	4.68	184.9	4.45
0.0285	0.0003	0.4	171.7	66.73	180.6	4.18	180.6	4.62
0.0285	0.0007	0.3	0.1	175.07	158.4	11.76	168.8	12.1
0.0286	0.0007	0.3	400.1	154.39	169.8	11.75	198.2	12.89
0.0286	0.0006	0.3	246.7	141.87	167.4	10.7	186.6	10.88
0.0287	0.0003	0.4	204.8	59.65	198.5	4.26	183.9	4.21
0.0288	0.0005	0.3	148.7	124.36	166.3	8.85	180.3	8.98
0.0288	0.0004	0.3	140.6	86.44	194.7	6.63	179.9	5.95
0.0288	0.0003	0.3	84.4	89.58	188.2	5.37	176.4	6.01
0.0289	0.0003	0.4	255	51.22	184.7	3.46	188.8	3.68
0.0289	0.0003	0.4	109.5	64.57	185.7	4.54	178.6	4.41
0.0289	0.0007	0.3	195.7	166.1	162.9	11.69	184.6	12.68
0.0291	0.0006	0.3	112.7	143.24	167.3	10.51	179.6	10.38
0.0292	0.0003	0.4	266.7	54.97	188.5	3.54	191.3	4.02
0.0292	0.0003	0.4	238.2	62.3	190.1	3.1	189.3	4.54
0.0292	0.0003	0.3	332.7	74.95	183.1	3.86	196.6	5.81
0.0292	0.0003	0.3	274.9	77.09	184.8	4.61	192.2	5.81
0.0292	0.0003	0.4	399.1	59.85	194.6	3.99	202.1	4.8
0.0292	0.0006	0.3	403.3	157.41	194.2	12.54	202.4	13.33
0.0292	0.0003	0.5	134.6	46.76	186.5	3.2	182.1	3.16
0.0293	0.0003	0.5	153.5	42.24	190.9	2.85	183.9	2.85

0.0295	0.0003	0.5	240.4	48.48	191.5	2.76	191.2	3.49
0.0295	0.0003	0.4	287.6	66.92	193.7	3.92	194.8	5.09
0.0296	0.0006	0.3	83.9	151.1	177.2	10.99	180.7	10.86
0.0298	0.0003	0.4	217.7	68.23	193.1	4.24	191.5	5.05
0.0299	0.0004	0.3	301.8	98.32	208.5	9.28	198.5	7.61
0.0301	0.0003	0.4	177	53.32	196.1	3.33	189.9	3.82
0.0301	0.0003	0.4	343.2	55.76	200.6	3.55	203	4.39
0.0302	0.0003	0.4	190.5	56.2	201	4.28	191.6	4.11
0.0303	0.0003	0.4	209.1	68.77	209.3	6	193.4	5.15
0.0303	0.0003	0.3	385.9	78.93	202.6	5.19	207.9	6.58
0.0303	0.0003	0.4	181.5	68.06	209.4	5.86	191.7	4.96
0.0304	0.0007	0.3	22.5	165.56	171.7	11.88	180.5	11.94
0.0306	0.0006	0.3	133.9	134.27	175.8	10.25	189.9	10.21
0.0306	0.0003	0.4	171.8	62.05	200.3	4.82	192.8	4.58
0.0309	0.0004	0.3	197.4	80.22	203.9	6.02	196.1	6.12
0.0313	0.0005	0.3	318.4	110.22	215.7	10.74	208.2	9.04
0.0315	0.0003	0.4	180.2	64.63	201.3	4.66	198.6	4.9
0.0318	0.0005	0.3	258.1	118.68	226.4	8.61	206.1	9.74
0.0318	0.0003	0.4	160.5	62.9	205.3	4.92	198.4	4.76
0.0319	0.0004	0.3	400.1	78.88	207.9	5.79	218.9	6.92
0.0325	0.0004	0.4	185.1	60.86	195	5.28	204.5	4.75
0.0326	0.0004	0.4	208.9	65	218.8	5.66	206.7	5.16
0.0328	0.0003	0.5	327.6	42.97	208.2	2.99	218.4	3.51
0.0334	0.0004	0.4	293.6	66.29	223.3	4.62	219	5.62
0.0340	0.0004	0.3	338.2	95.19	214.1	5.74	226	8.54
0.0340	0.0005	0.3	376.5	96.34	209.4	5.79	229.8	8.84
0.0345	0.0004	0.3	193.3	85.97	229	7.75	216.3	7.08
0.0345	0.0009	0.3	243	180.06	194	14.23	220.6	16.28
0.0348	0.0004	0.4	380.7	74.22	218.8	4.93	234.6	6.85
0.0356	0.0004	0.3	466.9	74.87	256.8	6.14	248	7.33
0.0359	0.0004	0.3	235.4	84.64	226.3	4.89	228.2	7.44
0.0359	0.0004	0.4	117.3	67.28	239.1	5.84	218.1	5.51
0.0360	0.0004	0.4	250.5	69.29	228.9	4.22	229.8	6.08
0.0364	0.0005	0.3	373.4	89.46	241	6.52	243.8	8.65
0.0380	0.0004	0.4	224	54.95	254.2	4.68	238.7	4.89
0.0382	0.0005	0.3	354	92.51	233.7	6.69	252.4	9.13
0.0390	0.0004	0.4	365.3	59.81	247.4	4.01	258.5	5.88
0.0458	0.0004	0.4	315.5	48.57	275.5	4.41	291.7	5.18
0.0477	0.0006	0.3	467.5	92.66	319.6	12.24	320.5	11.27
0.0502	0.0005	0.4	357.2	68.49	321.3	5.88	320.8	8.2
0.0540	0.0014	0.3	295.4	176	303.7	22.73	333.2	23.14
0.0542	0.0005	0.5	272.9	46.48	335.6	4.75	331.7	5.45
0.0574	0.0005	0.4	411.7	49.16	359	5.46	367.1	6.59
0.0588	0.0006	0.4	441.2	62.13	379.7	7.79	378.7	8.65
0.0596	0.0006	0.4	501.8	62.44	376.6	6.77	391.8	8.92
0.0597	0.0011	0.3	429.1	121.26	336.3	18.15	381.6	17.71
0.0609	0.0007	0.4	419.6	70.3	407.8	9.75	386.6	10.04
0.0619	0.0006	0.4	526.7	51.82	397.7	5.99	408.2	7.6
0.0655	0.0007	0.4	472.7	53.72	423.9	9.06	418.8	7.92
0.0732	0.0007	0.4	381.7	52.95	472.2	9.69	443.7	8.24
0.0848	0.0015	0.3	545.4	109.35	484.1	24.21	528.5	21.02
0.0889	0.0010	0.4	620.5	64.74	607.3	17.73	563.3	12.59
0.1231	0.0013	0.4	764.1	56.12	764.4	18.61	752.3	13.76

0.1400	0.0017	0.4	962.2	66.41	874.3	25.63	877.6	18.65
0.3012	0.0037	0.4	1786.6	60.31	1779.3	60.01	1737.5	26.57
0.0995	0.0015	0.3	697.7	93.82	715.9	41.4	629.9	20.19
0.0982	0.0009	0.5	556	42.77	682.7	23.75	593.8	8.39
0.0979	0.0010	0.5	607.6	46.3	689.7	25.09	603.3	9.38
0.0974	0.0010	0.5	545.4	51.05	643.5	24.15	588.2	10.16
0.0971	0.0010	0.4	639.2	58.49	620.9	27.46	606.1	11.93
0.0965	0.0009	0.5	615	44.7	611.6	25.07	598.3	8.87
0.0961	0.0012	0.4	608.4	66.88	579.9	27.38	595	13.73
0.0993	0.0017	0.4	595.2	102.89	633.7	37.52	607	21.94
0.1022	0.0023	0.3	514.7	141.86	564	42.88	603.4	30.56
0.0977	0.0008	0.6	627.9	34.72	654.2	19.97	606.7	6.75
0.0955	0.0008	0.6	641.1	36.36	620.5	20.99	599.3	7.1
0.0964	0.0009	0.5	627.3	39.17	629.1	22.17	600.6	7.74
0.0551	0.0008	0.3	382.2	101.63	357.6	18.78	350.2	13.17
0.0548	0.0005	0.5	325.8	44.71	333.6	7.81	341.7	5.45
0.0548	0.0005	0.5	314.5	48.72	328.7	8.33	340	5.97
0.0567	0.0006	0.4	274.1	53.9	349.5	9.63	344.8	6.71
0.0540	0.0006	0.4	301.8	64.82	339.3	11.25	334.4	7.83
0.0551	0.0005	0.5	304.8	47.47	329.8	8.42	340.6	5.73
0.0533	0.0006	0.4	311.3	68.37	304	10.54	331.9	8.39
0.0533	0.0009	0.4	235.4	106.51	289.7	14.68	322.4	12.96
0.0528	0.0012	0.3	361	142.09	310.7	20.95	335.2	18.78
0.0545	0.0005	0.6	334.8	36.05	318.8	5.65	341.3	4.24
0.0541	0.0005	0.5	319.8	39.37	329.2	6.9	337.5	4.64
0.0535	0.0005	0.5	288.9	41.83	334.1	7.2	330.1	4.86

$^{206}Pb/^{238}U$	1σ	D, %
159.8	1.75	1.4
162.9	1.64	0.5
163.8	1.72	1.9
166	1.85	2.5
167	1.62	-1.0
168.4	2.38	5.7
170.1	3.03	-0.2
170.4	1.6	-0.7
171	1.73	6.5
171.4	2.34	7.9
171.6	1.6	-2.2
171.8	2.25	-1.2
173.3	1.89	6.1
174.1	1.83	1.4
174.9	2.44	3.0
176.2	2.79	1.3
176.2	2.42	1.7
176.4	1.74	4.3
176.6	2.28	6.7
177.6	2.56	3.4
177.7	1.8	3.6
178.3	2.87	-2.4
178.9	1.61	1.2
180	2.61	-1.1
180.4	1.67	-0.3
180.4	2.55	1.5
180.6	2	-0.8
180.9	1.85	2.2
181.2	1.88	-0.3
181.4	4.57	-6.9
181.8	4.07	9.0
181.9	3.8	2.6
182.2	1.83	0.9
182.7	3.32	-1.3
182.9	2.25	-1.6
183.3	2.12	-3.8
183.5	1.7	2.9
183.9	1.97	-2.9
183.9	4.48	0.4
184.8	3.91	-2.8
185.2	1.78	3.3
185.3	1.81	2.2
185.4	2.04	6.0
185.5	2.03	3.6
185.6	1.86	8.9
185.6	4.01	9.1
185.7	1.7	-1.9
186.2	1.65	-1.2

187.1	1.68	2.2
187.2	1.91	4.1
188.2	3.92	-4.0
189.3	1.98	1.2
190	2.66	4.5
190.9	1.81	-0.5
191.1	1.86	6.2
191.6	1.93	0.0
192.1	2.08	0.7
192.4	2.15	8.1
192.5	2.01	-0.4
192.8	4.52	-6.4
194.5	3.82	-2.4
194.5	2.03	-0.9
196	2.29	0.1
198.7	3.02	4.8
200.1	2.05	-0.7
201.5	2.93	2.3
201.6	2.13	-1.6
202.3	2.26	8.2
206.1	2.17	-0.8
206.5	2.22	0.1
208.3	1.82	4.8
212	2.23	3.3
215.3	2.75	5.0
215.6	2.82	6.6
218.5	2.65	-1.0
218.6	5.53	0.9
220.3	2.49	6.5
225.3	2.5	10.1
227.4	2.57	0.4
227.6	2.42	-4.2
227.7	2.33	0.9
230.4	2.87	5.8
240.2	2.31	-0.6
241.6	2.95	4.5
246.7	2.4	4.8
288.6	2.6	1.1
300.6	3.93	6.6
315.6	3.29	1.6
338.8	8.61	-1.7
340	3.01	-2.4
359.9	3.31	2.0
368.4	3.8	2.8
373.1	3.77	5.0
373.9	6.87	2.1
381	4.18	1.5
387.3	3.64	5.4
408.9	3.9	2.4
455.6	4.45	-2.6
524.7	8.88	0.7
549.3	5.88	2.5
748.1	7.66	0.6

844.4	9.48	3.9
1697.2	18.38	2.4
611.5	8.65	3.0
603.6	5.42	-1.6
602	5.66	0.2
599.3	5.92	-1.9
597.3	6.11	1.5
593.8	5.33	0.8
591.4	6.77	0.6
610.1	9.85	-0.5
627.5	13.66	-3.8
600.7	4.96	1.0
588.1	4.96	1.9
593.2	5.15	1.2
345.5	5.1	1.4
343.9	3.13	-0.6
343.6	3.27	-1.0
355.3	3.56	-3.0
339.1	3.61	-1.4
345.7	3.13	-1.5
334.7	3.81	-0.8
334.5	5.38	-3.6
331.7	7.23	1.1
342	2.85	-0.2
339.9	2.91	-0.7
335.8	2.95	-1.7

X-Y Weighted Mean:
X = 0.28142±0.00033 2σ
Y = 0.039749±0.000032
X-Y error correlation = +0.673
MSWD = 1.18, Probability =

PRB72	1.1555	0.0190	0.0500	0.0018	0.0082	0.0002	0.1731	0.0060
PRB57	2.1293	0.0350	0.0496	0.0015	0.0080	0.0001	0.1750	0.0051
PRB22	0.1512	0.0027	0.0503	0.0016	0.0086	0.0003	0.1786	0.0054
PRB90	0.4214	0.0071	0.0507	0.0018	0.0089	0.0002	0.1824	0.0062
PRB19	0.5837	0.0100	0.0489	0.0013	0.0084	0.0002	0.1769	0.0044
PRB5	0.7865	0.0160	0.0525	0.0025	0.0092	0.0004	0.1916	0.0085
PRB42	0.7710	0.0211	0.0494	0.0027	0.0079	0.0004	0.1820	0.0097
PRB80	0.6123	0.0100	0.0491	0.0011	0.0088	0.0002	0.1813	0.0039
PRB78	1.2360	0.0203	0.0530	0.0015	0.0087	0.0002	0.1965	0.0054
PRB103	0.6125	0.0106	0.0538	0.0026	0.0082	0.0003	0.1999	0.0093
PRB83	0.6243	0.0103	0.0483	0.0011	0.0088	0.0002	0.1799	0.0037
PRB31	0.6244	0.0129	0.0489	0.0020	0.0084	0.0003	0.1820	0.0072
PRB26	0.5240	0.0096	0.0528	0.0017	0.0086	0.0002	0.1985	0.0059
PRB87	0.6243	0.0104	0.0503	0.0015	0.0090	0.0002	0.1898	0.0055
PRB4	0.7588	0.0156	0.0512	0.0023	0.0093	0.0004	0.1942	0.0083
PRB39	0.8900	0.0216	0.0503	0.0025	0.0083	0.0004	0.1921	0.0092
PRB35	0.9537	0.0210	0.0505	0.0020	0.0085	0.0003	0.1930	0.0076
PRB71	0.6742	0.0111	0.0519	0.0014	0.0088	0.0002	0.1986	0.0052
PRB29	0.8749	0.0167	0.0533	0.0023	0.0085	0.0003	0.2040	0.0085
PRB2	0.4028	0.0085	0.0515	0.0024	0.0095	0.0004	0.1984	0.0087
PRB13	0.4246	0.0075	0.0516	0.0014	0.0090	0.0002	0.1988	0.0050
PRB40	0.7503	0.0186	0.0484	0.0024	0.0083	0.0004	0.1871	0.0091
PRB77	0.6807	0.0111	0.0503	0.0010	0.0088	0.0001	0.1953	0.0036
PRB37	0.1087	0.0026	0.0491	0.0021	0.0084	0.0004	0.1918	0.0079
PRB59	0.3126	0.0052	0.0495	0.0012	0.0090	0.0002	0.1937	0.0044
PRB36	0.4416	0.0101	0.0505	0.0021	0.0088	0.0004	0.1977	0.0079
PRB30	0.8557	0.0164	0.0492	0.0015	0.0088	0.0002	0.1929	0.0056
PRB92	0.3366	0.0056	0.0509	0.0014	0.0099	0.0002	0.1997	0.0053
PRB25	0.5354	0.0096	0.0495	0.0014	0.0090	0.0002	0.1947	0.0054
PRB55	0.7384	0.0277	0.0460	0.0036	0.0079	0.0006	0.1808	0.0141
PRB49	0.3659	0.0118	0.0547	0.0040	0.0084	0.0006	0.2156	0.0154
PRB48	0.2792	0.0088	0.0511	0.0033	0.0083	0.0005	0.2018	0.0129
PRB91	0.4262	0.0071	0.0502	0.0013	0.0099	0.0002	0.1986	0.0050
PRB43	0.5882	0.0164	0.0490	0.0027	0.0083	0.0004	0.1943	0.0106
PRB8	1.0195	0.0195	0.0489	0.0019	0.0097	0.0003	0.1939	0.0070
PRB24	0.4552	0.0082	0.0477	0.0018	0.0094	0.0003	0.1898	0.0071
PRB73	0.3299	0.0054	0.0513	0.0012	0.0092	0.0002	0.2044	0.0044
PRB110	0.8839	0.0152	0.0482	0.0013	0.0092	0.0002	0.1924	0.0052
PRB53	0.7311	0.0265	0.0500	0.0038	0.0081	0.0006	0.1994	0.0150
PRB50	0.4886	0.0158	0.0483	0.0031	0.0083	0.0005	0.1935	0.0122
PRB21	0.6680	0.0115	0.0516	0.0013	0.0094	0.0002	0.2073	0.0048
PRB65	0.8271	0.0136	0.0509	0.0014	0.0095	0.0002	0.2049	0.0054
PRB23	1.2473	0.0219	0.0531	0.0018	0.0091	0.0002	0.2136	0.0070
PRB18	0.5525	0.0095	0.0518	0.0018	0.0092	0.0002	0.2084	0.0069
PRB17	0.7132	0.0122	0.0547	0.0015	0.0097	0.0002	0.2203	0.0058
PRB45	0.4725	0.0139	0.0548	0.0041	0.0097	0.0006	0.2206	0.0160
PRB84	0.3867	0.0064	0.0487	0.0010	0.0093	0.0002	0.1964	0.0037
PRB79	0.5262	0.0086	0.0491	0.0009	0.0095	0.0001	0.1986	0.0034
PRB58	0.5913	0.0097	0.0510	0.0011	0.0095	0.0001	0.2072	0.0042
PRB70	0.5597	0.0092	0.0521	0.0016	0.0096	0.0002	0.2115	0.0061
PRB47	0.5005	0.0154	0.0477	0.0032	0.0088	0.0006	0.1948	0.0128

PRB86	0.5701	0.0095	0.0505	0.0015	0.0096	0.0002	0.2076	0.0060
PRB3	0.4479	0.0094	0.0524	0.0023	0.0104	0.0005	0.2160	0.0091
PRB82	0.7329	0.0120	0.0496	0.0012	0.0098	0.0002	0.2057	0.0045
PRB81	0.7405	0.0122	0.0533	0.0013	0.0100	0.0002	0.2214	0.0053
PRB101	0.8361	0.0141	0.0499	0.0012	0.0100	0.0002	0.2076	0.0049
PRB102	0.2546	0.0044	0.0503	0.0015	0.0104	0.0003	0.2098	0.0061
PRB61	0.4714	0.0079	0.0544	0.0020	0.0101	0.0003	0.2272	0.0080
PRB14	0.2424	0.0043	0.0497	0.0015	0.0104	0.0003	0.2078	0.0059
PRB51	0.6696	0.0234	0.0465	0.0034	0.0085	0.0006	0.1945	0.0141
PRB46	0.4986	0.0150	0.0487	0.0029	0.0087	0.0005	0.2057	0.0121
PRB105	0.4605	0.0078	0.0495	0.0013	0.0100	0.0002	0.2091	0.0055
PRB109	0.4608	0.0080	0.0501	0.0018	0.0101	0.0003	0.2131	0.0073
PRB1	0.3950	0.0086	0.0528	0.0027	0.0107	0.0005	0.2276	0.0109
PRB89	0.4008	0.0067	0.0497	0.0014	0.0100	0.0002	0.2161	0.0059
PRB99	0.5015	0.0089	0.0514	0.0028	0.0113	0.0004	0.2250	0.0118
PRB106	0.6877	0.0117	0.0493	0.0014	0.0102	0.0003	0.2159	0.0057
PRB60	0.4029	0.0068	0.0547	0.0020	0.0103	0.0003	0.2405	0.0085
PRB108	0.2673	0.0046	0.0498	0.0013	0.0097	0.0003	0.2231	0.0057
PRB107	0.4130	0.0071	0.0503	0.0014	0.0109	0.0003	0.2258	0.0062
PRB56	0.4362	0.0072	0.0530	0.0010	0.0104	0.0002	0.2400	0.0043
PRB93	0.9444	0.0158	0.0522	0.0016	0.0111	0.0002	0.2407	0.0069
PRB98	0.9959	0.0170	0.0532	0.0023	0.0107	0.0003	0.2493	0.0105
PRB27	1.2138	0.0227	0.0541	0.0024	0.0104	0.0003	0.2539	0.0109
PRB10	0.4799	0.0090	0.0500	0.0019	0.0114	0.0004	0.2374	0.0086
PRB52	0.8075	0.0289	0.0511	0.0042	0.0096	0.0007	0.2427	0.0199
PRB97	1.2397	0.0209	0.0542	0.0018	0.0109	0.0003	0.2600	0.0085
PRB76	0.5244	0.0088	0.0564	0.0020	0.0128	0.0003	0.2767	0.0092
PRB74	0.8484	0.0141	0.0509	0.0019	0.0113	0.0002	0.2520	0.0092
PRB104	0.5237	0.0089	0.0484	0.0014	0.0119	0.0003	0.2397	0.0067
PRB68	0.7953	0.0131	0.0512	0.0016	0.0114	0.0002	0.2540	0.0075
PRB100	0.8421	0.0144	0.0541	0.0022	0.0120	0.0003	0.2713	0.0108
PRB85	0.5675	0.0094	0.0506	0.0012	0.0127	0.0002	0.2651	0.0061
PRB20	0.6194	0.0109	0.0536	0.0023	0.0116	0.0003	0.2822	0.0115
PRB64	0.8573	0.0141	0.0539	0.0015	0.0123	0.0002	0.2899	0.0075
PRB62	0.4843	0.0080	0.0527	0.0011	0.0137	0.0002	0.3328	0.0068
PRB9	0.4231	0.0082	0.0564	0.0024	0.0159	0.0006	0.3711	0.0152
PRB75	0.9673	0.0160	0.0537	0.0017	0.0160	0.0003	0.3716	0.0111
PRB54	0.7295	0.0271	0.0522	0.0043	0.0151	0.0011	0.3884	0.0316
PRB63	0.6364	0.0105	0.0517	0.0011	0.0167	0.0002	0.3864	0.0075
PRB67	0.7552	0.0124	0.0550	0.0013	0.0179	0.0003	0.4355	0.0093
PRB88	0.7582	0.0127	0.0557	0.0016	0.0190	0.0004	0.4520	0.0124
PRB69	0.8243	0.0137	0.0573	0.0016	0.0188	0.0003	0.4709	0.0129
PRB44	0.8507	0.0242	0.0554	0.0031	0.0168	0.0009	0.4562	0.0254
PRB94	0.6201	0.0106	0.0552	0.0018	0.0204	0.0005	0.4634	0.0145
PRB66	0.9359	0.0154	0.0579	0.0014	0.0199	0.0003	0.4948	0.0112
PRB16	0.3939	0.0068	0.0565	0.0014	0.0212	0.0005	0.5105	0.0118
PRB96	0.6416	0.0108	0.0543	0.0013	0.0236	0.0005	0.5481	0.0126
PRB41	0.6459	0.0174	0.0584	0.0030	0.0242	0.0012	0.6829	0.0348
PRB11	0.3084	0.0057	0.0605	0.0019	0.0305	0.0009	0.7416	0.0216
PRB28	0.6276	0.0118	0.0647	0.0018	0.0385	0.0010	1.0978	0.0284
PRB12	0.5093	0.0096	0.0712	0.0024	0.0442	0.0013	1.3733	0.0436
PRB7	0.6658	0.0131	0.1092	0.0037	0.0920	0.0032	4.5354	0.1448

GJ1	0.0268	0.0007	0.0627	0.0028	0.0361	0.0021	0.8597	0.0370
GJ10	0.0272	0.0005	0.0587	0.0012	0.0344	0.0012	0.7947	0.0148
GJ11	0.0268	0.0005	0.0601	0.0013	0.0347	0.0013	0.8115	0.0167
GJ12	0.0272	0.0005	0.0584	0.0014	0.0324	0.0012	0.7848	0.0179
GJ2	0.0269	0.0006	0.0610	0.0017	0.0312	0.0014	0.8165	0.0213
GJ3	0.0268	0.0006	0.0603	0.0013	0.0307	0.0013	0.8026	0.0157
GJ4	0.0295	0.0007	0.0601	0.0019	0.0291	0.0014	0.7968	0.0243
GJ5	0.0299	0.0009	0.0598	0.0029	0.0319	0.0019	0.8181	0.0393
GJ6	0.0314	0.0011	0.0576	0.0039	0.0283	0.0022	0.8117	0.0545
GJ7	0.0275	0.0005	0.0607	0.0010	0.0329	0.0010	0.8175	0.0121
GJ8	0.0268	0.0005	0.0611	0.0010	0.0312	0.0011	0.8045	0.0126
GJ9	0.0280	0.0005	0.0607	0.0011	0.0316	0.0011	0.8067	0.0138
PL1	0.0865	0.0019	0.0543	0.0026	0.0179	0.0010	0.4118	0.0183
PL10	0.0892	0.0015	0.0529	0.0011	0.0166	0.0004	0.4000	0.0075
PL11	0.0892	0.0015	0.0527	0.0012	0.0164	0.0004	0.3977	0.0082
PL12	0.0890	0.0015	0.0518	0.0012	0.0174	0.0005	0.4043	0.0093
PL2	0.0862	0.0016	0.0524	0.0015	0.0169	0.0006	0.3900	0.0107
PL3	0.0881	0.0015	0.0524	0.0011	0.0165	0.0004	0.3985	0.0079
PL4	0.0900	0.0018	0.0526	0.0016	0.0152	0.0005	0.3866	0.0115
PL5	0.0952	0.0025	0.0509	0.0024	0.0144	0.0007	0.3737	0.0175
PL6	0.0981	0.0033	0.0538	0.0036	0.0155	0.0011	0.3912	0.0257
PL7	0.0938	0.0016	0.0531	0.0009	0.0159	0.0003	0.3995	0.0058
PL8	0.0882	0.0015	0.0528	0.0009	0.0164	0.0004	0.3943	0.0064
PL9	0.0899	0.0015	0.0521	0.0010	0.0167	0.0004	0.3842	0.0066

0.0251	0.0003	0.3	194.6	81.75	164.4	3.03	162.1	5.22
0.0256	0.0003	0.4	175.3	69.01	161.6	2.17	163.7	4.38
0.0257	0.0003	0.3	209.7	70.96	173.3	5.95	166.9	4.62
0.0261	0.0003	0.3	226.6	78.88	179.7	4.81	170.1	5.29
0.0263	0.0003	0.4	142.3	59.74	169.7	3.32	165.4	3.75
0.0265	0.0004	0.3	307.7	102.68	185.6	7.75	178	7.28
0.0267	0.0005	0.3	165.4	121.69	158.5	8.17	169.7	8.33
0.0268	0.0003	0.4	150.8	52.2	177.3	2.98	169.2	3.34
0.0269	0.0003	0.4	328.5	63.38	174.9	2.96	182.2	4.55
0.0270	0.0004	0.3	362.2	104.26	164.6	5.69	185	7.9
0.0270	0.0003	0.5	115.9	50.25	176.6	2.96	167.9	3.16
0.0270	0.0004	0.3	140.5	93.07	169.9	5.82	169.7	6.19
0.0273	0.0003	0.4	320.4	69.32	172.6	4.41	183.8	5.03
0.0274	0.0003	0.4	207.6	68.8	180.7	3.91	176.5	4.72
0.0275	0.0004	0.3	251.3	99.39	186.5	7.93	180.2	7.03
0.0277	0.0005	0.3	208.3	109.54	167.8	7.41	178.5	7.83
0.0277	0.0004	0.4	218.9	90.9	170.5	6.28	179.2	6.46
0.0277	0.0003	0.4	281.5	61.77	177.7	3.21	184	4.43
0.0278	0.0004	0.3	339.6	94	171.4	5.16	188.5	7.14
0.0279	0.0004	0.3	264.3	102.11	190.7	8.88	183.7	7.36
0.0280	0.0003	0.4	266.9	60.23	180.3	4.37	184.1	4.26
0.0280	0.0005	0.3	117.9	112.38	167.6	7.62	174.1	7.74
0.0281	0.0003	0.5	209.1	44.91	177.3	2.67	181.1	3.05
0.0283	0.0004	0.4	153	96.31	169.6	7.73	178.1	6.76
0.0284	0.0003	0.4	170.9	54.49	180	3.48	179.8	3.7
0.0284	0.0004	0.4	218.1	92	176.7	7.01	183.1	6.69
0.0284	0.0003	0.4	158	68.63	177.3	4.69	179.1	4.73
0.0285	0.0003	0.4	234.8	62.2	198.8	4.68	184.9	4.45
0.0285	0.0003	0.4	171.7	66.73	180.6	4.18	180.6	4.62
0.0285	0.0007	0.3	0.1	175.07	158.4	11.76	168.8	12.1
0.0286	0.0007	0.3	400.1	154.39	169.8	11.75	198.2	12.89
0.0286	0.0006	0.3	246.7	141.87	167.4	10.7	186.6	10.88
0.0287	0.0003	0.4	204.8	59.65	198.5	4.26	183.9	4.21
0.0288	0.0005	0.3	148.7	124.36	166.3	8.85	180.3	8.98
0.0288	0.0004	0.3	140.6	86.44	194.7	6.63	179.9	5.95
0.0288	0.0003	0.3	84.4	89.58	188.2	5.37	176.4	6.01
0.0289	0.0003	0.4	255	51.22	184.7	3.46	188.8	3.68
0.0289	0.0003	0.4	109.5	64.57	185.7	4.54	178.6	4.41
0.0289	0.0007	0.3	195.7	166.1	162.9	11.69	184.6	12.68
0.0291	0.0006	0.3	112.7	143.24	167.3	10.51	179.6	10.38
0.0292	0.0003	0.4	266.7	54.97	188.5	3.54	191.3	4.02
0.0292	0.0003	0.4	238.2	62.3	190.1	3.1	189.3	4.54
0.0292	0.0003	0.3	332.7	74.95	183.1	3.86	196.6	5.81
0.0292	0.0003	0.3	274.9	77.09	184.8	4.61	192.2	5.81
0.0292	0.0003	0.4	399.1	59.85	194.6	3.99	202.1	4.8
0.0292	0.0006	0.3	403.3	157.41	194.2	12.54	202.4	13.33
0.0292	0.0003	0.5	134.6	46.76	186.5	3.2	182.1	3.16
0.0293	0.0003	0.5	153.5	42.24	190.9	2.85	183.9	2.85
0.0295	0.0003	0.5	240.4	48.48	191.5	2.76	191.2	3.49
0.0295	0.0003	0.4	287.6	66.92	193.7	3.92	194.8	5.09
0.0296	0.0006	0.3	83.9	151.1	177.2	10.99	180.7	10.86

0.0298	0.0003	0.4	217.7	68.23	193.1	4.24	191.5	5.05
0.0299	0.0004	0.3	301.8	98.32	208.5	9.28	198.5	7.61
0.0301	0.0003	0.4	177	53.32	196.1	3.33	189.9	3.82
0.0301	0.0003	0.4	343.2	55.76	200.6	3.55	203	4.39
0.0302	0.0003	0.4	190.5	56.2	201	4.28	191.6	4.11
0.0303	0.0003	0.4	209.1	68.77	209.3	6	193.4	5.15
0.0303	0.0003	0.3	385.9	78.93	202.6	5.19	207.9	6.58
0.0303	0.0003	0.4	181.5	68.06	209.4	5.86	191.7	4.96
0.0304	0.0007	0.3	22.5	165.56	171.7	11.88	180.5	11.94
0.0306	0.0006	0.3	133.9	134.27	175.8	10.25	189.9	10.21
0.0306	0.0003	0.4	171.8	62.05	200.3	4.82	192.8	4.58
0.0309	0.0004	0.3	197.4	80.22	203.9	6.02	196.1	6.12
0.0313	0.0005	0.3	318.4	110.22	215.7	10.74	208.2	9.04
0.0315	0.0003	0.4	180.2	64.63	201.3	4.66	198.6	4.9
0.0318	0.0005	0.3	258.1	118.68	226.4	8.61	206.1	9.74
0.0318	0.0003	0.4	160.5	62.9	205.3	4.92	198.4	4.76
0.0319	0.0004	0.3	400.1	78.88	207.9	5.79	218.9	6.92
0.0325	0.0004	0.4	185.1	60.86	195	5.28	204.5	4.75
0.0326	0.0004	0.4	208.9	65	218.8	5.66	206.7	5.16
0.0328	0.0003	0.5	327.6	42.97	208.2	2.99	218.4	3.51
0.0334	0.0004	0.4	293.6	66.29	223.3	4.62	219	5.62
0.0340	0.0004	0.3	338.2	95.19	214.1	5.74	226	8.54
0.0340	0.0005	0.3	376.5	96.34	209.4	5.79	229.8	8.84
0.0345	0.0004	0.3	193.3	85.97	229	7.75	216.3	7.08
0.0345	0.0009	0.3	243	180.06	194	14.23	220.6	16.28
0.0348	0.0004	0.4	380.7	74.22	218.8	4.93	234.6	6.85
0.0356	0.0004	0.3	466.9	74.87	256.8	6.14	248	7.33
0.0359	0.0004	0.3	235.4	84.64	226.3	4.89	228.2	7.44
0.0359	0.0004	0.4	117.3	67.28	239.1	5.84	218.1	5.51
0.0360	0.0004	0.4	250.5	69.29	228.9	4.22	229.8	6.08
0.0364	0.0005	0.3	373.4	89.46	241	6.52	243.8	8.65
0.0380	0.0004	0.4	224	54.95	254.2	4.68	238.7	4.89
0.0382	0.0005	0.3	354	92.51	233.7	6.69	252.4	9.13
0.0390	0.0004	0.4	365.3	59.81	247.4	4.01	258.5	5.88
0.0458	0.0004	0.4	315.5	48.57	275.5	4.41	291.7	5.18
0.0477	0.0006	0.3	467.5	92.66	319.6	12.24	320.5	11.27
0.0502	0.0005	0.4	357.2	68.49	321.3	5.88	320.8	8.2
0.0540	0.0014	0.3	295.4	176	303.7	22.73	333.2	23.14
0.0542	0.0005	0.5	272.9	46.48	335.6	4.75	331.7	5.45
0.0574	0.0005	0.4	411.7	49.16	359	5.46	367.1	6.59
0.0588	0.0006	0.4	441.2	62.13	379.7	7.79	378.7	8.65
0.0596	0.0006	0.4	501.8	62.44	376.6	6.77	391.8	8.92
0.0597	0.0011	0.3	429.1	121.26	336.3	18.15	381.6	17.71
0.0609	0.0007	0.4	419.6	70.3	407.8	9.75	386.6	10.04
0.0619	0.0006	0.4	526.7	51.82	397.7	5.99	408.2	7.6
0.0655	0.0007	0.4	472.7	53.72	423.9	9.06	418.8	7.92
0.0732	0.0007	0.4	381.7	52.95	472.2	9.69	443.7	8.24
0.0848	0.0015	0.3	545.4	109.35	484.1	24.21	528.5	21.02
0.0889	0.0010	0.4	620.5	64.74	607.3	17.73	563.3	12.59
0.1231	0.0013	0.4	764.1	56.12	764.4	18.61	752.3	13.76
0.1400	0.0017	0.4	962.2	66.41	874.3	25.63	877.6	18.65
0.3012	0.0037	0.4	1786.6	60.31	1779.3	60.01	1737.5	26.57

0.0995	0.0015	0.3	697.7	93.82	715.9	41.4	629.9	20.19
0.0982	0.0009	0.5	556	42.77	682.7	23.75	593.8	8.39
0.0979	0.0010	0.5	607.6	46.3	689.7	25.09	603.3	9.38
0.0974	0.0010	0.5	545.4	51.05	643.5	24.15	588.2	10.16
0.0971	0.0010	0.4	639.2	58.49	620.9	27.46	606.1	11.93
0.0965	0.0009	0.5	615	44.7	611.6	25.07	598.3	8.87
0.0961	0.0012	0.4	608.4	66.88	579.9	27.38	595	13.73
0.0993	0.0017	0.4	595.2	102.89	633.7	37.52	607	21.94
0.1022	0.0023	0.3	514.7	141.86	564	42.88	603.4	30.56
0.0977	0.0008	0.6	627.9	34.72	654.2	19.97	606.7	6.75
0.0955	0.0008	0.6	641.1	36.36	620.5	20.99	599.3	7.1
0.0964	0.0009	0.5	627.3	39.17	629.1	22.17	600.6	7.74
0.0551	0.0008	0.3	382.2	101.63	357.6	18.78	350.2	13.17
0.0548	0.0005	0.5	325.8	44.71	333.6	7.81	341.7	5.45
0.0548	0.0005	0.5	314.5	48.72	328.7	8.33	340	5.97
0.0567	0.0006	0.4	274.1	53.9	349.5	9.63	344.8	6.71
0.0540	0.0006	0.4	301.8	64.82	339.3	11.25	334.4	7.83
0.0551	0.0005	0.5	304.8	47.47	329.8	8.42	340.6	5.73
0.0533	0.0006	0.4	311.3	68.37	304	10.54	331.9	8.39
0.0533	0.0009	0.4	235.4	106.51	289.7	14.68	322.4	12.96
0.0528	0.0012	0.3	361	142.09	310.7	20.95	335.2	18.78
0.0545	0.0005	0.6	334.8	36.05	318.8	5.65	341.3	4.24
0.0541	0.0005	0.5	319.8	39.37	329.2	6.9	337.5	4.64
0.0535	0.0005	0.5	288.9	41.83	334.1	7.2	330.1	4.86

159.8	1.75	1.4
162.9	1.64	0.5
163.8	1.72	1.9
166	1.85	2.5
167	1.62	-1.0
168.4	2.38	5.7
170.1	3.03	-0.2
170.4	1.6	-0.7
171	1.73	6.5
171.4	2.34	7.9
171.6	1.6	-2.2
171.8	2.25	-1.2
173.3	1.89	6.1
174.1	1.83	1.4
174.9	2.44	3.0
176.2	2.79	1.3
176.2	2.42	1.7
176.4	1.74	4.3
176.6	2.28	6.7
177.6	2.56	3.4
177.7	1.8	3.6
178.3	2.87	-2.4
178.9	1.61	1.2
180	2.61	-1.1
180.4	1.67	-0.3
180.4	2.55	1.5
180.6	2	-0.8
180.9	1.85	2.2
181.2	1.88	-0.3
181.4	4.57	-6.9
181.8	4.07	9.0
181.9	3.8	2.6
182.2	1.83	0.9
182.7	3.32	-1.3
182.9	2.25	-1.6
183.3	2.12	-3.8
183.5	1.7	2.9
183.9	1.97	-2.9
183.9	4.48	0.4
184.8	3.91	-2.8
185.2	1.78	3.3
185.3	1.81	2.2
185.4	2.04	6.0
185.5	2.03	3.6
185.6	1.86	8.9
185.6	4.01	9.1
185.7	1.7	-1.9
186.2	1.65	-1.2
187.1	1.68	2.2
187.2	1.91	4.1
188.2	3.92	-4.0

189.3	1.98	1.2
190	2.66	4.5
190.9	1.81	-0.5
191.1	1.86	6.2
191.6	1.93	0.0
192.1	2.08	0.7
192.4	2.15	8.1
192.5	2.01	-0.4
192.8	4.52	-6.4
194.5	3.82	-2.4
194.5	2.03	-0.9
196	2.29	0.1
198.7	3.02	4.8
200.1	2.05	-0.7
201.5	2.93	2.3
201.6	2.13	-1.6
202.3	2.26	8.2
206.1	2.17	-0.8
206.5	2.22	0.1
208.3	1.82	4.8
212	2.23	3.3
215.3	2.75	5.0
215.6	2.82	6.6
218.5	2.65	-1.0
218.6	5.53	0.9
220.3	2.49	6.5
225.3	2.5	10.1
227.4	2.57	0.4
227.6	2.42	-4.2
227.7	2.33	0.9
230.4	2.87	5.8
240.2	2.31	-0.6
241.6	2.95	4.5
246.7	2.4	4.8
288.6	2.6	1.1
300.6	3.93	6.6
315.6	3.29	1.6
338.8	8.61	-1.7
340	3.01	-2.4
359.9	3.31	2.0
368.4	3.8	2.8
373.1	3.77	5.0
373.9	6.87	2.1
381	4.18	1.5
387.3	3.64	5.4
408.9	3.9	2.4
455.6	4.45	-2.6
524.7	8.88	0.7
549.3	5.88	2.5
748.1	7.66	0.6
844.4	9.48	3.9
1697.2	18.38	2.4

611.5	8.65	3.0
603.6	5.42	-1.6
602	5.66	0.2
599.3	5.92	-1.9
597.3	6.11	1.5
593.8	5.33	0.8
591.4	6.77	0.6
610.1	9.85	-0.5
627.5	13.66	-3.8
600.7	4.96	1.0
588.1	4.96	1.9
593.2	5.15	1.2
345.5	5.1	1.4
343.9	3.13	-0.6
343.6	3.27	-1.0
355.3	3.56	-3.0
339.1	3.61	-1.4
345.7	3.13	-1.5
334.7	3.81	-0.8
334.5	5.38	-3.6
331.7	7.23	1.1
342	2.85	-0.2
339.9	2.91	-0.7
335.8	2.95	-1.7